



8-2013

Human Motion Analysis with Wearable Inertial Sensors

Xi Chen
xchen46@utk.edu

Recommended Citation

Chen, Xi, "Human Motion Analysis with Wearable Inertial Sensors." PhD diss., University of Tennessee, 2013.
https://trace.tennessee.edu/utk_graddiss/2407

This Dissertation is brought to you for free and open access by the Graduate School at Trace: Tennessee Research and Creative Exchange. It has been accepted for inclusion in Doctoral Dissertations by an authorized administrator of Trace: Tennessee Research and Creative Exchange. For more information, please contact trace@utk.edu.

To the Graduate Council:

I am submitting herewith a dissertation written by Xi Chen entitled "Human Motion Analysis with Wearable Inertial Sensors." I have examined the final electronic copy of this dissertation for form and content and recommend that it be accepted in partial fulfillment of the requirements for the degree of Doctor of Philosophy, with a major in Biomedical Engineering.

Jindong Tan, Major Professor

We have read this dissertation and recommend its acceptance:

William R. Hamel, Xiaopeng Zhao, Qing Cao

Accepted for the Council:
Dixie L. Thompson

Vice Provost and Dean of the Graduate School

(Original signatures are on file with official student records.)

Human Motion Analysis with Wearable Inertial Sensors

A Dissertation

Presented for the

Doctor of Philosophy

Degree

The University of Tennessee, Knoxville

Xi Chen

August 2013

© by Xi Chen, 2013

All Rights Reserved.

DEDICATION

This dissertation is dedicated to my parents, Lifen Zhang and Haibo Chen.

Acknowledgements

I would like to express my sincere and deep gratitude to my advisor, Dr. Jindong Tan, for his continual support and guidance during the past five years. I appreciate his encouragement and enthusiasm for encountered problems in my research and my life.

I would like to thank Dr. William R. Hamel, Dr. Xiaopeng Zhao and Dr. Qing Cao, who gave me suggestions on my dissertation and served as my committee members of dissertation defense.

I would like to thank all my labmates at the Robotics and Wireless Sensor Networks lab at Michigan Technological University, from 2008 to 2012: Dr. Sheng Hu, Dr. Lufeng Shi, Dr. Fanyu Kong, Dr. Shuo Huang, Dr. Xinying Zheng, Dr. Ya Tian and Jian Lu. I appreciate their help on my research. Thanks also to Dr. Chen Li, Dr. Chen Liao, Rong Liu, Zhinan Wang for their encouragement and friendship since 2008.

I also want to thank all my labmates both at Michigan Technological University and the University of Tennessee, Knoxville. We all experienced the transfer and long distance moving from Houghton, MI to Knoxville, TN. Thanks for their support on my works and dissertation writing from 2012 to 2013: Dr. Hongsheng He, Zhenzhou Shao, Xiaolong Liu and Hao Zhang.

Finally, I would like to specially thank all my family members, who encourage me, support me and love me forever.

Abstract

High-resolution, quantitative data obtained by a human motion capture system can be used to better understand the cause of many diseases for effective treatments. Talking about the daily care of the aging population, two issues are critical. One is to continuously track motions and position of aging people when they are at home, inside a building or in the unknown environment; the other is to monitor their health status in real time when they are in the free-living environment. Continuous monitoring of human movement in their natural living environment potentially provide more valuable feedback than these in laboratory settings. However, it has been extremely challenging to go beyond laboratory and obtain accurate measurements of human physical activity in free-living environments. Commercial motion capture systems produce excellent in-studio capture and reconstructions, but offer no comparable solution for acquisition in everyday environments. Therefore in this dissertation, a wearable human motion analysis system is developed for continuously tracking human motions, monitoring health status, positioning human location and recording the itinerary.

In this dissertation, two systems are developed for seeking aforementioned two goals: tracking human body motions and positioning a human. Firstly, an inertial-based human body motion tracking system with our developed inertial measurement unit (IMU) is introduced. By arbitrarily attaching a wearable IMU to each segment, segment motions can be measured and translated into inertial data by IMUs. A human model can be reconstructed in real time based on the inertial data by applying

high efficient twists and exponential maps techniques. Secondly, for validating the feasibility of developed tracking system in the practical application, model-based quantification approaches for resting tremor and lower extremity bradykinesia in Parkinsons disease are proposed. By estimating all involved joint angles in PD symptoms based on reconstructed human model, angle characteristics with corresponding medical ratings are employed for training a HMM classifier for quantification. Besides, a pedestrian positioning system is developed for tracking users itinerary and positioning in the global frame. Corresponding tests have been carried out to assess the performance of each system.

Table of Contents

1	Introduction	1
1.1	Human Motion Analysis	1
1.2	Research Challenges	4
1.3	Research Goals	7
1.4	Contributions	9
1.5	Inertial Measurement Unit	12
1.6	Dissertation Outline	13
2	Inertial-Based Human Body Motion Tracking System	15
2.1	Introduction	17
2.2	Problem Formulation	19
2.2.1	Kinematics of Human Body	19
2.2.2	Body Motion Reconstruction	21
2.2.3	System Calibration	24
2.3	Motion Tracking with Twists and Exponential Maps	26
2.3.1	Quaternion-based Orientation Filter	26
2.3.2	Twists and Exponential Maps	29
2.3.3	Kinematic Chains and Full Body Motion	36
2.4	Estimation of Parameters	40
2.4.1	Estimation of Arbitrary IMU Placement	40
2.4.2	Estimation of Body Limb Length	43

2.5	Experiments	45
2.5.1	Experimental Setup	45
2.5.2	Upper Limb Motion Tracking	46
2.5.3	Full Body Motion Tracking	51
2.6	Related Work	58
2.7	Summary	61
3	Model-Based Quantification of Resting Tremor	62
3.1	Introduction	64
3.2	Human Arm Modeling and Joint Angle Estimation	67
3.2.1	Human Arm Modeling	67
3.2.2	Arm Joint Angle Estimation	70
3.3	Model-based Tremor Quantification	75
3.3.1	Tremor Feature Selection	75
3.3.2	Resting Tremor Severity Classification	79
3.3.3	Validation of EMG Assistance	82
3.4	Experiments	83
3.4.1	Resting Postures	84
3.4.2	Signal Pre-processing	85
3.4.3	Resting Tremor Simulation	86
3.5	Discussion and Summary	88
4	Model-Based Quantification of Lower Extremity Bradykinesia	92
4.1	INTRODUCTION	94
4.2	Human Lower Extremity Modeling and Joint Angle Estimation	97
4.2.1	Human Lower Extremity Modeling	97
4.2.2	Angle Estimation of Leg Joints	100
4.3	Model-based Bradykinesia Quantification	103
4.3.1	Bradykinesia Feature Selection	103
4.3.2	Bradykinesia Severity Classification	107

4.4	Experiments	109
4.4.1	Experimental Design	110
4.4.2	Signal Pre-processing	110
4.4.3	Bradykinesia Simulation	111
4.5	Discussion and Summary	112
5	Inertial-Based Pedestrian Positioning for Indoors	118
5.1	Introduction	120
5.2	System Overview	123
5.3	Activity Classification	125
5.3.1	Model description	125
5.3.2	HMM Training	126
5.3.3	Automatic Activity Classification	127
5.4	Pedestrian Dead Reckoning	127
5.4.1	Step Detection	127
5.4.2	Drift Correction	129
5.4.3	Heading Determination	130
5.4.4	Position Estimation	132
5.5	Experiments	133
5.5.1	Performance Evaluation	133
5.5.2	Straight Line Walking	134
5.5.3	Short Term Walking	134
5.5.4	Long Term Walking	137
5.6	Summary	139
6	Conclusions and Future Work	140
6.1	Conclusions	140
6.2	Future Work	142
Bibliography		144

List of Tables

2.1	Comparison of IMU angle and camera angle for each figure	57
3.1	UPDRS of tremor	79
3.2	Postures without subject movements	84
3.3	Postures after subject movements	84
3.4	Classification results of three features HMM with leave-one-out technique for elbow flexion-extension angle	88
3.5	Classification results of three Features HMM with leave-one-out technique for elbow pronation-supination angle	88
3.6	Classification results of three features HMM with leave-one-out technique for wrist flexion-extension angle	89
3.7	Classification results of single features HMM with leave-one-out technique	89
4.1	UPDRS of bradykinesia	107
4.2	Classification results of three features HMM with leave-one-out technique for hip and knee joint angle	115
5.1	Results of the straight line experiment	135
5.2	Results of the rectangle-shaped and U-shaped experiment	137
5.3	Absolute and relative average error of the long term experiment . . .	139

List of Figures

1.1	Wide applications of BSN	3
1.2	The goal and structure of this dissertation	8
1.3	The top view of IMU and its coordinate	13
2.1	Human body modeling	20
2.2	IMU position on arm and leg	22
2.3	The design of quaternion-based orientation filter	27
2.4	Quaternion rotations representation	28
2.5	Kinematic chains of upper and lower extremities	37
2.6	A kinematic chain of human model with forearm motion relative to the global frame at $t = t' + \Delta t$	39
2.7	Demonstration of IMU position estimation	41
2.8	Cylinder look of human limb	42
2.9	Limb length estimation by swinging around shoulder joint	44
2.10	A screenshot of the motion tracking procedure. Left figure shows the placement of markers and IMUs; Up-right figure shows real-time optical motion tracking result; Bottom-right figure shows real-time reconstructed arm motion in <i>MATLAB</i>	47
2.11	Upper limb motion tracking test 1: (a) angles between upper arm and trunk; (b) angles between upper and lower arm	48
2.12	Upper limb motion tracking test 2: (a) angles between upper arm and trunk; (b) angles between upper and lower arm	50

2.13 Angle changes of IMUs along 3 axes during upper limb motion tracking test 1	52
2.14 (a) The placement of IMUs and reflective markers on human body and (b) planned motions for experiment	54
2.15 Angle changes during elbow flexion-extension movements for (a) left arm and (b) right arm	55
2.16 Angle changes during knee flexion-extension movements for (a) left leg and (b) right leg	56
2.17 Angle changes of elbow joints and knee joints during full body test and corresponding movements	58
 3.1 Kinematic modeling of a human arm	68
3.2 Three major rotations of forearm used for extracting resting tremor features	75
3.3 HMM for tremor severity classification	81
3.4 Segments of elbow flexion-extension angle data, corresponding features: average angle change rate, energy and spectrum entropy and severities for HMM training.	87
 4.1 Kinematic modeling of a human lower extremity	99
4.2 Two rotations of lower extremity used for extracting bradykinesia features	104
4.3 HMM for bradykinesia classification	109
4.4 A screen shot of the video during the test and concurrently reconstructed body motions	112
4.5 Segments of hip joint angle data, extracted three features and corresponding severities for HMM training.	113
4.6 Segments of knee joint angle data, extracted three features and corresponding severities for HMM training.	114

5.1	A pedestrian positioning system design	121
5.2	The architecture of position estimation system	124
5.3	HMM for activity classification	126
5.4	IMU board and its placement	128
5.5	Some calculations for heading determination	130
5.6	Position estimation with IMU	132
5.7	The reconstruction of straight line trajectory. Black point and red point represent the starting and ending point.	134
5.8	Two short term walking experiments	136
5.9	Long term walking experiment	138

Chapter 1

Introduction

1.1 Human Motion Analysis

Human motion analysis has a wide range of applications, including telemanipulator control, athlete training, movie making, health status diagnosis and etc. Among these applications, biomedical related area is the most prospective and promising application for the coming aging era. The United States experienced the Baby Boom years during 40s to 60s in the last century ([Jones \(2009\)](#)). Till today, these “baby boomers” are gradually entering their retirement age and becoming ones of the aging population. As the age grows, especially after the age of 50, people are facing various issues and challenges physically and mentally. Among those issues, health problem affects the quality of daily living most and attracts significant attentions by society in the past decades. Familiar health problems that aging people are suffering are arthritis, stroke, Parkinson’ disease (PD) and etc. These illnesses have a common point, which is the impact on motor functions of aging people. As the development and deterioration of these illnesses, they are prone to be highly risky for the elderly. It would be necessary to monitor, track and analyze body motions of these patients by applying wearable sensors, without interrupting their free-living activities and meanwhile keeping watching their health status continuously.

Continuous tracking of human motions in natural environments potentially provides more accurate and intuitive feedback than in-lab settings. At present, however, it is difficult to achieve the goal of tracking and monitoring a patient's motion at anytime and anywhere. The restriction is from the tracking facilities, such as visual motion capturing systems, are too pricy and complicated to be practically applied for home use. Besides, a feasible motion tracking in the free-living environment is also not achievable.

Currently, patients are required to go to a lab or a clinic to have their treatment. An experienced clinician provides appropriate therapy based on their in-lab observations or subjective off-lab recall from patients themselves. As a matter of fact, aging people spend a large amount of time at home or walking outside. The disease, such as PD, varies in severity during a day according to patient's physical and mental status. The insufficient assessment during a day compared with in-lab observations is prone to induce inaccurate diagnosis, and then influence timely treatment.

After-treatment rehabilitation is essential for patients to recover their motor functions. It is a dynamic process to correct undesired motions by facilities and experienced clinicians. A better way to evaluate the rehabilitation is to continuously monitor patients' motions so that to identify and rectify problematic motion patterns at an early time. However, above restriction makes it unrealistic to continuously monitor motions in a free-living environment throughout the day.

Wireless body sensor network (BSN) has attracted increasing attentions due to its appealing applications, such as Figure 1.1 shows. Continuous monitoring by BSN provides information of patients, which is critical to discover their health problem in time. Besides, it is able to track motions and position of elders and quickly respond to potential emergencies they are having. A BSN consists of wearable sensor platforms, such as physiological sensors (electromyograph (EMG)) and bio-kinetic sensors (accelerometer, gyroscope). They can be used to monitor the health status and recognize the actions of body segments. Among these platforms, wireless inertial



Figure 1.1: Wide applications of BSN

sensors, such as accelerometers, gyroscopes and magnetometers, are small, easy to be set up and less cumbersome to the subject. They release the limitation of wired body sensors in capturing motions. Their advantage of wireless communication provides favorable opportunities for applying remote health care.

As a critical component of human motion analysis, a human motion tracking system with wearable inertial sensors can be developed for providing unlimited monitoring of users' status and motions. Compared with visual motion tracking technique, wearable inertial-based tracking fully satisfies the medical need of conveniently and continuously monitoring a patient's motions in free-living environment: Non-intrusive inertial sensors tracks human motions naturally and they are capable of providing long-term monitoring of daily activities accurately.

Besides, human motion analysis can be applied for other purposes, such as the quantification of PD, human positioning and etc. It effectively enables continuous monitoring, illness quantification and evaluation in one system and sends patient's information to the server. Care-givers can either locally or remotely diagnose and follow-up the progression of patient's illness conditions. Human motion analysis overcomes the restriction from current medical facilities. By innovating means of timely monitoring and diagnosis, the accurate treatment will be of great help in ameliorating the quality of elder people's life.

1.2 Research Challenges

Real-time human motion tracking can be applied to numbers of biomedical applications, such as clinical gait analysis, rehabilitation, joint motion analysis and etc. Several tracking technologies, such as mechanical tracking (*Gypsy 7TM**), magnetic tracking (*Liberty^{TM†}*) and visual tracking (*Vicon[‡], Qualisys[§], OptiTrack[¶]*) has been in used for many years. However, the complex infrastructure of these tracking technologies limits their usage in the controlled volume and is not practical in the free-living environment. Inertial tracking (*Xsens^{||}*) performs in a more natural way to track human motions in daily life. Especially as the development of sensor technology, wireless inertial tracking system is well accepted because of its small size, convenient installation, wireless communication, low power consumption and accurate monitoring of daily activities.

One challenge in current research of inertial motion tracking is low computational efficiency in motion tracking and model reconstruction. High-order calculations require a large amount of computational time for building a complicated human

*<http://www.metamotion.com/gypsy/gypsy-motion-capture-system.htm>

†<http://www.polhemus.com>

‡<http://www.vicon.com>

§<http://www.qualisys.com>

¶<http://www.naturalpoint.com/optitrack>

||<http://www.xsens.com>

model, which affects the efficiency of real-time tracking. Joint rotations are described by using product of rotation matrixes with one matrix for each rotation axis. When connecting multiple human segments in the system, the number of matrix increases as more number of degree of freedom (DoF) is added for tracking. This results in the increase of computational time during the motion reconstruction.

Similar to the function of rotation matrix, the twist representation and exponential maps techniques are capable of describing joint rotations and connecting rigid bodies. They have been employed in robotic manipulation and markerless visual tracking for years. These two techniques reduce the calculation complexity in traditional method, when reconstructing a human model by applying one matrix for each rotation joint. However, such techniques have not been researched for inertial human motion tracking so far and their advantages are necessary to be fully utilized.

Inertial sensors are attached to human segments for motion tracking, however, accurately estimate the sensor placement is challenging. At present, it always takes long to accurately estimate a placement where would be affected less by human soft tissue artifact and the anatomical structure of joints and body segments. Besides, arbitrary sensor placement by uses brings additional difficulty in placement estimation and it is easy to impact on tracking accuracy. Both issues bring challenges to researchers for discussing a way to rapidly and accurately estimate a sensor placement where could maximally reduce the errors and robust to users' arbitrary attachment ([Lin and Kulic \(2012\)](#)).

Inertial human body motion tracking system can be optimized for many medical applications. One of the potentially important applications is the quantification of PD through its specific symptoms. PD is a degenerative disorder of the central nervous system and it mostly occurs to the elderly over the age of 50. As PD progresses gradually, it impacts on motor and non-motor functions to variable degrees. As the two most apparent symptoms of PD, bradykinesia and resting tremor are usually analyzed for the quantification of PD severity. Although the medical rating scale for assessing symptoms of PD, such as Unified PD Rating Scale (UPDRS), has been

commonly used as a standard, it relies on a clinician's subjective observations and patients' subjective recall.

In recent years, some research has been developed for objectively quantifying PD symptoms with wearable inertial sensors. These inertial based works rely on individual sensors on analyzing tremor movements and always achieve low accuracy in quantification. Accelerometers are regularly applied since they can reflect moving trend of body segments. As a matter of fact, the acceleration of body segments is prone to be contaminated by subject's intentional movements and accumulated errors. Although based on the characteristic of tremor, gyroscopes performs much better in measuring recurrent movement, few research considers its superiority in quantifying resting tremor. Besides, resting tremor does not occur in only one joint, neighbor joints are also affected. Thus, a model based approach which analyzes the rotational movements of all involved joints simultaneously will greatly improve the accuracy of inertial based quantification approach. However, such model based approach is lacking in present research.

For the quantification of bradykinesia, similar to resting tremor, inertial sensors such as accelerometers and gyroscope sensors are commonly used to measure upper limb (wrist and finger) rotations, trunk stability and impaired gait for quantifying bradykinesia. One challenge of this research is still the lack of model based approach in quantification: measured inertial data is from single joint or segment for analysis. Since PD typically impact on patients' multiple body segments and their functions, it is necessary to develop a model based quantification to comprehensively analyze the motions. Moreover, a major impact of bradykinesia is on patients' motor functions of lower extremity (thigh and shank), but nevertheless very few research focuses on the quantification from lower extremity movements. This brings another challenge of current quantification of bradykinesia. Impaired lower extremity directly induces abnormal gaits. Therefore, it is preferable to assess the motor functions in entirety rather than from separate joints.

A human motion analysis system can position a human and record travelled itinerary. The wearable motion tracking only tracks human body motions locally but lack of tracking human position globally. Although for outdoor positioning, Global Positioning System (GPS) provides accurate and absolute position information, it is unreliable or even not available inside a building. For indoor positioning, local beacon positioning technique provides absolute position. However, the pre-installed infrastructure is not available in the unknown environment and it is not economical and practical to equip every point of such environment with beacons. Consequently, an inertial-based human positioning technique provides the solution, so that not only human motions can be tracked and monitored, human position also can be tracked and recorded.

In human positioning, many techniques of reducing the sensor drift, estimating step length and heading azimuth have made great advances, such as Zero Velocity Update (ZUPT) technique and Pedestrian Dead Reckoning (PDR) technique. As a newly developed technique in recent years, conventional PDR system encounters a challenging problem. It uses gyroscopes and compasses to estimate the heading orientation, however, the accuracy of orientation estimation by gyroscopes and magnetic compasses is easily to be affected by sensor drift and ambient perturbation of magnetic field. Thus, a method which can compensate the drift and magnetic field perturbation should be developed to increase the overall positioning accuracy and robustness.

1.3 Research Goals

This research aims to develop a human motion analysis system with wearable inertial sensors to address the challenges. It is capable of tracking human motions, reconstructing the human model, monitoring human health status, positioning and recording human itinerary in free-living environment. There are four major goals are discussed in this dissertation. The first goal is developing a wearable human

body motion tracking; the second and the third goal are two medical applications of body motion tracking in PD, which are the quantification of resting tremor and lower extremity bradykinesia; the fourth goal is developing a inertial-based human positioning.

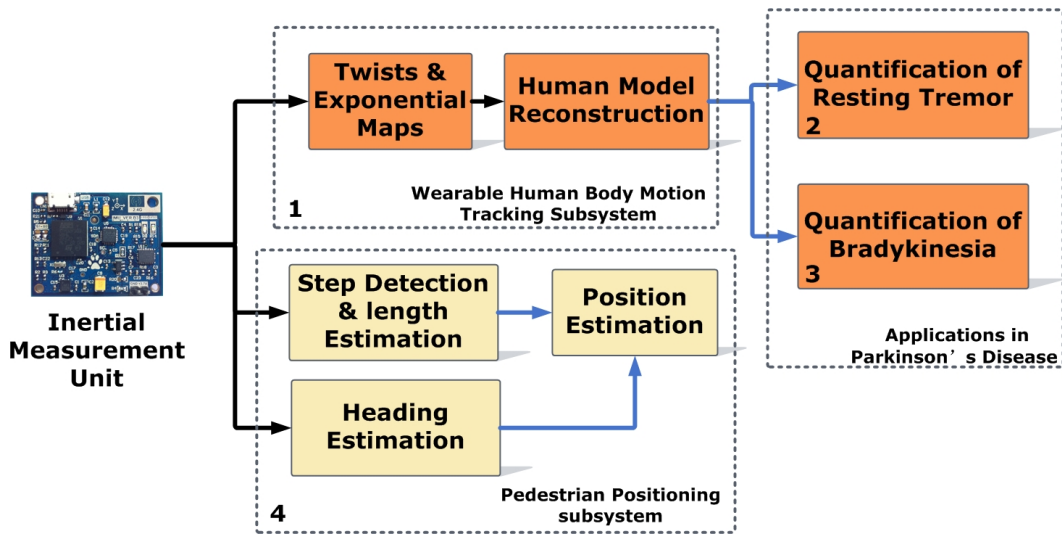


Figure 1.2: The goal and structure of this dissertation

Figure 1.2 illustrated 4 detailed goals of this dissertation. Our developed Inertial Measurement Unit (IMU) measures human body motions when attached to body. Captured inertial data and estimated quaternion by an embedded orientation estimation algorithm are employed for the first work and the fourth work in this research. A quaternion representation is introduced in the book by Kuipers (2002).

The first goal is to develop a wearable human body motion tracking system. Human body motions are captured and measured inertial data from IMUs are transmitted to computer via Bluetooth for processing by proposed motion tracking techniques. Joints' quaternions are translated into rotations and translations relative to neighbor joints. Limb kinematic chains are formed by connecting body segments

by joints. Finally, a human model is built by connecting chains to body trunk. By applying reconstructed human model, human joints are able to be located in a local tracking frame and absolute joint angles are easily estimated. Reconstructed model can simultaneously represent human motions and concrete rotational information around any joint axis is easily achieved from the joint quaternion representation for valuable joint analysis.

The second goal is a practical application of motion tracking system, which is developing a model-based approach for quantifying resting tremor of PD patient. Both wrist and elbow joint angles during some designed postures are measured from the reconstructed human body model. Selected features extracted from these angles are correlated with the severity of resting tremor. A trained classifier is capable of distinguishing the correlation from continuous features. Finally, by only analyzing upper extremity motions, resting tremor is going to be quantified.

The third goal is to apply the model-based approach for the quantification of lower extremity bradykinesia of PD. Both hip and knee joint angles during walking are measured. According to the difference of extracted features from healthy subjects and patients in various severities, proposed approach is going to quantify lower extremity bradykinesia based on pre-trained classifier.

The fourth goal is to develop a inertial-based human positioning system with our developed IMU. This work is mainly focusing on developing an orientation optimization method, in order to improve the accuracy of heading estimation and the robustness against both the accumulated gyroscope error and traditional fluctuation of magnetic field. Meanwhile, developed human positioning system records human travelled itinerary and positions human location for indoor or unknown environment.

1.4 Contributions

The major contributions of this dissertation are focusing on addressing the research challenges we mentioned. The details are specified as follows.

1. A wearable human body motion tracking system is developed based on a BSN consists of previously developed IMUs. IMUs are attached to body segments and measure the joint motions after a well-designed IMU calibration procedure. By applying twist and exponential maps techniques for representing segment motions and articulating segment chains, a human model is reconstructed by articulated segments and its motions are demonstrated by rotating joints within the global frame. Detailed contributions are summarized as follows
 - (a) The twist representation and exponential maps techniques are applied for estimating joint rotations and articulating neighbor segments by joints. Compared with traditional method that uses rotation matrix, proposed techniques are advanced by low-order calculations in building a human model. The highly efficient estimation guarantees the motion tracking in real time.
 - (b) A calibration procedure is designed for optimally estimating the position and orientation of attached IMUs. With the execution of this procedure, the spatial position of IMUs correlated to corresponding body segments can be estimated, regardless knowing the exact IMU placement by the subject. It significantly reduces the complexity in configuring the system and makes it simple to use for anyone.
2. Based on developed human body motion tracking technique, reconstructed human model is employed in developing a quantification method for resting tremor of PD. The model-based approach assesses a patient's resting tremor more complete from joint rotation of all involved joints, rather than from only one joint rotations. Moreover, specially selected features for analyzing joint rotations and trained Hidden Markov Model (HMM) for classifying those features from different severities obtain a high accuracy in discriminating severities of resting tremor that rated by the medical standard. Detailed contributions are summarized as follows

- (a) According to the character of resting tremor, absolute joint rotation angles are estimated by body motion tracking system. Compared with relative angular velocity or acceleration of single joint, absolute angle data is more promising for quantification and robust to human intentional movements.
 - (b) Angle related features are specially selected and extracted from absolute angle data. Those features can best describe the character of tremor movements.
 - (c) A discrete HMM classifier is chosen and trained with previously extracted features and their corresponding medical ratings. The training with multiple features greatly increases the classification accuracy of single feature training. Consequently, high accuracy of preliminary tests validates proposed quantification approach.
3. Based on developed human body motion tracking system, reconstructed human model is also employed in developing a quantification method for lower extremity bradykinesia of PD. The model-based approach assesses patient's motor functions of lower extremity by analyzing hip and knee joints motions. Specially selected features and HMM classifier are used to fulfill the quantification. The performance of proposed approach is validated with simulated data by leave-one-out mechanism.
4. A wearable inertial-based indoor positioning system is developed. By detecting step occurrence, estimating step length and heading azimuth, a subject's position and travelled itinerary can be tracked and monitored within the global frame, which is of great use for positioning a subject in the unknown environment where local positioning infrastructure is unavailable. Detailed contributions are summarized as follows
- (a) Zero Velocity Update (ZUPT) technique is implemented to correct the walking velocity. By resetting the walking velocity to zero at each step

stance phase, this technique lowers the accumulated drift in step length estimation and limits the error rate within a certain level.

- (b) A discrete HMM is introduced to detect step occurrence and classify the walking states by standing, walking, going upstairs and going downstairs.
- (c) In order to improve the accuracy of estimating heading azimuth in conventional Pedestrian Dead Reckoning (PDR) system, a novel combination of lateral acceleration and angular velocity are used for the estimation, which avoids the perturbation to magnetometer from local disordered magnetic field.

1.5 Inertial Measurement Unit

Inertial sensors can measure rigid kinematic motions, such as acceleration by accelerometers, angular velocity by gyroscopes and magnetic field intensity by magnetometers. A IMU is developed in our lab and introduced in the work of [Hu et al. \(2010\)](#), as is shown in Figure 1.3. It contains an integrated 6-axis motion tracking chip (*InvenSense* MPU-6000) which combines a 3-axis gyroscope, 3-axis accelerometer and a Digital Motion Processor. It also contains a 3-axis magnetometer (*Honeywell* HMC5843) and an embedded ARM-based processor (STM32F103) for computations. The sample rate for all the inertial sensors are 60 Hz and the interface between sensors and a computer is via Bluetooth. A micro-SD slot is optional to install on the board, so that if necessary the inertial data can be stored in the micro-SD when the communication is unavailable.

An embedded orientation estimation algorithm was proposed by our lab mate and the detail is introduced by [Tian et al. \(2012\)](#); [Tian and Tan \(2012\)](#). In this algorithm, an adaptive-gain complementary filter is combined with Gauss-Newton optimization algorithm to determine the gyroscope error and magnetic distortion and

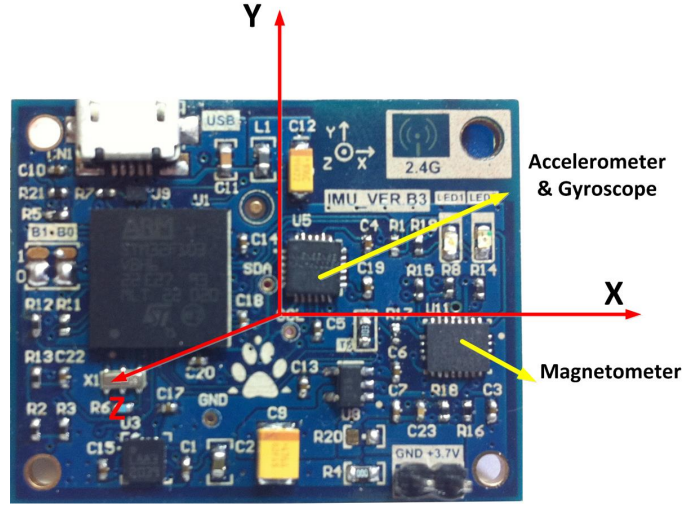


Figure 1.3: The top view of IMU and its coordinate

compensate gyroscope measurements. The quaternion representation is outputted from the algorithm to describe the 3-dimension rotations of a joint.

1.6 Dissertation Outline

This dissertation consists of four correlated papers which are arranged in the order as research goals summarized in Section 1.3. It is organized as follows:

Chapter 2 introduces the development of a human body motion tracking system with wearable inertial sensors. A well designed calibration procedure is effective to estimate the IMU position and orientation, regardless of arbitrary placement on the body segment. The twist and exponential maps techniques describe body movements and articulate segment chains to reconstruct a human model. Compared with traditional high-order product of rotational matrixes, low-order calculations from proposed techniques guarantee the real-time motion tracking. A series of upper extremity and full body motion tracking experiments are conducted, and the

comparisons with commercial systems validate the accuracy of developed wearable human body motion tracking.

Chapter 3 and Chapter 4 introduce two potential medical applications of developed motion tracking respectively, which are the quantification of two most apparent PD symptoms: resting tremor and bradykinesia. The upper extremity movements for resting tremor and lower extremity movements for bradykinesia are analyzed. With the help of reconstructed human model from the motion tracking system, absolute angles of all involved joints are simultaneously estimated. Three angle related features which can appropriately describe pathologic characters of these two symptoms are extracted. Features of different severities and correlated clinical ratings are used to train a discrete HMM classifier. Cross-validation of test data validates the accuracy in quantifying symptoms with various severities.

Chapter 5 introduces the development of a inertial-based human positioning system can be applied to locate and track human position for indoor environment and as a complementarity of human body motion tracking to provide global positioning. Developed human positioning system obtains the function by detecting step occurrence, estimating step length and heading azimuth. Currently available ZUPT algorithm is implemented and combines with a HMM to estimate step length, step occurrence and meanwhile classifies the walking patterns of the subject. An optimized PDR technique is developed to complement gyro rate with acceleration to improve the heading azimuth estimation, and to avoid electromagnetic perturbation that magnetometer suffers in conventional PDR system. A series of short term walking and long term walking tests are conducted. The performance of developed human positioning is validated by calculating position errors in both 2D and 3D itinerary reconstruction.

Finally, Chapter 6 concludes the dissertation and gives description of future works.

Chapter 2

Inertial-Based Human Body Motion Tracking System

Abstract

Wearable inertial tracking is well accepted due to its convenience for free-style motion tracking with high accuracy. Traditional tracking methods rely on complicated high-order calculations for human kinematic modeling. Besides, sensor placement issue is addressed by integrating multiple sensor measurements to estimate, in which researchers always ignore the importance of estimating a more accurate placement. In order to tackle the challenges of complexity in modeling and IMU placement estimation, a wearable human motion tracking system is developed by applying twist representation and exponential maps techniques. Joint positions are continuously updated based on these techniques and the rotational angles of each joint can be represented individually within the global frame, when the body segments are articulated by product of exponential maps. It is unnecessary to build a human kinematic model with high-order calculations, which brings more convenience and rapidness for real-time motion tracking. An IMU's position and orientation are optimally estimated in a well-designed calibration procedure regardless of knowing its placement. This chapter presents our approach and exemplifies the assessment of proposed motion tracking system. The comparisons with *Vicon* and *OptiTrack* motion capture systems verify the accuracy of several tests of limb motion tracking and full body motion tracking, which achieve satisfactorily high accuracy.

2.1 Introduction

Real-time human motion tracking has been applied to many applications in biomedical areas: clinical gait analysis, exercise rehabilitation, fall detection, biomechanical analysis of joints and etc. Several tracking technologies, such as mechanical tracking, magnetic tracking and visual tracking have been available for years. However, these tracking technologies lack the capability of tracking in free-living environments. Inertial tracking can track human motions in daily life with less intrusion.

Inertial tracking crosses over various areas that need tracking solutions and it provides more concrete information of subject's living status. As the progress of Micro-electromechanical Systems (MEMS) technology nowadays, inertial sensors are becoming smaller and can obtain accurate inertial measurements. The wireless sensor is less cumbersome to the subject, which makes human motion tracking available at anytime and anywhere. With its character of low power consumption, wearable sensor consequently provides long-term and accurate monitoring of daily activities in free living environment.

Wearable inertial tracking allows for unlimited estimation of limb orientations under fast motions, which could improve the performance of motion capture evidently. Its convenience for free-style movement tracking in daily life is well accepted. This research aims to develop a human body motion tracking system, which is capable of tracking arbitrary 3D motions, measuring joint angles and reconstructing a human model, by taking advantages of wireless sensors.

Current research has been focusing on achieving rapid and accurate tracking results. No matter how accurate and flexible the inertial tracking can achieve, a common procedure is building a human kinematic model to simulate the functionality of human links and coupling measured inertial data with the model to reconstruct a human model with 3D motions. Traditional inertial tracking algorithm mostly applies rotation matrix for representing rotations along each axis of joints. The inverse kinematics technique is a major way to address body link connections, which

uses product of rotation matrix to demonstrate the rotations of a joint with multiple DoFs or link connections with several joints. As an obvious drawback, the number of parameters needed in rotation matrixes will be raised linearly when connecting more links. The high-order calculations apparently increase the computational time for kinematic modeling and impact the feasibility of tracking in real time.

An approach to solving the challenge by adopting twist representation and exponential maps techniques is introduced in this chapter. A small amount of parameters (low-order) enables rapid calculations of joint angles, so that kinematic modeling can satisfy the needs for real-time model reconstruction. Besides, using forward kinematics to connect more human links together with mentioned techniques, much less parameters than rotation matrix would be added to the system, which almost does not affect real-time motion tracking. Without large amount of calculations, wearable body motion tracking system can estimate joint position rapidly and suffice real-time tracking.

Human soft tissue artifact is a main source of errors, no matter the wearable sensors are mounted on a garment or directly attached to skin. Besides, the spatial relationship of segment axes in a joint is actually much more complicated than it appears according to human anatomical structure. Both issues bring challenges to choose IMU placement on human body in typical tracking methods. Kalman filter and some extended methods discussed in the work of [Lin and Kulic \(2012\)](#) are generally utilized to integrate multiple sensor measurements to increase the reliability of sensor placement. The challenging task would still be, basically, to accurately estimate the sensor placement. In our developed system, a well-designed calibration procedure is developed to minimize the interference from IMU placement. Regardless of an arbitrary IMU placement, the procedure can estimate its position and orientation and couple its placement with corresponding joint, so that following tracking can base on the inertial data of corresponding joint but with less concern to the placement issue.

It will be practical to develop a wearable human body motion tracking system, which is convenient to be applied to free-style activities as well. The challenges of

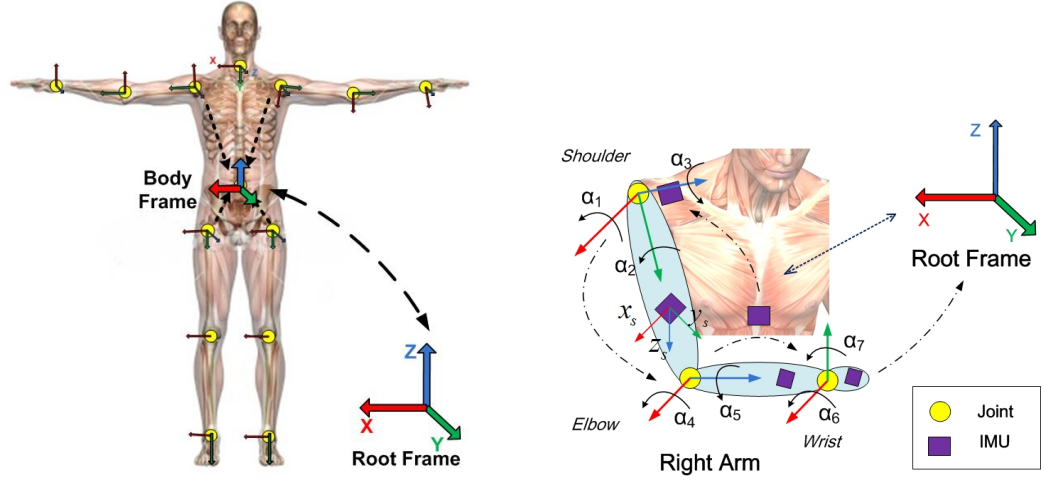
sensor placement and modeling rapidness, as a matter of fact, conceal the advantages of wearable tracking for use throughout our life. Even though traditional tracking technique achieves fairly high accuracy, the relatively complex initial configuration would confuse subjects and sway them to attempt a long term testing. Developing a “mount-n-use” system, which is non-intrusive to our daily life, becomes the purpose of this research.

Thus, a wearable body motion tracking system is introduced, which can estimate joint angles and demonstrate arbitrary 3D motions in real time simply from the inertial output of IMUs. A quaternion-based orientation filter is employed to pre-process inertial measurements and eliminate noises. A well designed calibration procedure optimally estimates the position and orientation of IMUs, regardless of arbitrary placement. Compared with traditional approach that constructs a human kinematic model with high-order calculations based on rotation matrix, proposed low-order calculations technique reflects more convenience to reconstruct 3D motions in real time. The twist representation and exponential maps techniques explicitly describe rigid body motions and articulate kinematic chains to achieve human modeling, which demonstrate aforementioned advantages. A series of movements of upper limb and full body are measured. The assessment of developed system is exemplified by the comparisons with commercialized motion capture systems on estimated joint angles between adjacent human links.

2.2 Problem Formulation

2.2.1 Kinematics of Human Body

A human body is modeled as an articulated model, which consists of 15 rigid body segments, 14 joints and 38 DoFs. It includes torso (waist-neck part and waist-hip part), head, upper limbs and lower limbs, as are shown in Figure 2.1a.



(a) Human full body model with joint coordinates

(b) Kinematic modeling of right arm with IMUs

Figure 2.1: Human body modeling

Human upper limb includes upper arm, forearm and hand, which has 10 DoFs in total. Taking the right arm as an example (Figure 2.1b). Shoulder is described as a ball and socket joint with 6 DoFs: 3-DoF rotations and 3-DoF translations. Rotation angles are assigned to flexion-extension α_1 , internal-external α_2 and abduction-adduction α_3 rotations. Elbow is modeled as 2 hinge joints with non-intersecting axes (Cutti et al. (2008)). Therefore, it is described by 2 DoFs: flexion-extension α_4 and pronation-supination α_5 rotations. Wrist is modeled as an ellipsoid joint with 2 DoFs: flexion-extension α_6 and radial/ulnar deviation α_7 rotations. For the left arm, similarly, rotation angles $\alpha_8 \sim \alpha_{14}$ are assigned to axes of shoulder, elbow and wrist joints.

Torso provides the orientation of body and it includes 2 joints: neck has 3 DoFs and waist is also considered to have 3 DoFs, so that the spinal movements can be simplified as the rotations around waist joint. Because developed system does not

consider the movements of head, there is no IMU corresponding to the neck. Rotation angles $\alpha_{15} \sim \alpha_{17}$ are assigned to waist joint.

Lower limbs have similar structure as upper limbs but relatively distinct functionalities; in fact, lower limbs perform less complicated motions than upper limbs. Here takes the right leg as an example, hip joint has similar structure as shoulder with 3-DoF rotations: flexion-extension α_{18} , internal-external α_{19} and abduction-adduction α_{20} . Knee joint has only 1 DoF, flexion-extension α_{21} . Ankle joint has a complicated anatomy as introduced in the work of Lundberg et al. (1989), thus without impact tracking accuracy, it is simplified as 1 DoF flexion-extension α_{22} rotation. For the left leg, the assignment of rotation angles are from α_{23} to α_{27} .

In order to reduce the complexity when modeling, the body parts are simplified as rigid bodies. When analyzing each joint, different axes along adjacent segments are regarded as intersect at the joint center. To be more specific, for example, the forearm pronation-supination movements are considered around the same center of elbow flexion-extension movements, ignoring the physiological fact that these two axes have no intersection and are not orthogonal (Perez et al. (2010); Cutti et al. (2008)). This simplification inevitably brings some errors to IMU placement estimation. Fortunately in our well designed calibration procedure, random IMU placement would not affect tracking results so that the accuracy can be guaranteed.

2.2.2 Body Motion Reconstruction

The proposed body motion tracking system mounts wireless IMUs on the main body segments to capture their movements. The coordinates of IMUs on the human arm and leg (feet are excluded) are defined as shown in Figure 2.2. In the left figure, four IMUs are mounted on the arm to capture arm movements: one is attached to upper arm near the elbow, over the distal humerus to measure shoulder rotations; one is attached to scapular to measure position change of shoulder joint; one is positioned over the distal flat surface of radius and ulna, corresponding to elbow joint movements;

one is mounted on the dorsal hand surface to capture hand movements. In the right figure, two IMUs are attached on the leg to capture leg movements: one IMU is attached to lower front part of thigh, close to knee joint, to measure hip joint movements; the other IMU is placed on the outside of lower shank, above the ankle, corresponding to knee joint movements. For the torso, two IMUs are attached on the torso: one is on the chest, which is used to measure the lumbar rotation and torso orientation; the other is on the low back over the pelvis, which is used to estimate the movement of pelvis.

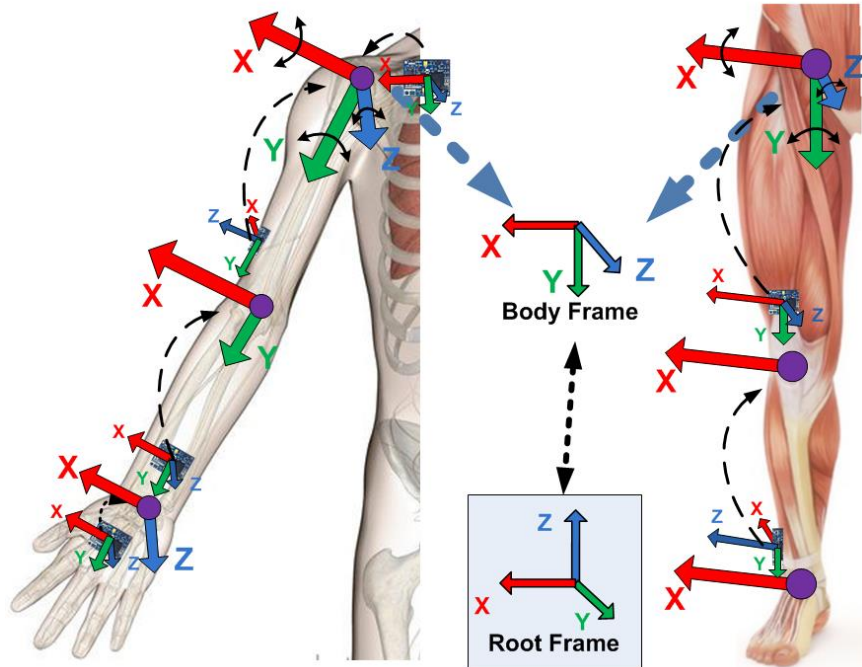


Figure 2.2: IMU position on arm and leg

Before linking IMUs to build a human kinematic model, a global frame \mathbb{R} (also called Root Frame in this dissertation) is defined. The Body Frame Σ_{body} (at

waist joint) shares the same coordinate with the global Root Frame, thus \mathbb{R} does not change with movements of human body. The end of four extremities (two shoulders and two hips) are connected to the torso, as shown in Figure 2.1a. All these four joints coordinates have direct relationship of translation and rotation to Σ_{body} , which means the 6-DoF transformation between their local coordinate and the Body Frame Σ_{body} is always considered as the transformation within \mathbb{R} . If transforming any extremity joint's coordinate to the global Root Frame, the procedure is achieved by first transforming joint frame to the local Body Frame Σ_{body} , then transforming from local Body Frame to the global Root Frame \mathbb{R} .

Here we take a human arm as an example to illustrate extremities' movements. After linking to the torso, rotations and translations of shoulder coordinate $\Sigma_{shoulder}$ are able to be captured within the Root Frame by direct " $\Sigma_{shoulder} \rightleftharpoons \Sigma_{body} \rightleftharpoons \mathbb{R}$ " transformation. As the adjacent joint of shoulder, elbow coordinate Σ_{elbow} only considers its rotation corresponding to $\Sigma_{shoulder}$ but not necessarily to Σ_{body} . With the known relationship, the spatial position of Σ_{elbow} within \mathbb{R} can be calculated. Wrist joint, similarly, only considers its rotation corresponding to Σ_{elbow} . In summary, except torso joint, all other joints consider their rotations with prior connected joint frame rather than with the Root Frame \mathbb{R} , so that each joint is correlated with prior joint and the inertial data from the IMU on each body segment represents the comprehensive movements from all previous joints.

Body parts are simplified as rigid bodies. IMUs cannot be placed at the joint center but attached to the surface of rigid bodies. Each IMU is placed on the far-end of the body segment, close to adjacent joint rather than its corresponding joint. Between the IMU and its corresponding joint, there keeps a distance. This arrangement is based on the consideration that keeping the measurement point away from the rotation center could represent rotations more clearly. No matter how a IMU is attached to the body, the rotations along each joint are reflected in the inertial input of the IMU. Motions are captured and then translated into more intuitive IMU output for our system: acceleration a , angular velocity ω and quaternion \mathbf{q} . After applying

proposed tracking technique, each joint is specified by its rotations and translations relative to others, and can be decomposed to rotation angles around each DoF. Joint movements are explained by combinations of quantified joint rotation angles, which would be significant for analysis.

An embedded quaternion-based orientation filter is utilized to pre-process and denoise raw IMU data and output filtered quaternion. In Figure 2.1b, the rotation angles of shoulder joint α_1, α_2 and α_3 , elbow joint α_4, α_5 and wrist joint α_6, α_7 are expressed by quaternion $s\hat{q}$ for shoulder frame, $E\hat{q}$ for elbow frame and $w\hat{q}$ for wrist frame, where “ $\hat{\cdot}$ ” denotes measurement value. Three quaternions integrate the movements of three arm joints instead of seven rotational matrixes $R(\alpha_1)…R(\alpha_7)$ for simplifying traditional expression. During movements, these three measurement values of quaternion compare with estimated quaternions $s\tilde{q}, E\tilde{q}, w\tilde{q}$ (for shoulder frame, elbow frame and wrist frame), and approach them after each time span t to minimize the difference $\delta = \|(s\hat{q}, E\hat{q}, w\hat{q}) - (s\tilde{q}, E\tilde{q}, w\tilde{q})\|_t$. Same idea is applied to other joints of the human body to update and keep joint motions being tracked.

After estimating rotation angles of each joint, we are aiming at estimating real-time update of joints’ position. As a principal part of this system, real-time position of IMUs within the Root Frame is calculated by proposed tracking technique first. Since the relative position between individual IMU and its corresponding joint is changeless with motions, then joints’ position in the Root Frame can be derived by applying translations from IMUs’ position.

2.2.3 System Calibration

In fact, mounting an IMU on human body is arbitrary. It is difficult to follow any strict regulations. Although IMUs can be preferred to place in certain position for optimizing the measuring, above restrain brings additional difficulties and inevitable errors to follow and for subjects it cannot be guaranteed to remember the same position for IMUs. Therefore, a convenient and reliable calibration procedure to

estimate the IMU placement is necessary, which includes the estimation of position and orientation.

The first step to estimate the position of an IMU is calculating the radius of rotation for each DoF. The gyroscope unit on the IMU is capable of capturing segment's circular motion around each axis, while other segments keep as still as possible. Circular motions around a joint axis generate angular velocity, and reminding the relationship between angular velocity and radius of rotation, a relative position of the IMU according to its rotating joint can be estimated when all axes of the joint are done. Besides the global position of IMU, the length of a human body segment between two joints is also requisite. The length works as an important parameter for configuring the human kinematic model and updating the joints position. Therefore, a method for estimating the length is developed. The method is to calculate a hypothenuse of one equilateral triangle based on two proportional triangles. The distance traveled by IMU when swing a human segment, *e.g.* arm or leg, acts as the base of a triangle and two neighboring IMUs give a proportional relation. Once the length is calculated, global position of both joint and IMU are estimated. In such ways, the initial position for each IMU and its corresponding joint are updated sequentially.

The calibration procedure is capable of estimating the IMU orientation, no matter how a subject mounts it to the body. IMU shares the same coordinate with \mathbb{R} , which is an essential prerequisite. Before mounting the IMU on the body, a human initial posture is required for both mounting IMUs and coupling local joint frames to the Root Frame. When an IMU is mounted, its orientation with respect to (*w.r.t.*) \mathbb{R} is calculated from its inertial output. Compared with corresponding joint frame, a rotational transformation is generated and represented by ${}^Y_X q$, which denotes the quaternion representation for rotational relationship from X frame to Y frame. During tracking body motions, quaternion of each joint is updated by the combination of corresponding IMU quaternion and their relationship quaternion. Therefore, proposed calibration approach estimates the position and orientation of

IMUs in a way that simple to be executed, before each time a subject uses the system, so that subsequent tracking procedures could be processed based on an accurate initialization prerequisite.

2.3 Motion Tracking with Twists and Exponential Maps

In this section, body tracking system with twists and exponential maps techniques is introduced. Due to the superiority of quaternion based rotation representation over Euler angle and rotation matrix, filtered unit quaternions from embedded IMU orientation filter are used as system input for calculating twist motions. Exponential maps for twists simplify the representation of rotation by reducing the computing complexity to one matrix per joint, compared with one rotation matrix per DoF in the traditional method. In order to track motions of a body with multiple joints and connected segments, a product of exponential maps, which borrows the idea from the *forward kinematics* technique, is employed to express the kinematic chain. The motion reconstruction will be accomplished based on human kinematic chains and rotation angles of each joint. Finally, a human model is reconstructed by describing the global position of each joint and articulating neighbor joints.

2.3.1 Quaternion-based Orientation Filter

In our previous work by Tian et al. (2012); Tian and Tan (2012), an adaptive-gain complementary filter was developed and combined with Gauss-Newton optimization algorithm to determine the orientation of the gyroscope measurement error. The framework of the filter is shown in Figure 2.3. A magnetic field selection scheme with adaptive measurement vectors and reference vector, which could significantly lessen the effect of severe magnetic distortion and highly dynamic movements, is applied to improve the performance of the filter. An accurate estimation of gyroscope bias then

compensates instantaneous gyroscope measurements, regardless of fast movement or magnetic distortion. The filter consumes short computing time, which satisfies the needs for real-time orientation measurement and filtered quaternion ${}_R\mathbf{q}$ denotes the IMU output within \mathbb{R} .

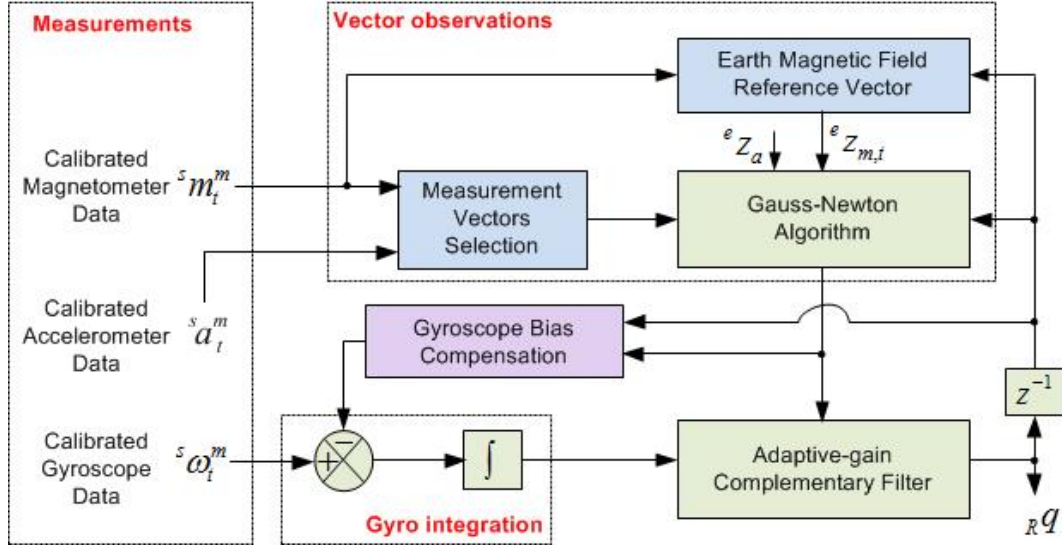


Figure 2.3: The design of quaternion-based orientation filter

Unit quaternion provides a convenient mathematical notation for representing orientations and rotations of objects in three dimensions (3D). Quaternion based rotation representation is adopted in view of its superiority: compared to Euler angle it is simpler to compose and avoid the problem of singularities (gimbal lock); compared to rotation matrix it is more numerically stable and more efficient. Any rotation in 3D can be represented as a combination of an axis vector and a rotation angle, as Figure 2.4 shows. Quaternion gives a simple way to encode this axis-angle representation in four numbers and apply the corresponding rotation to a position vector representing a point relative to the origin in \mathbb{R}^3 .

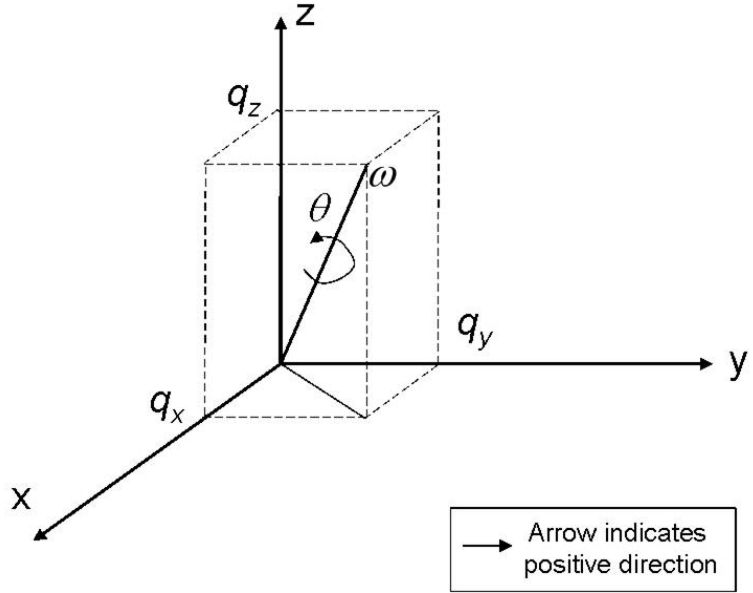


Figure 2.4: Quaternion rotations representation

Quaternion ${}_R\mathbf{q}$ is a vector quantity of the form

$${}_R\mathbf{q} = q_0 + q_1\mathbf{i} + q_2\mathbf{j} + q_3\mathbf{k} = (q_0, \vec{\mathbf{q}}) \quad (2.1)$$

where i, j and k are basis elements of a quaternion, q_0 is the scalar component of ${}_R\mathbf{q}$ and $\vec{\mathbf{q}} = [q_1, q_2, q_3]^T$ is the vector component. Given $\omega = [\omega_1, \omega_2, \omega_3]^T$, unit quaternion ($\|\omega\| = 1$) can be denoted by the form as

$${}_R\mathbf{q} = (\cos(\theta/2), \omega \sin(\theta/2)) \quad (2.2)$$

and given Equation (2.1), the corresponding rotation is extracted by setting

$$\theta = 2 \cos^{-1} q_0 , \quad \omega = \begin{cases} \frac{\vec{q}}{\sin(\theta/2)} & \text{if } \theta \neq 0, \\ \mathbf{0} & \text{otherwise,} \end{cases} \quad (2.3)$$

where, $\omega \in \mathbb{R}^3$ represents the unit axis of a rotation and $\theta \in \mathbb{R}$ is the angle of rotation about ω . In the example of shoulder joint, quaternion measurement ${}_S\hat{q}$ is represented by corresponding rotations of unit axes ω_S and angles about it θ_S .

2.3.2 Twists and Exponential Maps

The representation of general body motions includes both rotations and translations. Here we describe the position and orientation of a coordinate frame B relative to a coordinate frame A : let $p_{AB} \in \mathbb{R}^3$ be the position vector from the origin of frame A to the origin of frame B , and $R_{AB} \in SO(3)$ (special Orthogonal group) be the orientation of frame B relative to frame A . A configuration of the system consists of the pair (p_{AB}, R_{AB}) , and the configuration space of the system is the product space of \mathbb{R}^3 with $SO(3)$, which is denoted as $SE(3)$ (special Euclidean group)

$$\begin{aligned} SE(3) &= \{(p_{AB}, R_{AB}) : p_{AB} \in \mathbb{R}^3, R_{AB} \in SO(3)\} \\ &= \mathbb{R}^3 \times SO(3) \\ SO(3) &= \{R_{AB} \in \mathbb{R}^{3 \times 3} : R_{AB}R_{AB}^T = I, \det R_{AB} = +1\} \end{aligned}$$

More concretely, let $q_{\$}, q_{\mathbb{E}} \in \mathbb{R}^3$ be the coordinates of a point q relative to local Shoulder Frame $\$$ and local Elbow Frame \mathbb{E} respectively. Let $R_{\$E} = f(\alpha_1, \alpha_2, \alpha_3)$ indicates 3 DoF rotations of point q needed from $\$$ to \mathbb{E} . Given $q_{\$}$, we can calculate $q_{\mathbb{E}}$ from the transformation of the coordinate

$$q_{\mathbb{E}} = p_{\$E} + R_{\$E} \cdot q_{\$} \quad (2.4)$$

Let $g_{\$E} = (p_{\$E}, R_{\$E}) \in SE(3)$ be the specification of the configuration of the frame E relative to the frame $\$$. Using *homogeneous representation*, the linear form transformation is represented as

$$\bar{q}_E = \begin{bmatrix} q_E \\ 1 \end{bmatrix} = \begin{bmatrix} R_{\$E} & p_{\$E} \\ \mathbf{0} & 1 \end{bmatrix} \begin{bmatrix} q\$ \\ 1 \end{bmatrix} = \bar{g}_{\$E} \bar{q}\$ \quad (2.5)$$

Euler angles are commonly used to constrain a rotation matrix R to $SO(3)$, but they suffer from singularities and don't lead to a simple formulation. In contrast, the twist representation provides a more elegant solution and leads to a very simple linear representation of the motion model. For each homogeneous matrix $\bar{g} \in SE(3)$, there is a corresponding twist in the tangent space $se(3)$, we define

$$\begin{aligned} se(3) &= \{(v, \hat{\omega}) : v \in \mathbb{R}^3, \hat{\omega} \in so(3)\} \\ so(3) &= \{S \in \mathbb{R}^{n \times n} : S^T = -S\} \end{aligned}$$

where the inverse operator \wedge (wedge) is applied to ω and $\hat{\omega} \in so(3)$ here is the skew-symmetric matrix, defined as

$$\hat{\omega} = \begin{bmatrix} 0 & -\omega_3 & \omega_2 \\ \omega_3 & 0 & -\omega_1 \\ -\omega_2 & \omega_1 & 0 \end{bmatrix} \quad (2.6)$$

and v is the velocity of a point attached to the joint.

In homogeneous coordinates, we define $\xi \in \mathbb{R}^6$ to represent the twist coordinates and a twist $\hat{\xi} \in se(3)$ as

$$\hat{\xi} = \begin{bmatrix} v \\ \omega \end{bmatrix}^\wedge = \begin{bmatrix} \hat{\omega} & v \\ \mathbf{0} & 0 \end{bmatrix} \in \mathbb{R}^{4 \times 4} \quad (2.7)$$

where $v = -\omega \times r$ and r denotes the origin of rotation axis in the twist $\hat{\xi} \in se(3)$.

The exponential of $\theta\hat{\omega}$, $e^{\theta\hat{\omega}}$, is an element of $SE(3)$ and it indicates rotations during the movements and it can be calculated by the *Rodrigues' formula*

$$e^{\theta\hat{\omega}} = I + \hat{\omega}\sin\theta + \hat{\omega}^2(1 - \cos\theta) \quad (2.8)$$

Elements from $se(3)$ are mapped to $SE(3)$ using a exponential map for twists as shown in the following equation

$$\begin{aligned} e^{\theta\hat{\xi}} &= \begin{bmatrix} e^{\theta\hat{\omega}} & (I - e^{\theta\hat{\omega}})(\hat{\omega}v + \omega\omega^T v\theta) \\ \mathbf{0} & 1 \end{bmatrix} & \omega \neq \mathbf{0} \\ e^{\theta\hat{\xi}} &= \begin{bmatrix} I & v\theta \\ \mathbf{0} & 1 \end{bmatrix} & \omega = \mathbf{0} \end{aligned} \quad (2.9)$$

The 3-DoF rotation of shoulder relative to the Elbow Frame can be represented by $(e^{\theta\hat{\omega}})_{\mathbb{S}\mathbb{E}}$ and the transformation from \mathbb{S} to \mathbb{E} , which includes rotations and translations, is shown by a 4×4 matrix $(e^{\theta\hat{\xi}})_{\mathbb{S}\mathbb{E}}$, instead of the multiplication of three 3×3 rotational matrixes $R(\alpha_1) \cdot R(\alpha_2) \cdot R(\alpha_3)$. One body link transformation relationship is introduced above and the example of a connection of upper body links will be discussed next.

Firstly, IMUs are calibrated in \mathbb{R} , and their initial orientation ${}_{\mathbb{R}}q_0$ can translate to θ_0 for later use. After attaching IMUs to the human body, their orientation measurements on the body are rotated from initial ${}_{\mathbb{R}}q_0$ to ${}_{IB}\hat{q}$ for the IMU corresponding to waist in Σ_{body} , ${}_{IS}\hat{q}$ for the IMU corresponding to shoulder, ${}_{IE}\hat{q}$ for the IMU corresponding to elbow and ${}_{IW}\hat{q}$ for the IMU corresponding to wrist. In this procedure, the subject is asked to stand in order to mount the IMUs. The local coordinate of waist, shoulder, elbow and wrist refer to \mathbb{R} are initially defined as ${}_{B}q_{initial}(= \mathbb{R})$, ${}_{S}q_{initial}$, ${}_{E}q_{initial}$ and ${}_{W}q_{initial}$. The relationship between local joints'

coordinates and their corresponding IMUs are shown as

$$\begin{aligned}
{}^{\mathbb{R}}_B q_{initial} &= {}^S_{IB} q \otimes {}_{IB} \hat{q} \\
{}^{\mathbb{R}}_S q_{initial} &= {}^S_{IS} q \otimes {}_{IS} \hat{q} \\
{}^{\mathbb{R}}_E q_{initial} &= {}^E_{IE} q \otimes {}_{IE} \hat{q} \\
{}^{\mathbb{R}}_W q_{initial} &= {}^W_{IW} q \otimes {}_{IW} \hat{q}
\end{aligned} \tag{2.10}$$

where the relationship quaternion ${}^S_{IB} q$, ${}^S_{IS} q$, ${}^S_{IE} q$ and ${}^S_{IW} q$ will be used for updating real-time rotation measurements of joint quaternions. The conjugate of quaternion can be used to represent an orientation by swapping the relative frame and the sign * denotes the conjugate. For example, ${}^b_a q^* = {}^a_b q$ is the conjugate of ${}^b_a q$ and it denotes the orientation of the frame a *w.r.t.* the frame b , which can be denoted as

$${}^b_a q^* = {}^a_b q = [q_0, -q_1, -q_2, -q_3] \tag{2.11}$$

The quaternion product \otimes can be used to describe compounded orientations and the definition is based on the Hamilton rule ([Horn et al. \(1988\)](#)). For example, the compounded orientation ${}^c_a q$ can be defined by

$${}^c_a q = {}^c_b q \otimes {}^b_a q \tag{2.12}$$

and a quaternion product of two quaternion q and p is defined as

$$\begin{aligned}
q \otimes p &= [q_0, q_1, q_2, q_3] \otimes [p_0, p_1, p_2, p_3] \\
&= \begin{bmatrix} q_0 - q_1 - q_2 - q_3 \\ q_0 q_1 q_2 - q_3 \\ q_0 - q_1 q_2 q_3 \\ q_0 q_1 - q_2 q_3 \end{bmatrix} \begin{bmatrix} p_0 \\ p_1 \\ p_2 \\ p_3 \end{bmatrix}
\end{aligned} \tag{2.13}$$

Thus, the relationship quaternion ${}^S_{IB}q$, ${}^S_{IS}q$, ${}^S_{IE}q$ and ${}^S_{IW}q$ can be calculated from the transformation of Equation (2.10) as

$$\begin{aligned} {}^S_{IB}q &= {}^R_B q_{initial} \otimes {}_{IB}\hat{q}^* \\ {}^S_{IS}q &= {}^R_S q_{initial} \otimes {}_{IS}\hat{q}^* \\ {}^S_{IE}q &= {}^R_E q_{initial} \otimes {}_{IE}\hat{q}^* \\ {}^S_{IW}q &= {}^R_W q_{initial} \otimes {}_{IW}\hat{q}^* \end{aligned} \quad (2.14)$$

The Body Frame Σ_{body} shares the same coordinate with R . We assume the starting position of its initial configuration is known as ${}^R P_B$. An IMU mounted on the chest (upper body and denoted by b-IMU) is used to estimate the orientation of upper trunk and two IMUs mounted on each scapula (sc-IMU) are measuring the linear acceleration of shoulder movements. The translational calculation from body to shoulder p_{BS} in the homogeneous matrix $g_{BS}(0)$ includes ${}^R P_B$, initial spacial relationship of shoulder relative to waist ${}_0 p_{BS}$ and the real-time update of the shoulder position from sc-IMU inertial measurements \hat{p}_{sc-IMU} within Σ_{body}

$$p_{BS} = {}^R P_B + {}_0 p_{BS} + \hat{p}_{sc-IMU} \quad (2.15)$$

Following the forward kinematics idea, the aim here is to estimate updated shoulder position within R . As the subject moves, the quaternion of b-IMU continuously updates waist joint quaternion measurement ${}^R_B \hat{q}$ by

$${}^R_B \hat{q} = {}^S_{IB}q \otimes {}_{IB}\hat{q} \quad (2.16)$$

With the waist quaternion measurements are calculated, the position of shoulder joint can be updated by

$$\begin{aligned} {}^B\hat{q} &\rightarrow \theta_B, \omega_B \\ \{\theta_B, \omega_B, p_{BS}\} &\xrightarrow{\text{exp map}} {}^R\hat{P}_S \end{aligned} \quad (2.17)$$

where ${}^R\hat{P}_S$ denotes updated shoulder position within \mathbb{R} .

Updated position of shoulder joint is ${}^R\hat{P}_S$ and the translational calculation from shoulder to elbow p_{SE} is achieved by combining ${}^R\hat{P}_S$ and initial spacial relationship of elbow relative to shoulder ${}_0p_{SE}$ within $\Sigma_{shoulder}$

$$p_{SE} = {}^R\hat{P}_S + {}_0p_{SE} \quad (2.18)$$

As the subject moves, the quaternion of s-IMU (short for the IMU attached to the upper arm, corresponding to shoulder) continuously updates shoulder joint's quaternion measurement ${}^S\hat{q}$ as

$${}^S\hat{q} = {}_{IS}^S q \otimes {}_{IS}\hat{q} \quad (2.19)$$

With shoulder measurements are calculated, the elbow joint position can be updated by

$$\begin{aligned} {}^S\hat{q} &\rightarrow \theta_S, \omega_S \\ \{\theta_S, \omega_S, p_{SE}\} &\xrightarrow{\text{exp map}} {}^R\hat{P}_E \end{aligned} \quad (2.20)$$

where ${}^R\hat{P}_E$ denotes updated elbow position within \mathbb{R} .

For adjacent lower arm link, updated position of elbow joint is ${}^R\hat{P}_E$ and the translational calculation from elbow to wrist p_{EW} is achieved by combining ${}^R\hat{P}_E$ and

initial spacial relationship of wrist relative to elbow ${}_0p_{EW}$ within Σ_{elbow}

$$p_{EW} = {}^R\hat{P}_E + {}_0p_{EW} \quad (2.21)$$

Then, the elbow quaternion measurement by e-IMU (short for the IMU corresponding to elbow) is similarly updated as

$${}^R_E\hat{q} = {}^E_{IE}q \otimes {}_{IE}\hat{q} \quad (2.22)$$

The wrist joint position can be updated by

$$\begin{aligned} {}^R_E\hat{q} &\rightarrow \theta_E, \omega_E \\ \{\theta_E, \omega_E, p_{EW}\} &\xrightarrow{\text{exp map}} {}^R\hat{P}_W \end{aligned} \quad (2.23)$$

Therefore, the procedure of updating wrist quaternion ${}^R_W\hat{q}$ and estimating hand position ${}^R\hat{P}_{hand}$ in \mathbb{R} are easy to get by first calculating the translation from wrist to hand p_{Wh} within Σ_{wrist}

$$p_{Wh} = {}^R\hat{P}_W + {}_0p_{Wh} \quad (2.24)$$

then updating the hand position by

$$\begin{aligned} {}^R_W\hat{q} &= {}^W_{IW}q \otimes {}_{IW}\hat{q} \\ {}^R_W\hat{q} &\rightarrow \theta_W, \omega_W \\ \{\theta_W, \omega_W, p_{Wh}\} &\xrightarrow{\text{exp map}} {}^R\hat{P}_{hand} \end{aligned} \quad (2.25)$$

The rotations of each joint in above example are represented by $\{\theta_B, \theta_S, \theta_E, \theta_W\}$. Their corresponding twists are shown as $\{\hat{\xi}_B, \hat{\xi}_S, \hat{\xi}_E, \hat{\xi}_W\}$. The exponential map for twists of each joint is in the form of $e^{\theta\hat{\xi}}$, as Equation (2.9) shows.

If the initial configuration of an IMU corresponding to \mathbb{R} is $g(0)$, the final configuration of the IMU corresponding to \mathbb{R} with rotation angle θ is given by

$$g(\theta) = e^{\theta \hat{\xi}} g(0) \quad (2.26)$$

For the right arm discussed above, the connection is demonstrated by the product of all joints' exponential maps

$$\prod_{i=B}^W e^{\theta_i \hat{\xi}_i} = e^{\theta_B \hat{\xi}_B} \cdot e^{\theta_S \hat{\xi}_S} \cdot e^{\theta_E \hat{\xi}_E} \cdot e^{\theta_W \hat{\xi}_W} \quad (2.27)$$

If we let $g_{wrist,hand}(0)$ represent the initial configuration of hand *w.r.t.* wrist, then the final configuration of hand *w.r.t.* the Body Frame $g_{body,hand}$, which are connected by rotation angles $\Theta = (\theta_B, \theta_S, \theta_E, \theta_W)$, is given by

$$\begin{aligned} g_{body,hand}(\Theta) &= \prod_{i=B}^W e^{\theta_i \hat{\xi}_i} \cdot g_{wrist,hand}(0) \\ &= \exp\left(\sum_{i=B}^W \theta_i \hat{\xi}_i\right) \cdot g_{wrist,hand}(0) \end{aligned} \quad (2.28)$$

This final configuration contains the position of hand within \mathbb{R} , which achieves our aforementioned aim. Meanwhile, the advantage of twists and exponential maps techniques are revealed by transforming the multiplication of exponentials to summations, which substantially reduces the complexity of motion estimation of multiple body links, compared with rotation matrix representations.

2.3.3 Kinematic Chains and Full Body Motion

A human body model consists of a set of body segments connected by joints. For upper limbs and lower limbs, four kinematic chains are modeled and they branch out around the torso. The kinematic chain describes the relationship between rigid body movements and motions of joints. A *forward kinematics* technique, which is

introduced in robotic control, is utilized to determine the configurations of each pair of adjacent segments. The product of exponential maps gives an expression of the kinematics of each joint, which is generated by twists associated with the joint axis.

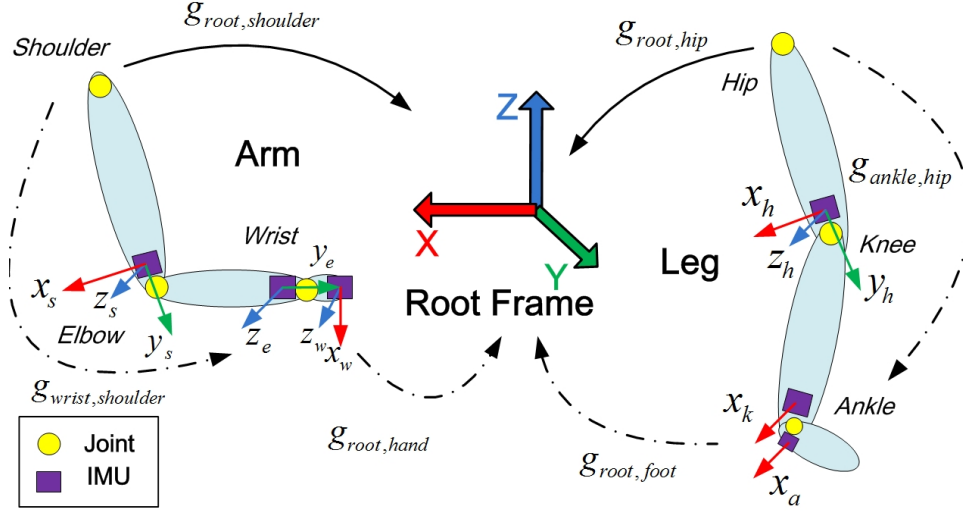


Figure 2.5: Kinematic chains of upper and lower extremities

In this system, the goal of building a human kinematic chain is to find the independent configuration for each joint and the relationship with the Root Frame, such as shown in Figure 2.5. Four kinematic chains of upper and lower limbs are built, which describe 10-DoF arm movement and 5-DoF leg movement. Each joint is able to transform from local coordinate to \mathbb{R} by twist representation.

For the upper limb, a kinematic chain that representing the wrist frame relative to the body frame is modeled as

$$g_{body,hand}(\Theta) = \exp(\theta_{body}\hat{\xi}_{body} + \theta_{shoulder}\hat{\xi}_{shoulder} + \theta_{elbow}\hat{\xi}_{elbow} + \theta_{wrist}\hat{\xi}_{wrist}) \cdot g_{wrist,hand}(0) \quad (2.29)$$

and for the lower limb, the ankle frame relative to the body frame is modeled as

$$g_{body,foot}(\Theta) = \exp(\theta_{body}\hat{\xi}_{body} + \theta_{hip}\hat{\xi}_{hip} + \theta_{knee}\hat{\xi}_{knee} + \theta_{ankle}\hat{\xi}_{ankle}) \cdot g_{ankle,foot}(0) \quad (2.30)$$

where Θ represents the set of rotation angles of joints involved in the final configuration.

A full body model is reconstructed by linking all the limb kinematic chains to the torso and mapping individual sensor frames into unified \mathbb{R} . Figure 2.6 shows a example of human forearm movements, from $t = t'$ to $t = t' + \Delta t$, with only elbow rotation occurs. Here we use ξ_m to represent the m^{th} joint among total n joints with the rotation angle $\theta_{m,\Delta t}$.

Full body motion estimation considers twists of all body segments within the Root Frame, so that motions of segments can be displayed as a coherent reconstruction. The Body Frame of a human model is defined as the root that connecting all four limb chains, so that it can better demonstrate the human motions. The IMU on the chest is used to capture the motion of waist joint and represent torso direction. Based on the fact that all the limb chains are connected to torso, \mathbb{R} is placed at human waist. By linking all the limb kinematic chains to torso, full body pose can be estimated. For example, the motion of a lower arm (corresponding to the elbow joint) relative to human foot (corresponding to the ankle joint) is shown by

$$g_{ankle,elbow}(\Theta) = \exp\left(\sum_{ankle}^{hip} \theta_i \hat{\xi}_i + \sum_{hip}^{body} \theta_i \hat{\xi}_i + \sum_{body}^{shoulder} \theta_i \hat{\xi}_i + \sum_{shoulder}^{elbow} \theta_i \hat{\xi}_i\right) \cdot g_{shoulder,elbow}(0) \quad (2.31)$$

As an extension, some kinematic characteristics of human skeleton can be referred as parameters to optimize tracking results, such as elbow has no abduction/adduction movement, elbow carrying angle is 5 to 15 degrees for healthy people and etc. Those

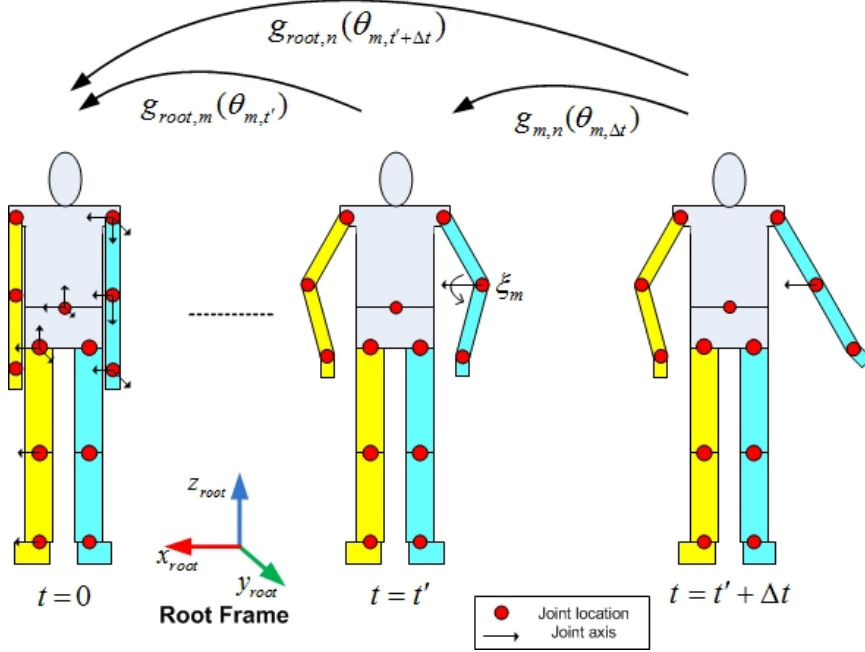


Figure 2.6: A kinematic chain of human model with forearm motion relative to the global frame at $t = t' + \Delta t$

limitations can be assigned as a threshold to the updated value of joint angles and to reduce errors when tracking human motions in specific circumstance. For the requirements of different applications, the tracking system sometimes will not set those boundaries when reconstructing human motions. Optimized joint angles quantify motion tracking, so that the joint angle based information could greatly help researchers analyze and diagnose the status of subjects.

2.4 Estimation of Parameters

In order to cooperate inertial measurements from IMU with a human kinematic model, some parameters are estimated, which include the IMU orientation, IMU position relative to corresponding joint and human limb length.

2.4.1 Estimation of Arbitrary IMU Placement

Mounting an IMU on the human body is recurrent and an accurate position of IMU is highly demanded to be guaranteed. Since it is not expected that the subjects could place the IMU on the same position every time, a calibration procedure for estimating the position when it is randomly positioned can be considerable helpful for tracking. A more reasonable way to estimate the position of IMU is introduced in this section, compared with measuring the distance by measuring instruments. According to the fact that the rotation of human limb is a synthetic action of more than one bone, therefore, human limb movement is considered as a cylinder rotating around various axes. Although the simplification would not remove the errors caused by human muscle sliding and soft tissue artifact, the accuracy is acceptable for tracking human body motion. By repeating human limb rotations around each axis, stable sampling from inertial measurements averages the distance between joint center and IMU, and further, estimates spatial position of the IMU. The random position estimation is designed for initializing the motion tracking, thus, the tradeoff between adding complexities to calibration procedure and improving the accuracy of body tracking system is worthwhile.

When an IMU is mounted on the body and ready to initialize the system, adjacent limbs are required to hold still and the target limb rotates repeatedly around corresponding joint solely. For example as Figure 2.7 shows, we want to estimate the position of the IMU mounted on the lower arm. The upper arm is held still while rotating the lower arm around X axis (flexion/extension) and Y axis (pronation/supination). In order to obtain better estimation results, it is highly

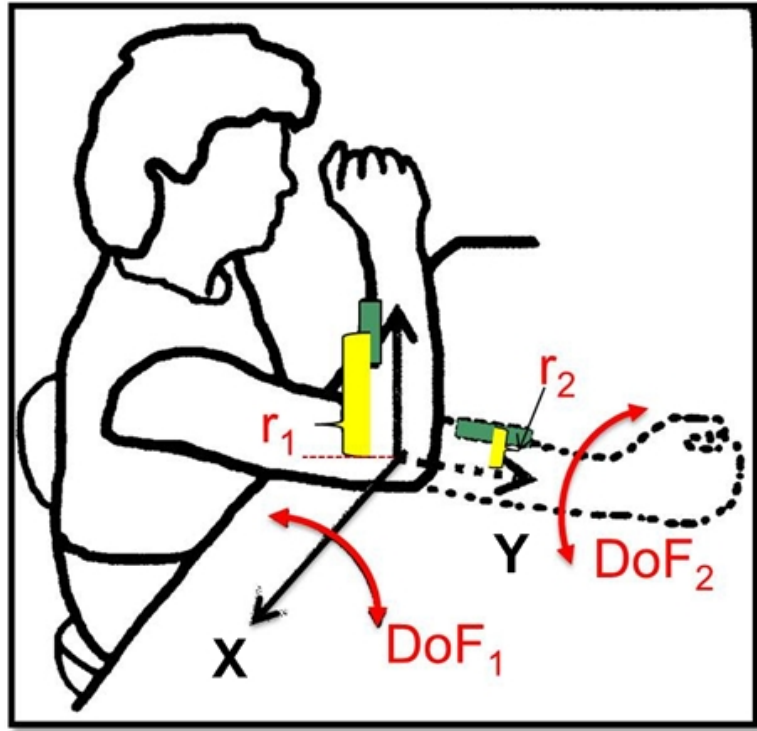


Figure 2.7: Demonstration of IMU position estimation

suggested that the IMU is mounted on the far end of lower arm, which is close to the wrist joint. When rotating the lower arm, a longer distance between elbow joint center and IMU provides a larger swing range and as a result, achieves clearer inertial measurements for position estimation.

Inertial measurements from an IMU include angular velocity ω and acceleration a , which are applied for estimating the IMU position relative to the joint center. The calculation of the distance inbetween is given by

$$r_{DoF} = \frac{a_{centripetal}}{\omega_{DOF}^2} \quad (2.32)$$

where DoF indicates the rotation axis. $a_{centripetal}$ is the acceleration pointing to the joint center and ω is the angular velocity generated by rotations. Each rotation around certain axis is repeated for several times, in case that averaged rotation radius r_{DoF} is more convincing and accurate.

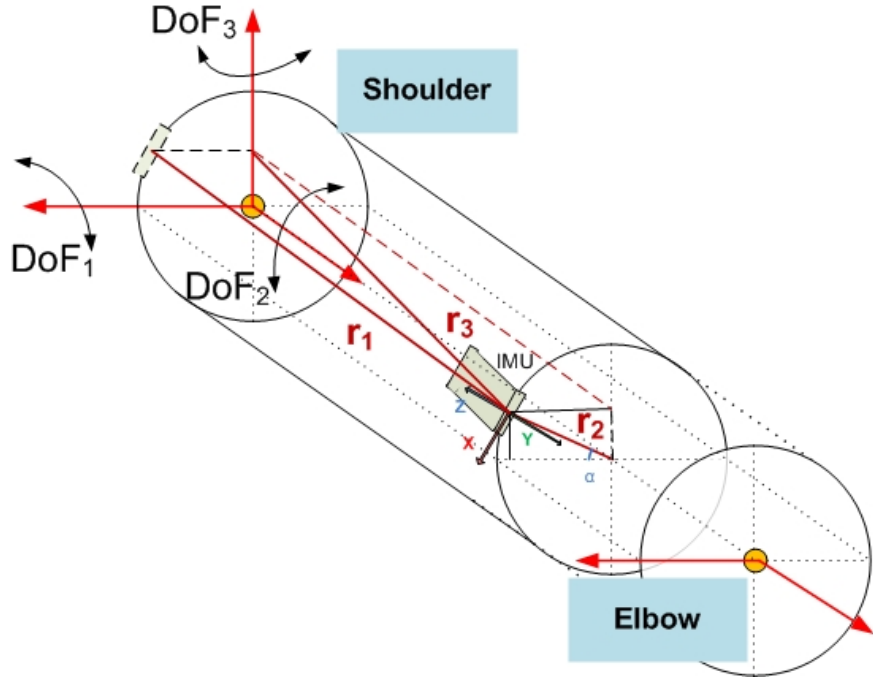


Figure 2.8: Cylinder look of human limb

For the upper arm example in Figure 2.8, an IMU is mounted close to elbow joint to measure the shoulder movement. For all three rotation axes, DoF_1 , DoF_2 and DoF_3 , the calculation of the radii about each axis are r_1 , r_2 and r_3 in the figure. These distances compose the position vector introduced in Section 2.3.2. In this example, assuming the altitude angle is α , the origin of the shoulder joint is $[X_S, Y_S, Z_S]$ and the axes corresponding to DoF_1 , DoF_2 and DoF_3 are X , Y and Z . From the origin of the Shoulder Frame S to the IMU Frame I , the position of IMU

is estimated by position vector $p_{\$I}$, as

$$p_{\$I} = \begin{bmatrix} X_S + r_2 \cos(\alpha) \\ Y_S + r_1 \\ Z_S + \sqrt{r_3^2 - r_1^2} \end{bmatrix} \quad (2.33)$$

For the joint with two DoFs, *e.g.* elbow joint, the length of r in the “missing” axis is still able to be calculated by using r_1, r_2 and the altitude angle α ; for the joint with only one DoF, *e.g.* knee joint and ankle joint, the distance parameters in the two “missing” axes are need to be estimated manually. Besides the IMU position relative to its corresponding joint, the position of adjacent joint is also important. In the above example, if the distance between the shoulder and elbow (length of upper arm) is $d_{\$E}$, the position vector from $\$$ to E within $\$$ will be $p_{\$E} = [X_S, Y_S + d_{\$E}, Z_S]$. So, in the following part, the estimation of the length of human segment is introduced.

2.4.2 Estimation of Body Limb Length

Another critical part of the calibration procedure is to estimate the length of human limbs. Since the twists and exponential maps presented above need the position of adjacent joint to maintain the integrity of human limb and connectivity of limbs, an accurate estimation of human limb length will guarantee excellent results of human motion tracking. Although human body limbs are simplified as rigid bodies, measuring the length manually causes more errors than applying inertial estimations which achieve high precision from IMU measurements. Therefore, an IMU based method for estimating the body limb length is developed by employing the twist representation. Inertial measurements provide changes in spatial position and attitude, and with estimated IMU position, body limb length is calculated by solving the spatial relation of two connected body limbs.

In order to assure the stability of estimation results, subjects are required to extend their limbs and swing gently around certain joint. For the example in Figure

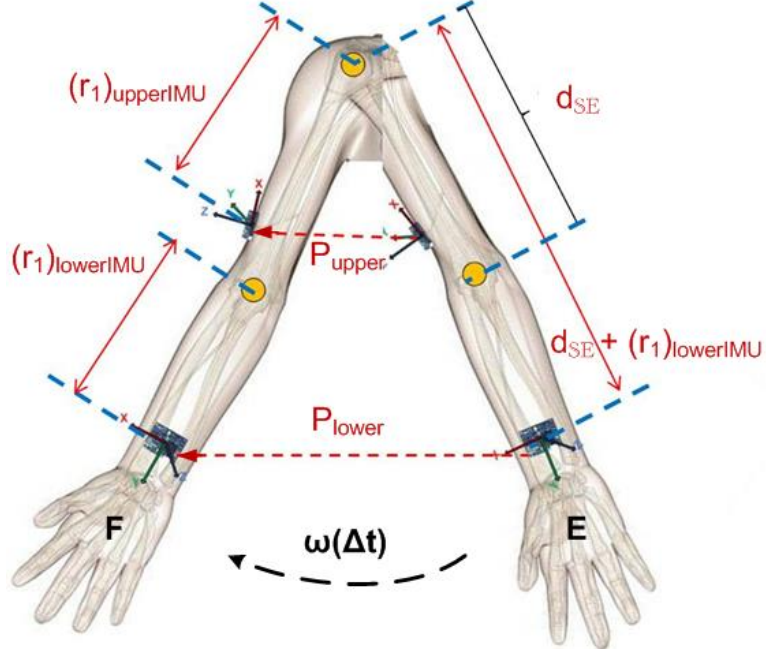


Figure 2.9: Limb length estimation by swinging around shoulder joint

2.9, the process is estimating the length of upper arm. A subject is required to extend the arm and swing gently around shoulder joint. Assuming during δt , the arm rotates from position E to F with the angular velocity of ω . The spatial changes of the IMU on the upper arm $(P_{E \rightarrow F})_{upperIMU}$ and lower arm $(P_{E \rightarrow F})_{lowerIMU}$ (denoted by P_{upper} and P_{lower} in Figure 2.9) can be derived from the twist representation ξ

$$(P_{E \rightarrow F})_{upperIMU} : \xi_{upper}(E, t) \rightarrow \xi_{upper}(F, t + \Delta t) \quad (2.34)$$

$$(P_{E \rightarrow F})_{lowerIMU} : \xi_{lower}(E, t) \rightarrow \xi_{lower}(F, t + \Delta t) \quad (2.35)$$

Positions of IMUs relative to corresponding joints can be estimated from previous Section 2.4.1. As is shown in Figure 2.9, here uses $(r_1)_{upperIMU}$ and $(r_1)_{lowerIMU}$ to

represent the distance of r_1 in Figure 2.8 for upper arm and lower arm respectively. The length of upper arm d_{SE} is calculated from the proportional relationship

$$\frac{P_{upper}}{P_{lower}} = \frac{(r_1)_{upperIMU}}{d_{SE} + (r_1)_{lowerIMU}} \quad (2.36)$$

Similarly, the length of lower arm can be calculated when extend lower arm and hand, swinging around elbow joint. For any human body limb, it is able to be estimated by extending and swinging around its joint. When the length of body limbs and position of IMUs are estimated, following motion tracking technique will apply those estimates to reconstruct.

2.5 Experiments

2.5.1 Experimental Setup

The IMU was developed in our lab and the detail was introduced in the work of [Chen et al. \(2011\)](#). The commercialized *Vicon* and *OptiTrack* motion capture systems are separately utilized as the benchmark. Six cameras are set up at the frequency of $100Hz$, while IMUs are working at $40Hz$. A series of upper limb and full body motions are designed to validate our tracking system. For the upper limb tracking, three ranges of movements are executed, including arm lifting up-down, arm swinging left-right and lower arm flexion-extension. A commercialized product *Vicon* is used as the benchmark. For the full body tracking, three ranges of movements commonly performed in medical rehabilitation process are tested and *OptiTrack* is used as the benchmark. Each range is repeated twice to clearly demonstrate the motion and apart from other ranges. Two participants are asked to test developed system by using these motions. Before the tests, the participants are required to stand upright in T-pose to attach IMUs on the body. During the tests, motion capture system and our tracking system are manually started to capture the motions simultaneously. The

inertial measurements from IMUs are analyzed and joint positions captured by *Vicon* and *OptiTrack* are recorded for later calculations and comparisons.

2.5.2 Upper Limb Motion Tracking

To ensure the accuracy of proposed tracking system, two sets of parameters are estimated: the placement of IMUs and the length body limbs, from the calibration procedure. These parameters are also validated by *Vicon* system so that to make sure those estimated parameters for proposed algorithm are satisfactory as expected. A reliable and convenient method for estimating these parameters avoids the reliance on *Vicon* when calibrating proposed system.

Figure 2.10 shows a screenshot of the motion tracking test. The participant with reflective markers affixed on the arm is asked to move gently as designed motions and *Vicon* system captured his motion simultaneously and animated. Inertial measurements are transmitted wirelessly to the computer via Bluetooth and tracked motions are reconstructed by deploying twists and exponential maps techniques, as shown in the bottom right of Figure 2.10. *Vicon* system instantly captures arm movements as shown in the top right of the figure.

Each test is analyzed graphically as curves of angle against frame. After the motion data are transmitted to the computer, two different kinds of angles are calculated: rotational angles of a joint center and angles between two adjacent body segments. By comparing calculated angles with the benchmark results calculated by *Vicon* system, the accuracy of developed motion tracking system can be evaluated.

In the tests, shoulder angles (between trunk and upper arm) and elbow angles (between upper and lower arm) are calculated from IMU data and compared with *Vicon* truth. In the comparison figures, the red curve represents angles calculated based on captured markers' position from *Vicon* system and the blue curve shows the angles estimated by proposed tracking system based on IMU measurements.

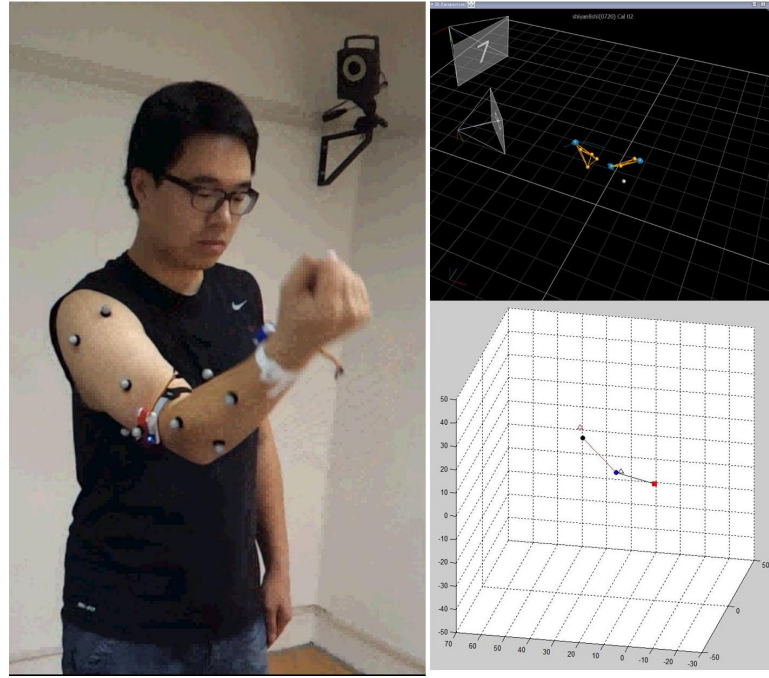


Figure 2.10: A screenshot of the motion tracking procedure. Left figure shows the placement of markers and IMUs; Up-right figure shows real-time optical motion tracking result; Bottom-right figure shows real-time reconstructed arm motion in *MATLAB*

Test 1

Figure 2.11a shows the angle between body trunk and upper arm. The 1st range movement, arm lifting up-falling back, is shown by the first two wave peaks and troughs. The 2nd range movement, arm swinging to left-right, is represented by the following flat curve. For these two ranges, the IMU tracking performs well in matching the *Vicon* truth. However for the 3rd range, lower arm flexion-extension, IMU tracking does not match *Vicon* data very well. The reason of this unmatch is from additional vibration of the soft tissue artifact, due to contractions of biceps

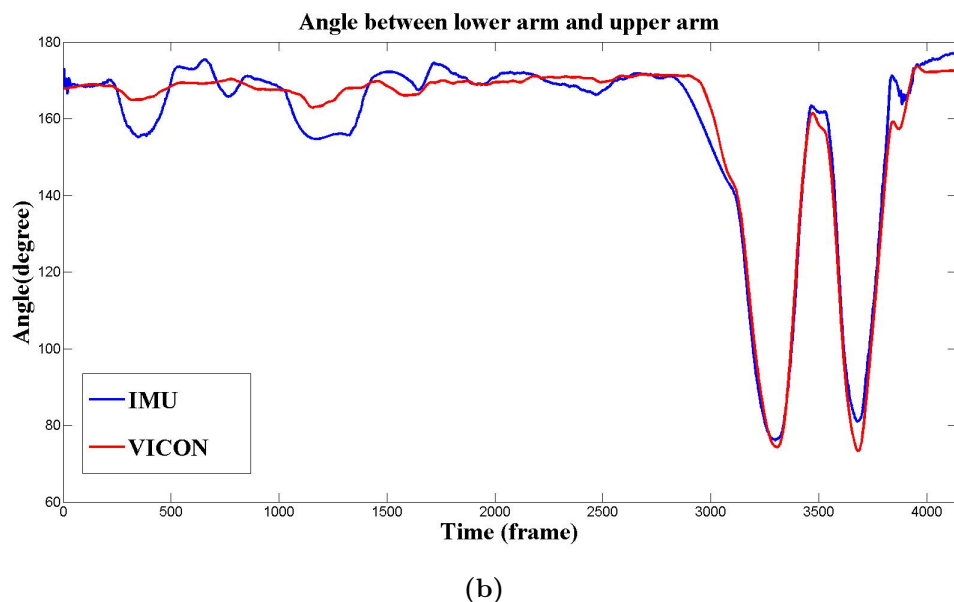
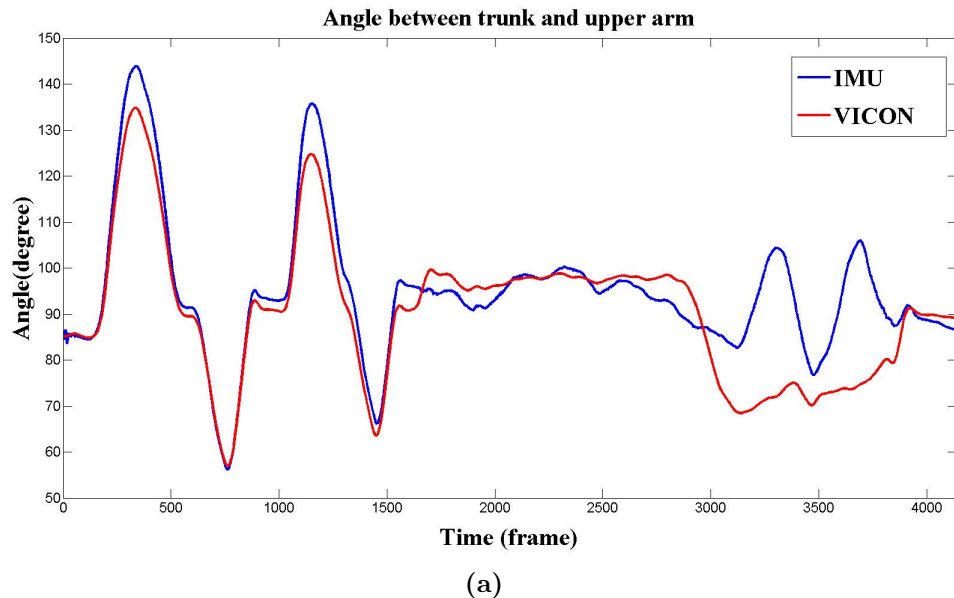


Figure 2.11: Upper limb motion tracking test 1: (a) angles between upper arm and trunk; (b) angles between upper and lower arm

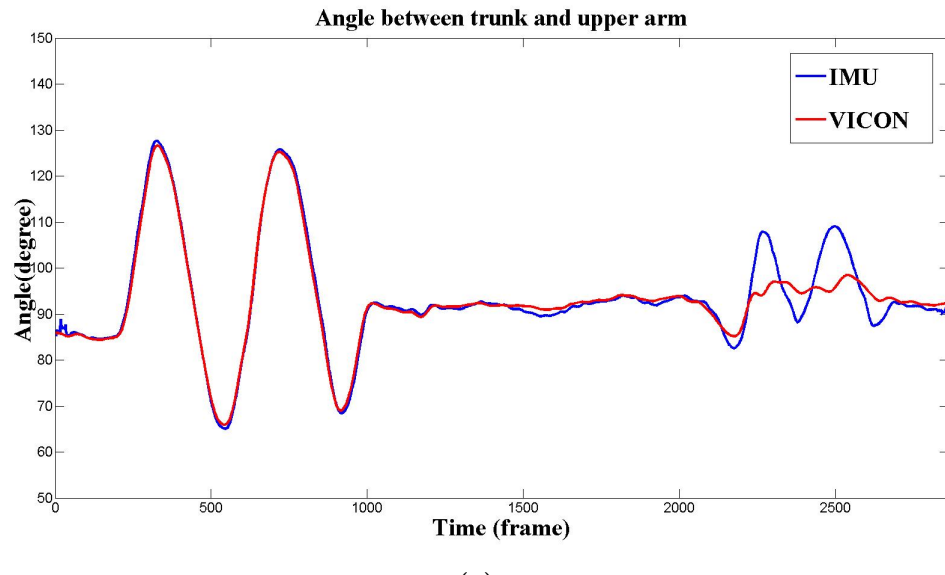
brachii. Even though the IMU is placed on the flat sulcus bicipitalis lateralis, it can hardly avoid vibrations but try to minimize it. This little but inevitable vibration is magnified by sensitive IMU sensors and then lost precise capture. The average difference for these two angle curve is 6.3° , and the similarity (correlation) of two curves is 0.8354.

Figure 2.11b shows the angle between lower arm and upper arm. During the 1st and 2nd range movements, this angle should not vary too much because of fixed angle of elbow joint. It can be observed from the curves, IMU tracking in the 1st and 2nd range fluctuates. The fluctuation at first is from gyroscope errors, since the gyroscope encountered a sudden start of movement. Although embedded orientation filter (in Section 2.3.1) in the IMU is capable of calibrating and recovering the impact from errors, a short time is needed. Whereafter, proposed filter takes effect gradually on the 2nd range movement and corrects the orientation of IMU tracking, which causes the curve remaining flat. The 3rd range performs elbow flexion-extension and the IMU tracking matches the *Vicon* truth mostly and is not affected by previous fluctuation clearly. The average difference for these two angle curve is 3.5° and the similarity (correlation) of two curves is 0.9824.

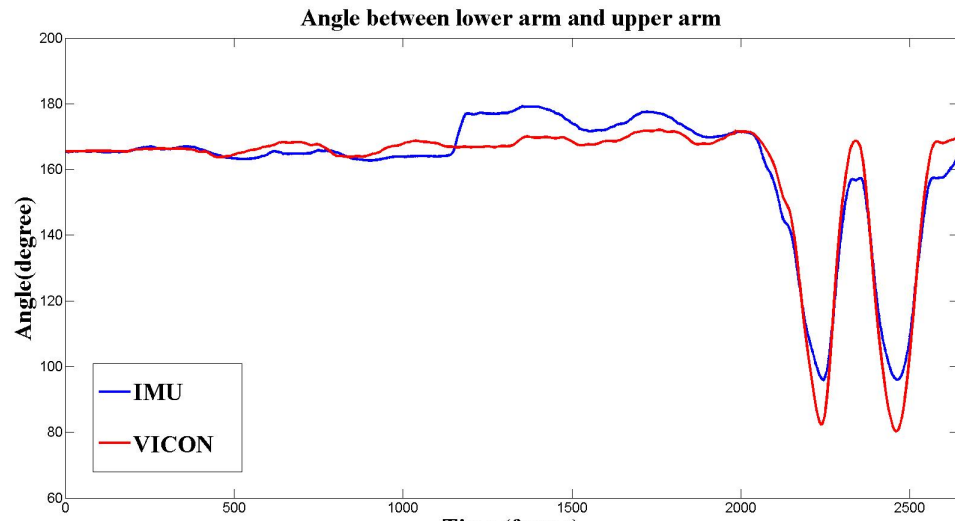
Test 2

We removed IMUs from the first subject and reboot the system and then all the IMUs are mounted on another subject's arm again to execute a second test. Test 2 repeated the activities in test 1, so that calculated results can have an intuitive comparison with test 1. The placement of each IMU is slightly different from test 1, because the exactly same IMU placement is not guaranteed but a closer position is acceptable for contrast.

Figure 2.12a shows the angle between body trunk and upper arm. During the 1st range and 2nd range movement, the IMU tracking performs better than in matching the *Vicon* truth in Figure 2.11a. For the 3rd range, there still remains the unmatch between IMU tracking and *Vicon* capture, but the performance is better than in test



(a)



(b)

Figure 2.12: Upper limb motion tracking test 2: (a) angles between upper arm and trunk; (b) angles between upper and lower arm

1, since this time a new IMU placement for upper arm is applied. The vibrations still comes from the soft tissue artifact caused by biceps brachii. However, the placement of upper arm IMU is adjusted, and obviously, the new position tolerated some vibrations and reduced errors. Overall, test 2 achieves better performance in capturing arm motions and the average difference and similarity (correlation) of two curves is 2.6° and 0.9643 for test 2.

Figure 2.12b shows the angles between lower arm and upper arm for test 2. All the movements are captured precisely and the two curves in the figure mostly matches. A jump occurred after 1st range movement, but two curves approximates afterward due to the help of orientation filter. The 3rd range performs elbow flexion-extension and the IMU tracking matches the *Vicon* truth but these is an difference in angles calculated from IMU data. The estimated angles are from the integral of angular velocity, differences are generated from very slow motions in test 2. In the contrast, the faster motions in test 1 achieve less angle difference. The average difference of two curves is 4.1° and the similarity (correlation) is 0.9651 for test 2.

For clinical analysis of human motions, the angles around three axes for each joint are concernful. These angles can be reflected by IMU rotations within its local coordinate and then translates to the rotations of each joint coordinate. Figure 2.13 shows a example of all the angles of six axes from shoulder IMU and elbow IMU, and their changes according to subject's pose during the test 1. Six red lines indicate three ranges of movement and represent motions which are shown by A to F. From the curve, it is clearly legible to discriminate all the joints orientation during each movement and diagnose the body posture.

2.5.3 Full Body Motion Tracking

A 3-range movement is performed in the full body tracking procedure. The participant with markers and IMUs is started with "T-pose" and is requested to accomplish arm abduction, arm forward flexion, standing leg lifts and keeping balance, as are shown in

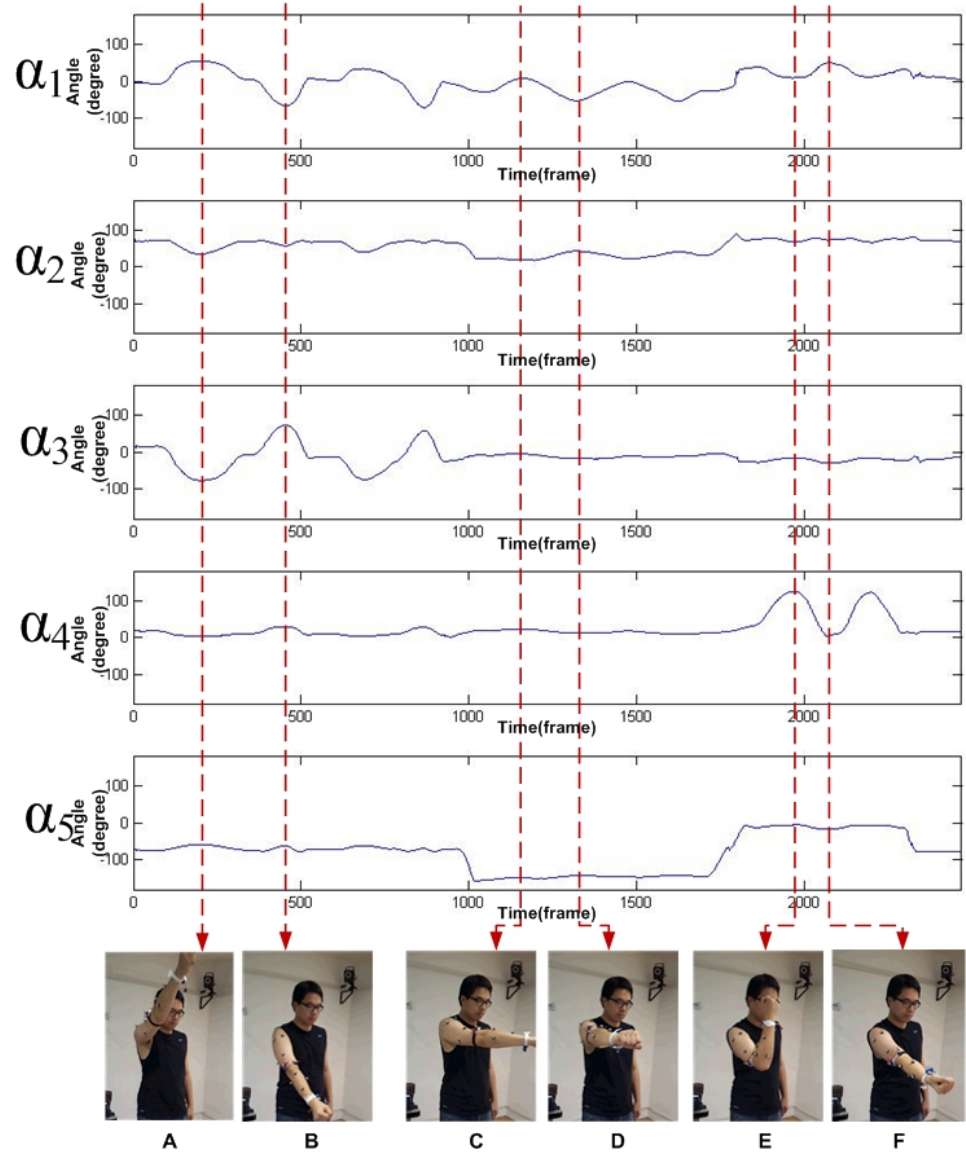


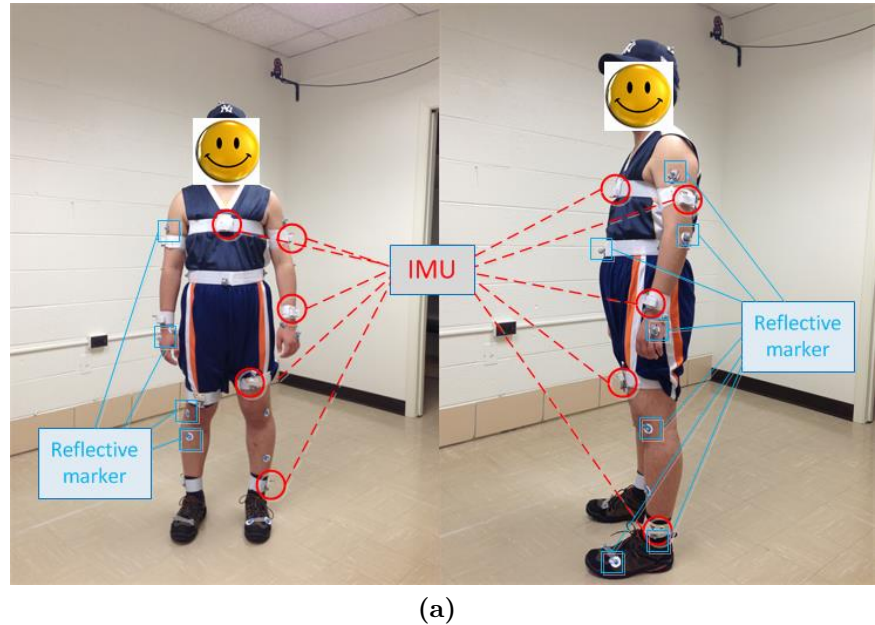
Figure 2.13: Angle changes of IMUs along 3 axes during upper limb motion tracking test 1

Figure 2.14b. Figure 2.14a describes the placement of IMUs and markers on the body. For full body tracking, *OptiTrack* motion capture system is used as the benchmark. Similar as the upper limb tracking test, full body tracking is analyzed as curves of angle against frame. Four angles are our concern and calculated for comparison: elbow angles (between upper arm and lower arm) for each arm and knee angles (between thigh and shank) for each leg. Compared with the angles calculated from *OptiTrack* truth, the accuracy for developed system is further evaluated.

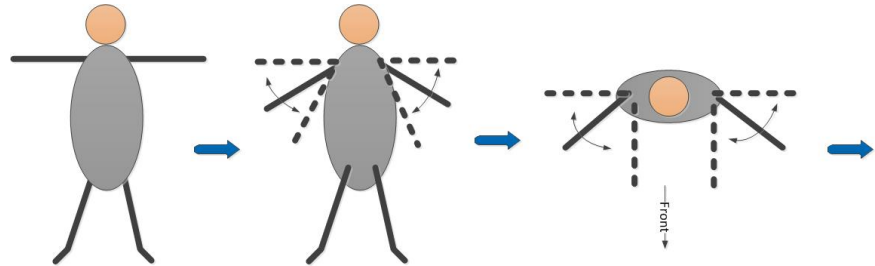
In the following comparisons, the red curve represents angles calculated from the camera system and the blue one shows angels estimated by our developed system.

Figure 2.15 shows the angle between upper arm and lower arm for left arm (Figure 2.15a) and right arm (Figure 2.15b), which also can be called elbow flexion-extension angle. Three ranges of movements are performed during the test. First two ranges of movements are basically arm motions. Because the elbow is not fixed when rotating shoulder joint, the figure clearly shows angle changes of elbow joint by four wave troughs and fluctuations. The 3rd range of movements is lifting legs while keeping body balance. During these movements, arms shake a bit for keeping the balance, which is reflected as the fluctuations of the IMU curve in the 3rd range. The overall results show that angles from IMU and from camera system match very well. The fluctuations of the IMU curve are basically caused by sensitive sensing, while the camera software processes the marker position to make it smoother. The sample rate for the camera system is 100Hz and for IMU is 40Hz, thus the interpolation procedure is applied to inertial data for comparison.

Figure 2.16 shows the angle between thigh and shank for left leg (Figure 2.16a) and right leg (Figure 2.16b), which also can be called knee flexion-extension angle. The 3rd range of movement is lifting thigh and bending knee, so the two wave troughs denote these movements. From the figure, it is clear that IMU curves match the camera truth better for right leg than left leg. This result can be explained that while lifting right leg, left leg is able to better keep body balance than the other side, since our subject is right-handed. Because of the same reason, the right arm has less

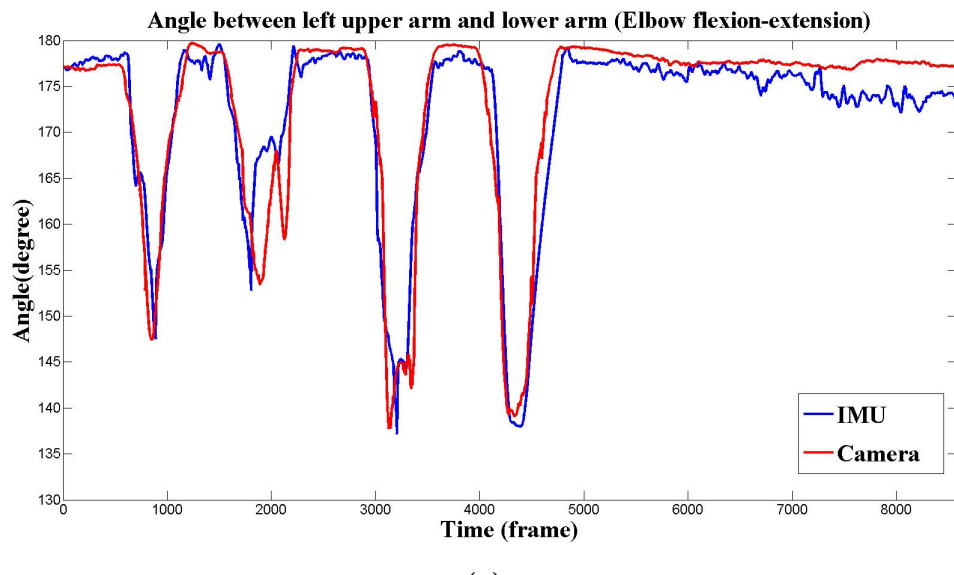


(a)

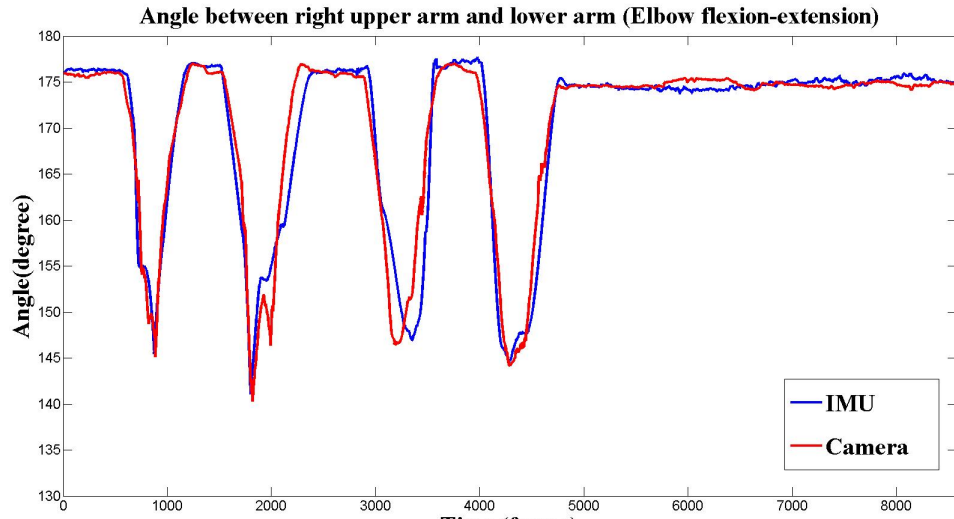


(b)

Figure 2.14: (a) The placement of IMUs and reflective markers on human body and (b) planned motions for experiment

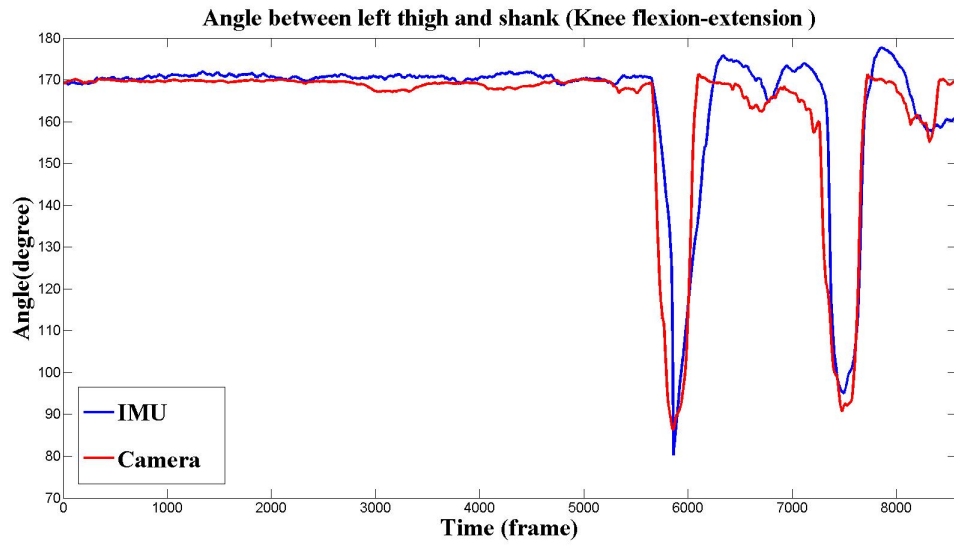


(a)

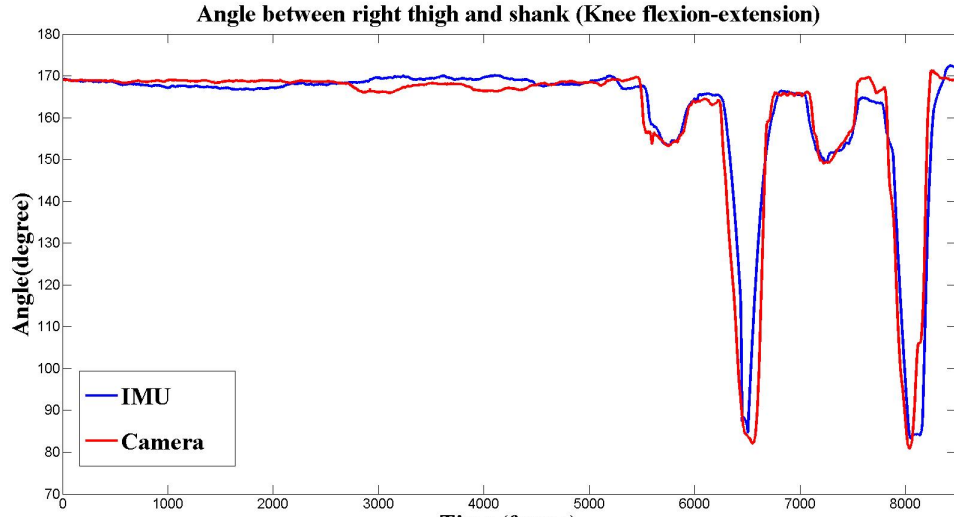


(b)

Figure 2.15: Angle changes during elbow flexion-extension movements for (a) left arm and (b) right arm



(a)



(b)

Figure 2.16: Angle changes during knee flexion-extension movements for (a) left leg and (b) right leg

fluctuations during the 3rd range of movements. Although at the end of the test, the angle difference increases, the orientation filter in the IMU will be able to calibrate and recover the inertial data quickly when subject's motion turns into gentle and slow. For overall results, our inertial tracking technique is capable of capturing and calculating the body motions accurately. The average difference of angle comparisons for these four figures and their similarity (correlation) are summarized in Table 2.1.

Table 2.1: Comparison of IMU angle and camera angle for each figure

	Left	Right	Average difference	Correlation
Elbow	×		2.6°	0.9349
		×	1.5°	0.9625
Knee	×		4.2°	0.9052
		×	3.1°	0.9447

Four angles of elbow and knee flexion-extension are merged and shown in Figure 2.17, thus the motions of body are clearly indicated. The angle changes are corresponding to different ranges of movements as the small figure shows. For a right-handed subject as is discussed before, a preliminary find is that for keeping the body balance, the right arm and left leg are more capable than the other side with less shakes and fluctuations. More angles of human joints also can be calculated by using developed tracking system. By analyzing joints rotations and monitoring the reconstructed human motions, the status of a subject is achievable remotely and in either virtual display or quantitative summary in real-time process.

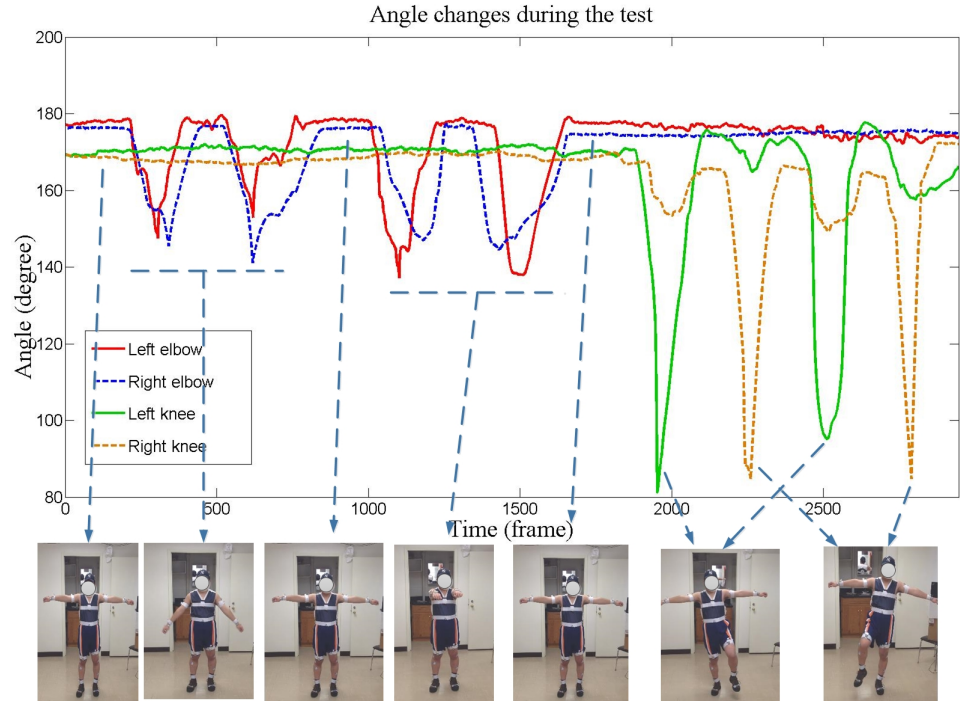


Figure 2.17: Angle changes of elbow joints and knee joints during full body test and corresponding movements

2.6 Related Work

Considering the tracking accuracy of a capturing system, most current research of human motion tracking is concentrated on visual tracking. The most popular approach is marker-based visual tracking, which is capable of fast response to motions accurately. Due to this advantage, it is widely adopted for entertainment, medical care and supporting as the ground truth for non-vision based motion tracking. Some visual tracking systems such as *Vicon* and *Qualisys* are widely utilized and proved to be with high resolution and accuracy. Notwithstanding marker-based visual tracking system is well accepted, the costly camera infrastructures, numbers of reflective markers and

massive computing for data analysis limit its operations better in controlled volumes (labs or studios) and not suitable for portable usage in daily life.

Markerless tracking approaches reduce those limits that marker-based method has and give more flexibility to subjects. Since at least one calibrated camera view would reconstruct a 3D rigid body model by applying markerless visual tracking, motions of a subject can be captured consecutively within a larger space. To better represent the motion of rigid body parts, a twists and product of exponential maps for kinematic chains techniques from the robotic manipulation was introduced to complement visual capture for robust estimation ([Rosenhahn and Brox \(2007\)](#); [Bregler and Malik \(1998\)](#); [Liu and Chellappa \(2007\)](#)). This technique could simplify the estimation procedure without losing tracking accuracy, and provide a convenient way to describe motions of body segments attached by joints. Unfortunately, markerless visual tracking is still interfered by intensity of lights. Furthermore, the motion of body segments is ambiguous in certain degree of freedom (DoF) and fast motions cause noises to the images. Thus, [Pons-Moll et al. \(2010\)](#) developed a hybrid human motion tracker that combines video with inertial sensors to improve the performance of motion capture. Inertial sensors allowed for drift-free estimation of limb orientations under fast motions, compensated accurate position information obtained from video data.

In the research by [Zhou et al. \(2006\)](#), the authors placed an inertial sensor on the wrist and obtained its position by double integrating the measured accelerations. Elbow position was then computed from wrist position by the Euler relationship between them. Although an optimization technique was adopted to minimize the estimate errors, the wrist position was easily suffering from the drift problem by integration. In order to track the upper limb and body motion, a kinematic chain was modeled by linking the rotations of each joint with inverse kinematics ([Perez et al. \(2010\)](#); [Jung et al. \(2010\)](#); [Zhu and Zhou \(2004\)](#)). The calculations of associate joints were based on the inertial data from multiple inertial sensors mounting on the body model. However, no matter the sensors were mounted on a garment or directly on the skin, the noises were generated anyway by following reasons: the soft tissue artifact

over the bony structure does not keep sensor locations constant, and the orientation of each joint axis is actually much more complicated than it appears according to anatomical analysis.

For minimizing the drift problems and optimizing tracking performance, some authors utilized Kalman filter to integrate accelerometers with gyroscopes and magnetometers ([Lin and Kulic \(2012\)](#); [Zhu and Zhou \(2004\)](#)). In the research by [Lee and Park \(2009\)](#), the authors developed a situational measurement vector selection procedure to avoid effects from sudden dynamics and ferromagnetic disturbances. Combined with Gauss-Newton method, a quaternion-based orientation optimizer was presented for finding the best-fit quaternion, whose idea was adopted in our previous work for orientation filtering. Arm physical geometry constraints introduced in the work of [Lin and Kulic \(2012\)](#) are particular ways to further improve the tracking accuracy, such as elbow adduction angle and carrying angle ([Zhang et al. \(2009\)](#); [Luinge et al. \(2007\)](#); [Cutti et al. \(2008\)](#)): the elbow of a healthy subject cannot permit abduction/adduction movement, thus whose adduction angle is restricted to a very small angle. With the arms extended at the sides and the palms facing forward, the forearm and hands are normally slightly away from the body. This is elbow carrying angle, which is 5 to 15 degrees for healthy people.

In the work of [Dejnabadi et al. \(2006\)](#), lower limbs orientation was estimated by placing virtual sensors at the centers of rotational joints. The virtual sensors could yield estimates of segment orientation with minimized drift and noise problems. Although in this paper the method was operated within sagittal plan, the technique could extend to 3D orientation estimation and reduce the restriction of placing sensors over bony structure. Besides, it initiates the mechanism of applying non-model based motion tracking. Also in the work of [Cutti et al. \(2008\)](#), a protocol was developed to measure the scapulothoracic, humerothoracic and elbow 3D kinematics. The upper-limb kinematic model was anatomically defined so that the placement of sensor units could optimally describe the movement of joints with less impact from soft tissue artifact. The idea of choosing optimal IMU placement was helpful to by our proposed

method. However, the protocol was validated based on single-joint-angle movement, which lacked a cross-talk test with other joints for practical activities.

2.7 Summary

In this chapter, a wearable motion tracking system is developed, which is portable and accurate for daily usage. IMUs are mounted on body segments and regardless of their placement, our well-designed calibration procedure can estimate their position and orientation accurately. IMU inertial measurements are pre-processed by developed quaternion-based orientation filter for eliminating noises. With the superiority over rotational matrix, the twist representation and exponential maps techniques describe body movements accurately and articulate body segments conveniently to build a human model. Our low-order computational system enables the needs for real-time reconstruction of body motion and model. Besides, quantitative status of tracked subject can be analyzed and diagnosed rapidly. The comparisons with commercialized *Vicon* and *OptiTrack* motion capture systems assess the accuracy of proposed body motion tracking system. Analysis of joint angle provides quantified tracking results and accurate illumination for motion status.

Chapter 3

Model-Based Quantification of Resting Tremor

Abstract

Parkinson’s Disease (PD) gradually impacts the daily living quality of patients to a variable degree. As the second most apparent symptom, resting tremor mainly affects patients’ motor function by impairing their upper extremities. Using inertial sensors to measure and quantify this symptom has been explored in recent years. However, applying single inertial sensors is not able to provide complete analysis on tremor and it affects the accuracy of quantification. In this chapter, a model-based quantification approach is proposed to improve current quantification. A human body motion tracking system is employed to estimate joint angles from the reconstructed human model. By using a model-based approach, the estimation of joint angle is robust to the contamination from human intentional movements and ambient noise from the gravity component. Since resting tremor is always appeared as recurrent movements of upper extremities, upper extremity joint angles are estimated for quantification. Features that best describe the data characteristics are specially selected for each joint and extracted. A discrete Hidden Markov Model (HMM) classifier is trained by features and their corresponding clinical ratings. The accuracy of classification is cross-validated by the leave-one-out mechanism. In the future work, Electromyogram (EMG) sensors also can be applied to corresponding muscles to measure their fluctuations. The tests are isolated from inertial sensor based tests and are prone to validate the potential help in detecting and quantifying early-stage resting tremor. Experiments achieve high classification accuracy and preliminary results prove the practicability of proposed approach and its feasibility in improving current clinical methods.

3.1 Introduction

Parkinson's disease is a degenerative disorder of the central nervous system, characterized by a large number of motor and non-motor features which impact on function to a variable degree. It is more common in the elderly, with most cases occurring after the age of 50. As PD progresses, it results in more severe difficulties in activities of daily life and becomes more challenging in clinical management in advanced PD. PD shows four major motor features including bradykinesia, resting tremor, rigidity and postural instability ([Jankovic \(2008\)](#)). Resting tremor is the second most apparent symptom of PD (after bradykinesia) and it occurs maximally when the limb is at rest and supported against gravity. The frequency of resting tremor typically ranges from 3 to 6 Hz and may increase with mental stress or contralateral voluntary motion ([Grimaldi and Manto \(2010\)](#)). Most resting tremor is prominent in upper extremity unilaterally (*e.g.* hand tremors) in early-stage PD and spread to bilateral later. Therefore, an assessment of how the resting tremor affects patients' daily life would be necessary.

Currently, a number of rating scales are applied to assess clinical tremor, such as UPDRS, Schwab and England Activities of Daily Living Scale, Hoehn and Yahr Scale, and Webster Scale. Although most of these scales have not been evaluated for reliability, as the most well established one, UPDRS are commonly used. However, these scales rely on a clinician's subjective observations and lack of comparisons with objective standard. Moreover, the severity of resting tremor varies during daily living activities, which induces insufficiency for assessing the tremor severity by minutes' observations in lab or clinic. Thus, an objective quantification method for detecting and quantifying resting tremor can greatly assist the clinical diagnosis of PD.

Several researchers have proposed their works to detect and quantify tremor. The research included the detection and assessment of resting tremor by [Rissanen et al. \(2008\)](#); [Askari et al. \(2010\)](#), discrimination and quantification of resting/action tremor by [Rigas et al. \(2012\)](#); [Salarian et al. \(2007\)](#); [Rissanen et al. \(2010, 2011\)](#); [Heldman](#)

et al. (2011); Powell et al. (2009) and estimation of tremor severity by Rigas et al. (2012); Heldman et al. (2011); Patel et al. (2009). Based on the fact that tremor rating is typically obtained in a clinic with the presence of a clinician, it is unpractical to capture a patient's tremor fluctuations throughout the day. In order to study and evaluate the methods during activities of daily living, Heldman et al. (2011) quantified the tremor of PD patients during non-standardized activities of daily living tasks in lab environment. Salarian et al. (2007) took a 4 hours long monitoring to record and analyze free moving of PD patients, focusing on tremor and bradykinesia. Although long term monitoring, such as days or weeks long, will definitely valuable for analyzing how the tremor impact patients' daily life, no such research had been done because of the limitations on applying body sensors.

The advantages of using body sensors, such as high accuracy tracking, long-term monitoring, non-intrusiveness and easy setup have been brought to clinical assessments for motor abnormalities of PD patients. Accelerometers and gyroscopes have been used to measure the movement of body segments (Rigas et al. (2012); Mellone et al. (2011); Palmerini et al. (2011); Salarian et al. (2007); Heldman et al. (2011); Powell et al. (2009); Patel et al. (2009)). Although the use of accelerometers can distinctly reflect motion trend, whose drawback is often ignored by current research. The acceleration of body segments are prone to be contaminated by intentional motions of the subject him/herself. Accumulated errors and ambient noises also make the measured acceleration unreliable.

Tremor is mostly appeared as recurrent movements around certain body axis or the combination of axes. Gyroscopes, as its fundamental function is measuring angular velocity, perform better than accelerometers and represent legible readings to tremor. However, current usage of gyroscopes was less taken into consideration than accelerometers. Although the advantages of BSN for tremor quantification has been recognized that the correlation of multi-sensor data could generate more meaningful kinematic information, the practical use of BSN still mostly relies on individual function of each sensor rather than multi-sensor correlations in real network. Rigas

et al. (2012) measured the angles between different axes of accelerometers, whereas additional acceleration generated by intentional movements would still bring errors to measured results.

Using electromyography (EMG) can be potentially helpful for current researches. Applying EMG and its combination with inertial sensors for PD diagnosis provided an objective assessment of tremor through muscular fluctuations, which directly studied the source of tremor (Askari et al. (2010); Rissanen et al. (2008, 2010, 2011)). At early-stage of PD tremor, the fluctuation of body segments is mild, which is hardly noticed visually from acceleration/angular velocity data, whereas EMG can detect such mild fluctuations from the muscular signal. Consequently, the use of EMG would help the detection of early-stage PD tremor and improve the assessment of severity. Furthermore, for the current research that employed sensors to measure kinematic data, the variation in sensor placement each time could affect the selected features for the quantification approaches, which could result in errors in tremor estimations.

As a rapid developing research area, wireless BSN based motion tracking system utilizes multiple wireless sensors mounted on the human body to capture human motions and build a body network. It isolates traditional visual tracking system and provides more flexible and convenient motion tracking mechanism without losing accuracy. Building a body model possesses an irreplaceable advantage, which allows inertial sensors to be randomly placed on human segments and unnecessarily knowing their position. By applying the motion tracking technique, a novel model-based approach for quantifying resting tremor is proposed in this chapter.

The frequent fluctuations of elbow/wrist joint angles of PD patients during resting are selected as major features for detection and later quantification of resting tremor in the inertial-based study (first study). Joint angles calculated from our developed IMU are chosen and angle related features are extracted to achieve appropriate illustrations for assessment. Unlike most researches using accelerometers to measure tremor movements, proposed angle related technique can ignore the impact from different posture of the subject. Because calculated angles have no relationship with the gravity

component and only absolute angles are employed, the advantage of robustness for measuring subject's tremor with more flexibility appears clearly. A discrete HMM is trained by using selected features which could best describe resting tremors. Both the start/end and the severity of resting tremor of PD patients are classified and quantified by trained HMM classifier. The assessment of our model-based tremor quantification approach is verified by correlations with UPDRS, which was rated by professional PD clinicians while the patients are holding defined postures.

In the future IMU+EMG study (second study), EMG of patient's upper arm will be measured and certain features will be extracted, accompanying those features from IMU, to potentially enhance the accuracy of both detection and quantification of PD tremors. After correlated with UPDRS, the correlations for both studies are going to be compared and examined, to discover the necessity of using both EMG and IMU in improving IMU-only mechanism.

Compared with current researches, proposed model-based approach not only provides an alternative and more robust tremor assessment, but patients' real-time motion can be monitored through reconstructed human model, which simplifies the clinician-patient interaction at anytime and anywhere. This advantage of model-based approach makes it unique among current researches.

3.2 Human Arm Modeling and Joint Angle Estimation

3.2.1 Human Arm Modeling

Most resting tremor is prominent in upper extremity, therefore, arm segments are primarily chosen for analysis. A human arm can be modeled as a kinematic chain comprises three arm segments (upper arm, lower arm and hand) and three joints (shoulder, elbow and wrist). Correspondingly, three IMUs are respectively mounted on the upper arm near elbow (over the distal humerus), on the lower arm near wrist

(over the distal flat surface of radius and ulna) and on the dorsal hand surface. According to the experiences, those positions are considered to have less effects from soft tissue artifact. An arm has seven rotational DoFs, as are shown in Figure 3.1: shoulder has three (flexion-extension α_1 , internal-external α_2 and abduction-adduction α_3), elbow has two (flexion-extension α_4 and pronation-supination α_5) and wrist has two (flexion-extension α_6 and radial/ulnar deviation α_7).

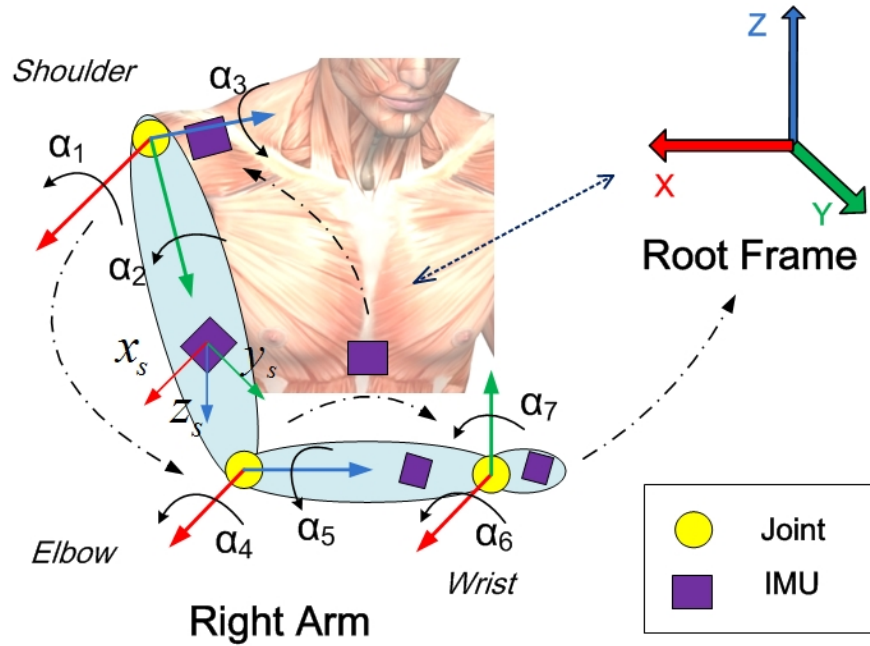


Figure 3.1: Kinematic modeling of a human arm

A Root Frame \mathbb{R} is defined as the global reference and the rotations of shoulder coordinate $\Sigma_{shoulder}$ are captured within the Root Frame. As the adjacent joint of shoulder, elbow coordinate Σ_{elbow} only considers its rotation corresponding to $\Sigma_{shoulder}$, and the wrist joint, similarly, only considers its rotation corresponding to Σ_{elbow} . Each joint considers rotations within prior connected joint frame, so that

rotations of each joint are closely related to the prior joint's position and the inertial data from IMU of each local frame are closely correlated with previous IMU output. It is clear that the joint motions are caused by the combination of rotations along different axes, *e.g.* in Figure 3.1, elbow rotation angle combines α_4 and α_5 and wrist rotation angle combines α_6 and α_7 . When joint motion occurs, IMU directly measures combined effects of involved angles. Meanwhile, the rotation angles along each axis are simple to be transformed from joint quaternion output of IMU.

Once joint motions are captured, joint quaternion \mathbf{q} is computed for representing 3D rotations. Quaternion provides a convenient mathematical notation for representing orientations and rotations of objects in three dimensions. Quaternion-based rotation representation is adopted because of its superiority: compared to Euler angles they are simpler to compose and avoid the problem of singularities (gimbal lock); compared to rotation matrices they are more numerically stable and more efficient. Any rotation in three dimensions can be represented as a combination of an axis vector and an angle of rotation. Quaternion gives a simple way to encode this axis-angle representation in four numbers and apply the corresponding rotation to a position vector representing a point relative to the origin in \mathbb{R}^3 . It is a vector quantity of the form

$$\mathbf{q} = q_0 + q_1\mathbf{i} + q_2\mathbf{j} + q_3\mathbf{k} = (q_0, \vec{q}) \quad (3.1)$$

where i, j and k are basis elements of a quaternion, q_0 is the scalar component of \mathbf{q} and $\vec{q} = (q_1, q_2, q_3)^T$ is the vector component. Given that $\omega = [\omega_1, \omega_2, \omega_3]^T$ represents the unit axis of rotation and $\theta \in \mathbb{R}$ represents the angle of rotation about ω , another form for quaternion is as ${}_R\mathbf{q} = (\cos(\theta/2), \omega \sin(\theta/2))$. Thus, the corresponding rotation is extracted by setting

$$\theta = 2 \cos^{-1} q_0 \quad , \quad \omega = \begin{cases} \frac{\vec{q}}{\sin(\theta/2)} & if \quad \theta \neq 0, \\ \mathbf{0} & otherwise, \end{cases} \quad (3.2)$$

The rotation angles of shoulder joint α_1, α_2 and α_3 , elbow joint α_4, α_5 and wrist joint α_6, α_7 are expressed by measured quaternion $s\hat{q}$ for shoulder frame, $E\hat{q}$ for elbow frame and $w\hat{q}$ for wrist frame. Three quaternions integrate the movements of three arm joints, which achieves high computational efficiency, instead of traditionally applying the product of seven rotational matrixes from $R(\alpha_1)$ to $R(\alpha_7)$ for expressing rotations.

3.2.2 Arm Joint Angle Estimation

By updating quaternions of each joint during the movements, their rotation angles around each DoF can be decomposed from updated quaternions. However, mounting an IMU on human body acts more random than to follow any strict regulations and the orientation of mounted IMU could be in any direction. Thus in order to reliably measure the rotations of joint, IMU orientation is estimated before arm motions and the mapping relationship between IMU coordinate and joint coordinate is calculated for later transformation. A calibration procedure is designed to estimate the IMU orientation, no matter how a subject mounts it to the body.

IMU shares the same coordinate with the global Frame \mathbb{R} , which is an essential prerequisite. Before mounting the IMU on the body, a human initial posture is required for both mounting the IMU and coupling local joint frames to the Root Frame. When an IMU is mounted, its orientation *w.r.t.* \mathbb{R} is calculated from inertial output. Compared with corresponding joint frame, a rotational transformation is generated and represented by ${}_X^Y q$, which denotes the quaternion representation of rotational relationship from X frame to Y frame. Thus, during tracking the arm motions, quaternion of each joint is updated by combination of corresponding IMU quaternion and their relationship quaternion.

Initially, IMUs are calibrated within \mathbb{R} . After being attached to the human arm, their orientation measurements on the arm are rotated from initial orientation ${}_{\mathbb{R}} q_0$ to ${}_{IS} \hat{q}$ for the IMU corresponding to the shoulder, ${}_{IE} \hat{q}$ for the IMU corresponding

to the elbow and $_{IW}\hat{q}$ for the IMU corresponding to the wrist. During this process, the subject is asked to hold their arm still as pre-defined posture in order to mount the IMUs and calibration. The local coordinate of the shoulder, elbow and wrist refer to \mathbb{R} are initially defined as ${}^{\mathbb{R}}_S q_{initial}$, ${}^{\mathbb{R}}_E q_{initial}$ and ${}^{\mathbb{R}}_W q_{initial}$ for the initial posture. The rotational relationship quaternion ${}^Y_X q$ between local joint coordinates and their corresponding IMU orientations are shown as

$$\begin{aligned} {}^S_{IS} q &= {}^{\mathbb{R}}_S q_{initial} \otimes {}^S_{IS} \hat{q}^* \\ {}^E_{IE} q &= {}^{\mathbb{R}}_E q_{initial} \otimes {}^E_{IE} \hat{q}^* \\ {}^W_{IW} q &= {}^{\mathbb{R}}_W q_{initial} \otimes {}^W_{IW} \hat{q}^* \end{aligned} \quad (3.3)$$

where IS , IE and IW denote corresponding IMUs for shoulder, elbow and wrist. The quaternion product \otimes is used to describe compounded orientations, which is based on the Hamilton rule (Horn et al. (1988)). ${}_a^b q^* = {}_b^a q$ denotes the conjugate of a quaternion ${}_a^b q$. The relationship quaternion ${}^S_{IS} q$, ${}^E_{IE} q$ and ${}^W_{IW} q$ will be used for updating real-time rotation measurements of shoulder ${}^{\mathbb{R}}_S \hat{q}$, elbow ${}^{\mathbb{R}}_E \hat{q}$ and wrist ${}^{\mathbb{R}}_W \hat{q}$ joint

$$\begin{aligned} {}^{\mathbb{R}}_S \hat{q} &= {}^S_{IS} q \otimes {}^S_{IS} \hat{q} \\ {}^{\mathbb{R}}_E \hat{q} &= {}^E_{IE} q \otimes {}^E_{IE} \hat{q} \\ {}^{\mathbb{R}}_W \hat{q} &= {}^W_{IW} q \otimes {}^W_{IW} \hat{q} \end{aligned} \quad (3.4)$$

The resting tremor is generally displayed as the rotations on elbow and wrist joint, therefore three rotations around these joints are measured for later feature extraction, which are elbow flexion-extension, elbow pronation-supination and wrist flexion-extension rotations. In order to avoid the impact of rotation superposition on transforming Euler angle directly from quaternion, elbow angle is calculated from intersection angle between upper arm and lower arm and wrist angle is between lower arm and hand. The joint position calculation is described below.

Let $p_{\mathbb{A}\mathbb{B}} \in \mathbb{R}^3$ be the position vector from the origin of frame \mathbb{A} to the origin of frame \mathbb{B} , and $R_{\mathbb{A}\mathbb{B}} \in SO(3)$ (special Orthogonal group) be the orientation of \mathbb{B} , relative to \mathbb{A} . A configuration of the system is defined as a pair $g_{\mathbb{A}\mathbb{B}} = (p_{\mathbb{A}\mathbb{B}}, R_{\mathbb{A}\mathbb{B}}) \in SE(3)$. The linear form transformation from a given point $q_{\mathbb{A}}$ in \mathbb{A} to its coordinate in \mathbb{B} is represented as

$$\bar{q}_{\mathbb{B}} = \begin{bmatrix} q_{\mathbb{B}} \\ 1 \end{bmatrix} = \begin{bmatrix} R_{\mathbb{A}\mathbb{B}} & p_{\mathbb{A}\mathbb{B}} \\ \mathbf{0} & 1 \end{bmatrix} \begin{bmatrix} q_{\mathbb{A}} \\ 1 \end{bmatrix} = \bar{g}_{\mathbb{A}\mathbb{B}} \bar{q}_{\mathbb{A}} \quad (3.5)$$

For each homogeneous matrix $\bar{g} \in SE(3)$, there is a corresponding twist $\hat{\xi}$ in the tangent space $se(3)$, defined as

$$\hat{\xi} = \begin{bmatrix} v \\ \omega \end{bmatrix}^\wedge = \begin{bmatrix} \hat{\omega} & v \\ \mathbf{0} & 0 \end{bmatrix} \in \mathbb{R}^{4 \times 4} \quad (3.6)$$

where $v = -\omega \times r$ and r denotes the origin of rotation axis in the twist $\hat{\xi} \in se(3)$. The exponential of $\theta\hat{\omega}$, $e^{\theta\hat{\omega}} = I + \hat{\omega}\sin\theta + \hat{\omega}^2(1 - \cos\theta)$, is an element of $SE(3)$ and it indicates the rotations. Elements from $se(3)$ are mapped to $SE(3)$ using the exponential map for twists as shown in following equation

$$e^{\theta\hat{\xi}} = \begin{bmatrix} e^{\theta\hat{\omega}} & (I - e^{\theta\hat{\omega}})(\hat{\omega}v + \omega\omega^T v\theta) \\ \mathbf{0} & 1 \end{bmatrix} \quad \omega \neq \mathbf{0}$$

$$e^{\theta\hat{\xi}} = \begin{bmatrix} I & v\theta \\ \mathbf{0} & 1 \end{bmatrix} \quad \omega = \mathbf{0} \quad (3.7)$$

If the initial configuration of one IMU corresponding to \mathbb{R} is $g(0)$, the final configuration of the IMU, which contains the final position, corresponding to \mathbb{R} with rotation angle θ is given by

$$g(\theta) = e^{\theta\hat{\xi}} g(0) \quad (3.8)$$

Take arm model as an example. The assumed position of shoulder joint is ${}^{\mathbb{R}}\hat{P}_S$ and the translational calculation from shoulder to elbow p_{SE} is achieved by combining ${}^{\mathbb{R}}\hat{P}_S$ and initial spacial relationship of elbow relative to shoulder ${}_0p_{SE}$ within $\Sigma_{shoulder}$

$$p_{SE} = {}^{\mathbb{R}}\hat{P}_S + {}_0p_{SE} \quad (3.9)$$

As the subject moves, the quaternion of s-IMU (short for the IMU corresponding to shoulder) ${}^S\hat{q}$ is continuously updated. With shoulder measurements are calculated, the elbow joint position can be updated by

$$\begin{aligned} \theta_S, \omega_S &\leftarrow {}^S\hat{q} \\ \{\theta_S, \omega_S, p_{SE}\} &\xrightarrow{\text{exp map}} {}^{\mathbb{R}}\hat{P}_E \end{aligned} \quad (3.10)$$

where ${}^{\mathbb{R}}\hat{P}_E$ denotes updated elbow position within \mathbb{R} .

For adjacent lower arm, the updated elbow position is ${}^{\mathbb{R}}\hat{P}_E$ and the translational calculation from elbow to wrist p_{EW} is achieved by

$$p_{EW} = {}^{\mathbb{R}}\hat{P}_E + {}_0p_{EW} \quad (3.11)$$

Then, the wrist joint position can be updated by

$$\begin{aligned} \theta_E, \omega_E &\leftarrow {}_E\hat{q} \\ \{\theta_E, \omega_E, p_{EW}\} &\xrightarrow{\text{exp map}} {}^{\mathbb{R}}\hat{P}_W \end{aligned} \quad (3.12)$$

The procedure of updating wrist quaternion ${}^W\hat{q}$ and estimating hand position ${}^{\mathbb{R}}\hat{P}_{hand}$ in \mathbb{R} are similar to get by first calculating the translation from wrist to hand p_{WH} within Σ_{wrist}

$$p_{WH} = {}^{\mathbb{R}}\hat{P}_W + {}_0p_{WH} \quad (3.13)$$

then updating the hand position

$$\begin{aligned} \theta_W, \omega_W &\leftarrow {}^R_W \hat{q} \\ \{\theta_W, \omega_W, p_{\text{Wh}}\} &\xrightarrow{\text{exp map}} {}^R \hat{P}_{\text{hand}} \end{aligned} \quad (3.14)$$

The rotation of each joint of above example are represented by $\{\theta_S, \theta_E, \theta_W\}$ and their corresponding twists are $\{\hat{\xi}_S, \hat{\xi}_E, \hat{\xi}_W\}$. The exponential map for twists of each joint is in the form of $e^{\theta_i \hat{\xi}_i}$ and the connection of joints is demonstrated by product of all joints' exponential maps

$$\prod_{i=S}^W e^{\theta_i \hat{\xi}_i} = e^{\theta_S \hat{\xi}_S} \cdot e^{\theta_E \hat{\xi}_E} \cdot e^{\theta_W \hat{\xi}_W} \quad (3.15)$$

If we let $g_{\text{wrist}, \text{hand}}(0)$ represent the initial configuration of hand *w.r.t.* wrist, then the final configuration of hand *w.r.t.* shoulder $g_{\text{shoulder}, \text{hand}}$, connected by rotation angles $\Theta = (\theta_S, \theta_E, \theta_W)$ is given by

$$\begin{aligned} g_{\text{shoulder}, \text{hand}}(\Theta) &= \prod_{i=S}^W e^{\theta_i \hat{\xi}_i} \cdot g_{\text{wrist}, \text{hand}}(0) \\ &= \exp\left(\sum_{i=S}^W \theta_i \hat{\xi}_i\right) \cdot g_{\text{wrist}, \text{hand}}(0) \end{aligned} \quad (3.16)$$

The final configuration contains the position of the target joint. Thus, once the elbow, wrist and hand position are achieved, our interested elbow flexion-extension and wrist flexion-extension angles can be easily calculated. And based on the character of elbow pronation-supination rotation, its angle α_5 is directly transformed from e-IMU quaternion ${}^R_E \hat{q}$.

3.3 Model-based Tremor Quantification

3.3.1 Tremor Feature Selection

Model-based tremor quantification approach is a practical application of developed human body motion tracking system in Chapter 2. A human model is reconstructed from the exponential maps of connected body segments, whose twist movements are captured and measured by IMUs mounted on the segments. An advanced characteristic of this tracking technique is its robustness to the IMU placement, which means the reconstruction of human model can be achieved regardless of the placement and orientation of corresponding IMU (to the joint).

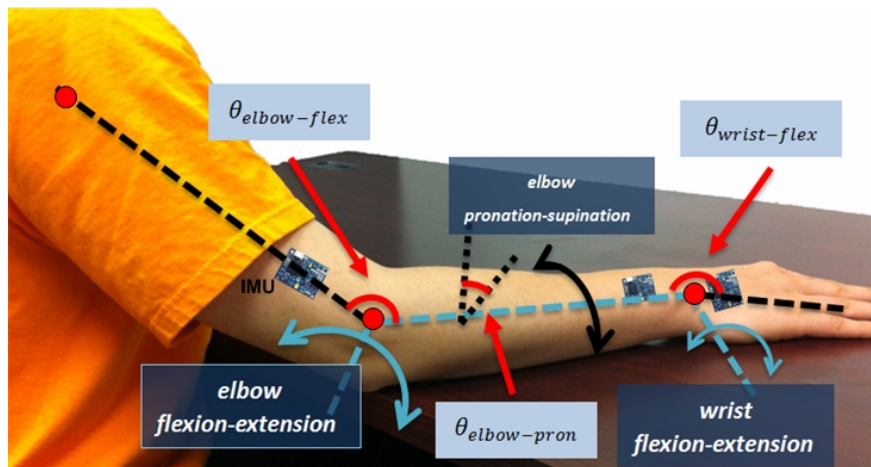


Figure 3.2: Three major rotations of forearm used for extracting resting tremor features

The IMUs mounted on arm provide acceleration a , angular velocity ω and quaternion q of arm segments. The quaternion representation can properly represent the twist motions of each joint. In this work, the quaternion of shoulder joint ${}^S\hat{q}$, elbow joint ${}^E\hat{q}$ and wrist joint ${}^W\hat{q}$ are employed and to estimate the position of

elbow, wrist and hand. As are shown in Figure 3.2, elbow flexion-extension $\theta_{elbow-flex}$, elbow pronation-supination $\theta_{elbow-pron}$ and wrist flexion-extension $\theta_{wrist-flex}$ are the interested angles for monitoring and quantifying resting tremor. As is mentioned before, the rotation of these angles are the combined effects from α_4 , α_5 , α_6 and α_7 . The quaternion representation is capable of estimating the 3D rotations of corresponding joint, and if needed, each involved angles can be decomposed from quaternion to analysis separately. Aiming at those three concerned angles, three features for describing resting tremor are selected and extracted.

Angle Related Features

Resting tremor in PD is characterized by rhythmic movement induced by rotating motion of certain joints. According to such character, rotation angles are calculated and directly segmented for feature extraction. Since the tremor regularly lasts for long duration of time once it starts, the signal is divided into a 3s duration window and 75% overlapping. Using a 3s moving window technique considers the fact that a shorter window would bring heavy computation and a longer window, in the opposite, would reduce the resolution and accuracy of extraction.

Three angle related features are estimated from the signal, as listed below. Among the features, 1 is angle based feature; 2 and 3 are frequency-spectrum based features, which are extracted from the frequency-spectrum of the signal using a fast Fourier transform.

1. Average angle change rate:

The average change rate of angle (unit: $^{\circ}/s$) calculates the average changes of relative joint angle between two connected body segments in a certain time span. It is defined as

$$\bar{\theta} = \frac{\theta(i+1) - \theta(i)}{1/f} \quad (3.17)$$

where f is the frequency of the signal.

2. Angle energy:

Resting tremor in PD behaves as involuntary movement of body parts within certain range of frequency, thus, the energy (unit: dB/s) of such harmonic motion is considered as a feature. It gives a quantitative measure of the wobbling in certain frequency range. From the frequency-spectrum of the signal, the energy is given as

$$E = \frac{1}{2} \sum_{f \in [3-6Hz]} f P(f) \quad (3.18)$$

where $P(f)$ is signal spectrum.

3. Angle spectrum entropy:

The high energy concentration in specific frequency also reflects the character of signal. Thus, the spectrum entropy H is calculated as follows

$$H = - \sum_f p(f) \log p(f) \quad (3.19)$$

where $p(f) = \frac{P(f)}{\sum_f P(f)}$.

The severity of PD resting tremor correlates with the amplitude and frequency of the tremor. The three features can commendably describe the character of resting tremor for each rotation, and the feature vector is defined as

$$F = [\bar{\theta}, E, H] \quad (3.20)$$

For analyzing the arm resting tremor, as mentioned before, three rotation angles, $\theta_{elbow-flex}$, $\theta_{elbow-pron}$ and $\theta_{wrist-flex}$, about elbow and wrist joints are utilized. Hence, $F_{elbow-flex}$, $F_{elbow-pron}$ and $F_{wrist-flex}$ are calculated. Each angle extracts three angle related features for each 3-second segment, and if monitored signal lasts for 20s, then there are 23 segments and the total features are $3 \times 3 \times 23 = 207$. For PD patients,

extracted features can guarantee the needs for classifying their symptoms and keeping low computational complexity for quantifying resting tremor.

EMG Features

Two features can be used for extracting EMG signal from the overlapping epochs. The discrimination of EMG signal from PD patients and healthy control is clear by these two features, which can greatly help identifying the invisible muscular movement of PD patients from healthy control.

1. Kurtosis:

The kurtosis is defined as the fourth centered moment of a time series x

$$k = \frac{E\{(x - \mu)^4\}}{\sigma^4} \quad (3.21)$$

where μ is the mean of the sample values, $E\{*\}$ is the expectation and σ is the standard deviation. It can assess the sharpness of the EMG distribution. Because the PD-like EMG signals are regularly more spiky, the kurtosis is expected to achieve higher value for PD-like EMG signals than from healthy controls.

2. Crossing rate:

Crossing rate (CR) expansion is defined by calculating the number of crossing at given threshold levels. A crossing is described as two neighboring value in a time series are on opposite sides of the threshold. The width of the expansion is made on the purpose of obtaining a good and clear representation as possible, and the height is defined as the maximum value of crossing value at all threshold level. The CR is calculated as the width/height of the expansion. Since PD-like EMG signal has narrower CR expansions, the expected CR of PD patients is lower than healthy controls.

The severity of PD resting tremor is quantified by both EMG features and angle related features. The feature vector is defined as

$$F = [\dot{\theta}, E, H, k, CR] \quad (3.22)$$

The total features for the 20-second trial are $3 \times 5 \times 23 = 345$. Although the number is a little bigger, it will not bring any reductions in HMM training efficiency, and the quantification with this feature vector is expected to achieve better results even for very mild tremor. Besides, it is expected to discover whether there are correlations between angle changes and EMG signals from the quantification procedure.

3.3.2 Resting Tremor Severity Classification

Classified features are correlated with UPDRS motor scores for quantification. The feature vectors which contains the patients' feature data of different severities and healthy controls' feature data are sent to a HMM for training. Their corresponding UPDRS from 0 to 4 (as in Table 3.1) are sent to the HMM as observation states. After training the HMM, dataset are randomly merged with leave-one-out mechanism to validate the performance of HMM classification. By going through all the dataset and leaving each subject outside the dataset once, total results are averaged.

Table 3.1: UPDRS of tremor

0	Absent
1	Slight and infrequently present
2	Moderate; bothersome to patient
3	Severe; interferes with many activities
4	Marked; interferes with most activities

Many research in this field apply heuristic rules to classify bio-signal, such as decision tree and fuzzy logic, or apply statistical rules, such as discriminant analysis, k-NN and HMM. HMM is a statistical model that can better describe the characteristics of time dependent signal and can be well characterized as a parametric random process. It preserves structural information of characteristic signal and no thresholds used by the heuristic rules are needed in HMM. The supervised studying mechanism enables HMM to learn new model and optimize current classification strategy based on its intrinsic probability-based discrimination. Therefore in our research where multiple features are requested for classification, HMM is chosen because of its adaptation.

A HMM is defined by a brief triplet $\lambda = (A, B, \pi)$, where A is the matrix of state-transition probabilities, B is observation probabilities and π is the vector of initial state probabilities. Classic Baum-Welch algorithm is adopted to estimate HMM parameter by maximizing the likelihood $P(O|\lambda)$ using an iterative procedure. Viterbi method is chosen to find the most likely state sequence in the model that produces the observations and optimize the model construction.

PD patients' tremor has disparities of duration, amplitude and frequency more or less. Single HMM model experiences deficiency for applying to different subjects and multiple features. The retrain procedure for single HMM is time consuming and short of universality. In order to simplify the HMM training and make general use for different patients, a discrete, multiple feature HMM is proposed as Figure 3.3 shows.

The state space consists of 5 patterns: 0-4, which represents the tremor severity from scale 0 to scale 4. The state transitions are equiprobable and the classification result is mainly determined by the observation probability, which is obtained through calculating the probability of particular output sequence. In the training process, we consider possible state transitions, such as the direct transitions between scale 0 (no visible tremor) and other scales (0-1, 0-2, 0-3, 0-4), the transitions between adjacent scales (0-1, 1-2, 2-3, 3-4); some jumps between states, such as scale 1-3, 2-4, 1-4, were ignored because of its impracticability.

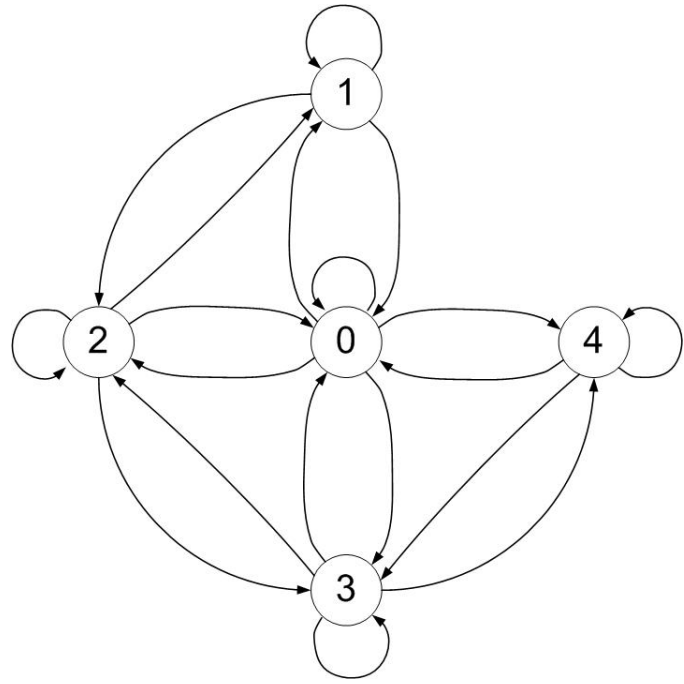


Figure 3.3: HMM for tremor severity classification

The severity classification can be considered as a decoding procedure. Each moment a transition from scale 0 to other scale begins, it is noted as the start of tremor; similarly, the end of tremor is defined as the moment that other scale turns back to scale 0. Corresponding features from a patient's measurements are selected as the input of HMM and marked with the severity scale that estimated professionally by a clinician. After fulfilling model training with dataset including various severity scales, a leave-one-out mechanism is applied to verify the accuracy of classification and value the availability of proposed model-based approach.

3.3.3 Validation of EMG Assistance

The inertial sensors are sensitive to body movements, even mild tremors of PD patients. However, for the potential elders at very early-stage of PD, tremors sometimes are too weak to be noticed by both clinician and self-diagnosis, which also causes difficulty in distinguishing tremor from measured inertial signal. Nevertheless, the tremor does exist in the muscles for this situation and they can be clearly detected by EMG signal. EMG measuring is an objective method to assess muscular function, however it is not yet used for clinical PD diagnosis currently (Rissanen et al. (2008)). In order to enhance potential PD diagnosis at early-stage and also verify whether EMG signal could assist to enhance the severity quantification, both EMG and IMU are employed in the second study.

The severity of UPDRS 0 is considered as no tremor in the first study. However, the EMG signal could give another explanation to early-stage PD in the second study. In the second study, severity 0 is divided into 0- and 0+ for more precise classification: severity 0- represents the state of healthy control, and severity 0+ represents the state for early-stage PD resting tremor which cannot be visually monitored. The start of resting tremor is defined, consequently, as the classification from 0- to other state, and the end of resting tremor is the state that goes back to 0- from other state. Therefore, the quantification of resting tremor in the first study can achieve decent PD description with higher HMM training efficiency; whereas in the second study, a more detailed classification can be more persuasive, even though more sensors and sample data are needed for HMM training.

The tremor is always weakened when the muscle gets loaded. Therefore, when the surface EMG is measured, the patients are required to relax and lay the arm over any object that can hold it stable. The reference electrodes are placed on the surface of the Biceps Brachii (BB) muscles and surface EMG signal is measured since both elbow flexion-extension and pronation-supination rotations have direct relation with BB muscles. For measuring the EMG signal when rotating wrist angles, the

electrodes are attached to the surface of extensor carpi ulnaris muscle. The EMG of PD patients has discrepancies in the characteristics from those of healthy subjects, such as magnitude and frequencies. Features of EMG signal are extracted from related character and sent to HMM classifier for training as the procedure in the first study. Besides those selected features, the coherence of EMG and angle changes are analyzed to validate the correlation of muscular movements and tremor.

The application of EMG in PD resting tremor diagnosis is a validation of EMG assistance for inertial technique. More accurate classification and severity estimation are expected for the cooperation of EMG and IMU, whereas EMG electrodes are required to affix to the surface of muscles, which would bring certain bothers to subjects. Although the introducing of EMG could improve the accuracy, the tradeoff between accuracy and convenience is identified. The choice depends on the requirements under various situations. Again, both the first study and the second study can verify the availability of proposed model-based approach in quantifying the severity of PD resting tremor. The study possesses the novelty among current research in this area, even though it is still at the beginning.

3.4 Experiments

In this section, the experimental procedure and results of proposed classification method are presented. The tremor simulation is started by defining three different severities of tremor. Calculated angles of three joints are extracted by applying three aforementioned feature extraction methods. Selected features are used for HMM classification and HMM are validated by leave-one-out technique to verify overall tremor assessment.

Table 3.2: Postures without subject movements

	Tests without movement
T1	Lying on bed
T2	Sitting on chair
T3	Sitting on chair with arm held on table
T4	Standing with hands in rest

Table 3.3: Postures after subject movements

	Tests after movement
T5	Repeat T1, after walk around for 10 seconds
T6	Repeat T2, after nose-touching for 5 times
T7	Repeat T3, after grab a cup and drink
T8	Repeat T4, after lift and extend arms for 5 times

3.4.1 Resting Postures

A sequence of eight tasks are performed by each subject, including four tests without subject's movements (Table 3.2) and four tests after subject's movements (Table 3.3). The postures in the tests are chosen based on routine activities in daily living and it is convincing to estimate the resting tremor of PD patients under a circumstance that similar to our daily life. Before the tests, each subject is asked to get familiar with the tasks and the subject's tremor is evaluated once using UPDRS. Then the subject is asked to perform the four tests in the sequence from test 1 to test 4 and each test holds for 30s. After a rest period of 3-5min, the subject is asked to perform the four tests after doing some movements, such as described in the sequence from test 5 to test 8, with a 30s rest period between each two tests. The later four tests are chosen to evaluate the interference of daily activities to resting tremor. The kinematic data

measured by IMU and the muscular signal measured by EMG are transmitted to computer for processing and feature extraction.

3.4.2 Signal Pre-processing

IMU Measurements

Tremor has to be discriminated from patients' voluntary movements before tremor classification and severity quantification. In the PD patients' movements, the low frequency components ($< 3Hz$) are typically from patients' intentional movements, whereas the high frequency components could consist of different types of tremors and noise. A 20-second long segments of inertial data are chosen from the middle of the 30s test data, which is smoothly recurrent and don't contain sudden changes. Based on the rhythmic frequency range of resting tremor from $3Hz$ to $6Hz$, a band-pass finite-impulse-response (FIR) filter is employed to filter resting tremor signal from kinematic data. This signal pre-processing procedure is applied to calculated joint angles, based on our previous description, from the data measured by accelerometers and gyroscopes on the IMU. Finally, the angle data are processed into overlapping epochs of 3s length with 75% overlap. Subsequent extraction of angle related features are executed in accordance to processed joint angles as data source.

EMG Measurements

The pre-processing procedure for EMG signal is similar to the pre-processing procedure of IMU measurements. Firstly, corresponding 20s long segment of EMG are chosen from the smooth trials during the 30s test data. In order to make typical spikes and bursts for PD-like EMG signals clear to identify, a band-pass FIR filter between $3Hz$ and $12Hz$, is applied to the regular PD-like EMG frequency. The signal segments are also divided into overlapping epochs as for angle signals.

3.4.3 Resting Tremor Simulation

Feature Extraction

In the resting tremor simulation experiments, three different severities of tremor are defined: severity 0, represents healthy control without tremor; severity 1, represents mild tremor, with the frequency around 2Hz ; severity 2, represents severe tremor, with the frequency around 4Hz . A healthy control is asked to simulate these three severities of tremor while the arm is held on a table. For each angle, the subject is asked to sequentially perform the tremor in different severity and each severity lasts for 30s. Finally, 22 segments are captured from elbow flexion-extension and elbow pronation-supination rotations, 25 segments are captured from wrist flexion-extension rotations.

For each angle, three features are extracted and denoted by feature A: angle average change rate; feature B: energy; feature C: spectrum entropy. In Figure 3.4 shows the example of segments of captured elbow flexion-extension angle data and extracted corresponding features A, B and C. On the bottom shows corresponding severities.

Tremor Severity Classification

For tremor severity classification, the leave-one-out cross-validation technique is employed to validate the HMM performance. The training process considers the transition among state 0,1 and 2. The validation is also applied to single feature training HMM, which only uses single feature to classify our data, so that to clearly demonstrate the advantage of using multiple features for HMM training. The performance of the validation is defined as the average accuracy of matching classification states with predefined states of segments. Table 3.4-3.6 present the results of the tremor severity classification of three features trained HMM, including angle name, classification for each class and average classification accuracy. Table 3.7 presents the results of the tremor severity classification of single feature trained HMM,

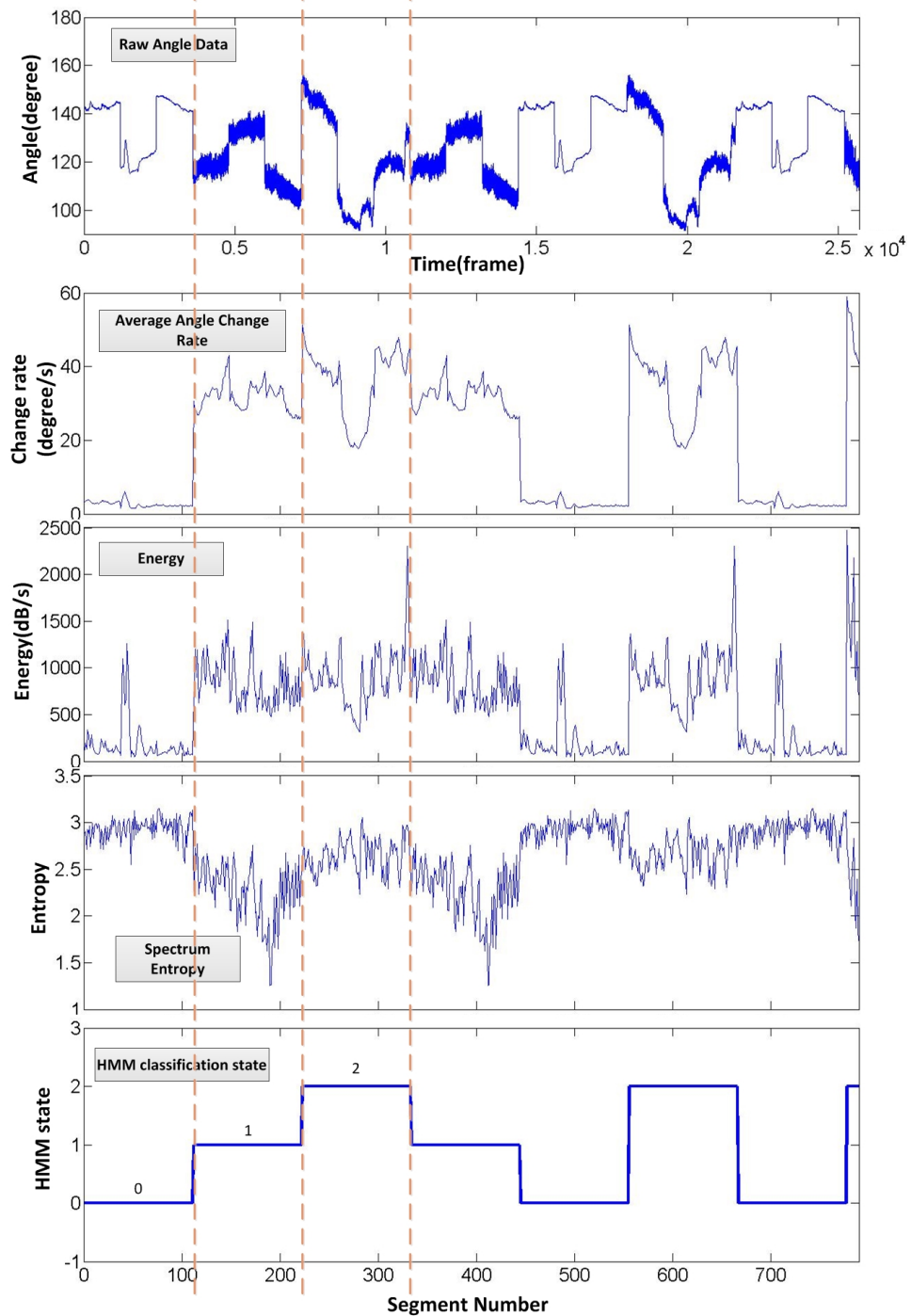


Figure 3.4: Segments of elbow flexion-extension angle data, corresponding features: average angle change rate, energy and spectrum entropy and severities for HMM training.

Table 3.4: Classification results of three features HMM with leave-one-out technique for elbow flexion-extension angle

Elbow-flex	Classified as			Leave-one-out Validation Accuracy per Class
	0	1	2	
0	6993	0	0	100%
1	0	4662	0	100%
2	0	2	4993	99.96%
Overall Accuracy				99.99%

Table 3.5: Classification results of three Features HMM with leave-one-out technique for elbow pronation-supination angle

Elbow-pron	Classified as			Leave-one-out Validation Accuracy per Class
	0	1	2	
0	6993	0	0	100%
1	0	4914	0	100%
2	0	0	4662	100%
Overall Accuracy				100%

including angle name, applying feature and validation average accuracy. Besides, three sets of tremor simulation for each angle are randomly captured without assigned postures for the subject. The angle related features are extracted and classified by trained HMM parameters in previous training. The validation accuracy for all the three angles are 100%.

3.5 Discussion and Summary

A model-based quantification method for assessing the resting tremor in PD is proposed. IMUs are not limited to be attached to certain positions. Elbow and wrist joint angles are calculated based on estimated joint positions in space, which provides

Table 3.6: Classification results of three features HMM with leave-one-out technique for wrist flexion-extension angle

Wrist-flex	Classified as			Leave-one-out Validation Accuracy per Class
	0	1	2	
0	6576	0	0	100%
1	0	4632	0	100%
2	0	3	4557	99.93%
Overall Accuracy				99.98%

Table 3.7: Classification results of single features HMM with leave-one-out technique

Angle	Applying Features	Leave-one-out Validation Average Accuracy
Elbow-flex	Feature A	93.50%
	Feature B	77.92%
	Feature C	97.60%
Elbow-pron	Feature A	96.45%
	Feature B	96.44%
	Feature C	95.05%
Wrist-flex	Feature A	91.78%
	Feature B	89.66%
	Feature C	88.60%

a solution with more robustness and flexibility, compared with current research which uses acceleration and/or angular velocity as raw data. Achieved angles are analyzed and three features are extracted and sent to a HMM for classification. The HMM relies on time-dependent features and forward-backward probabilities of multiple tremor symptoms. Thus, the classification accuracy is high.

More dataset is used for training the HMM, more accurate the new data can be classified. The HMM employed in proposed classifier is discrete, which means that continuous data are divided and sorted into different bins in HMM model. The bin to bin transition probabilities are trained previously. If new input are sorted into the bin that does not have probability to other bins, the classification will have errors. That is why more training data can definitely increase the accuracy of HMM classification. Although in our simulation experiments, each segment has 33 continuous data and totally less than 30 segments are collected for HMM training, the average accuracy is still very high. Therefore, more angle data from different severity and subjects, trained HMM would at least maintain such high classification accuracy. Current misclassifications when validating the HMM occurs only to neighbored classes region, which is difficult even for experienced clinician to discriminate adjacent tremor severities. These misclassifications in our tests, however, are very few, which proves the HMM classifier to be high accuracy for classification.

There are no direct comparisons with the results of current research, due to the differences in choosing dataset materials (subject numbers), classification methods and validation metrics. However, a rough comparison can be obtained. The accuracy of tremor recognition in the work of Salarian et al. (2007) is summarized by sensitivity and specificity, which are 99.5% and 94.2% in comparison to a video reference; the tremor correlation to the UPDRS is $r=0.87$ and bradykinesia correlation is $r=-0.83$ by Pearson correlation. Patel et al. (2009) implement a support vector machine for classification and use estimation error to define the performance, which is 2.5%. In the work of Rigas et al. (2012), a HMM is also implemented to classify both resting and action tremor, and the overall accuracy is 87% in correlation with UPDRS.

Developing a reliable and convenient quantification approach for PD symptom is considerably important from the clinical point of view. It can be used for in-lab evaluation, off-line follow-up and remotely monitoring the progression of PD after therapy. Proposed new approach may change the clinician's concentration from short term in-lab observation to long term assessment during our daily life, since the fact that PD symptoms vary throughout the day. In addition, developed IMU is small, low energy consumption and accessible for capturing daily motions. Thus, it is potentially useful for home, outdoor and clinical environments to evaluate the progression of PD. Proposed model-based quantification approach can make the diagnosis of resting tremor more flexible.

In the future work, both inertial information and EMG of PD patient are going to be measured for the quantification of resting tremor. For early stage PD or potential PD monitoring, the timely diagnosis would be helpful for clinician to assess the evolutive disease and make early decision for treatment.

Chapter 4

Model-Based Quantification of Lower Extremity Bradykinesia

Abstract

This chapter presents a model-based quantification approach for bradykinesia by assessing the motor functions of lower extremity. Bradykinesia is one of the most apparent symptoms of Parkinson's disease. It mainly affects patients' motor function by impairing limb motor functions, which also could cause many related problems. Currently, a lot of research is focusing on the quantification of upper limb bradykinesia by using inertial sensors to analyze certain motions and also focusing on patients' gait using specialized tools. However, very little research is working on lower extremity bradykinesia, which affects human motor ability the most. Therefore in this chapter, we focus on the quantification of lower extremity bradykinesia. A human body motion tracking system is utilized to build a human body model. The joint rotations around different axis are closely correlated with others within the network, so that the estimation of joint angles is robust to the contamination from human intentional movements and gravity component. Patients with different symptom severities suffer from variable degrees of leg joint bending. Therefore, the rotation angles of hip and knee joints are estimated for quantification. Features that best describe the angle character are selected and extracted. A discrete HMM classifier is trained by features and corresponding clinical ratings. The accuracy of classification is cross-validated by leave-one-out mechanism. Since the feature discrepancy of bradykinesia and healthy subjects in walking is distinct, high classification accuracy of preliminary results proves that proposed objective approach is feasible in quantifying lower extremity bradykinesia.

4.1 INTRODUCTION

Bradykinesia is usually regarded as the most apparent symptom of PD. It is defined as the abnormal slowness of movement and it not only affects the upper and lower limb motor functions (Kim et al. (2011); Jun et al. (2011); Salarian et al. (2007)), but also patients' gait and body posture during walking through the whole stage of PD (Heldman et al. (2012); Koop et al. (2008); Louie et al. (2009)). The traditional way to assess how bradykinesia impacts on the daily life of PD patient is performing a quantification of bradykinesia. Based on the dominant appearance, the quantification of bradykinesia can be focusing on the motor functions of impaired limb and/or gait with various observations and measurement tools.

It is necessary to accurately assess the motor symptoms for diagnosis, treatment and continuous monitoring of pathologic development. Currently, the most widely used clinical rating scale for evaluating PD motor disability, is part III (motor disability score) of the Unified Parkinson's Disease Rating Scale (UPDRS-III), which rates a range on 0-none, 1-minimal, 2-mild, 3-moderate, and 4-marked scale. However, it relies on subjective experiences of a clinician and the patients' physical conditions during the time visiting a clinic. An objective quantification method for persistent monitoring and quantifying bradykinesia can be of great help in the diagnosis of PD.

Current studies have been focusing on using gyroscope sensor to measure the rotation of human limb for bradykinesia quantification because it tolerates the effects of gravity. The assessment of upper limb bradykinesia during forearm (wrist) pronation-supination rotation is well studied. The quantification applies root-mean-squared angular velocity in the work of Jun et al. (2011); Salarian et al. (2007); Koop et al. (2008); Louie et al. (2009), measured by a gyro sensor attached to the dorsal part of the distal forearm. The authors instruct their subject to pronate and supinate their hands repetitively as large amplitude and fast as possible for short term tests (less than 30 s). Besides angular velocity, rotation angle integrated from angular velocity is also estimated as a performance parameter for quantification (Jun

et al. (2011); Salarian et al. (2007)). Such as in the work of Kim et al. (2011); Koop et al. (2008); Louie et al. (2009), the quantification of bradykinesia is conducted by assessing tapping velocity, angular velocity and integrated finger angle in finger tapping task. These performance parameters are statistically analyzed and evaluated by the correlation with bradykinesia score rated by clinicians.

Impaired gait is a typical manifestation of PD bradykinesia. Human motion tracking systems are capable of quantifying impaired gait of PD patients, e.g. mechanical tracking and optical tracking. However, these systems are not designed for home use due to their system complexity and pricy cost. Applying sensors to quantify gait is a more flexible and less cumbersome way to subjects. Actigraph system, such as *Nike+* in shoe sensor, is focusing on recording overall activities and calculate user steps approximately. However, this sensor cannot analyze abnormal gait. Other sensor, such as pressure sole, has been employed to quantify abnormal gait by analyzing the change of center of gravity. However, quantifying PD bradykinesia only from gait is indirect, because the gait of PD patients is closely correlated with the motor function of lower extremity.

Presently, there is very little research on quantifying lower extremity bradykinesia using body sensors. It provides a good opportunity to explore the availability of using wearable sensors for the quantification of bradykinesia. Heldman et al. (2012) place a motion sensor unit on the heel of subject and four motor assessment tests (toe-tapping, leg agility, gait and freezing of gait) are executed. Angular velocity, integrated angle, integrated linear velocity and corresponding task time are calculated as quantitative features and used to develop multiple linear regression models for predicting motor scores. The deficiency of this study is the lacking of quantified analysis for leg joints when quantifying lower extremity bradykinesia. As a matter of fact, bradykinesia impacts the motor function of PD patients on leg movement gradually and further on patients' gait. Thus, using body sensors to directly assess leg movement performs better in quantifying lower extremity bradykinesia.

Related research also includes the posture of trunk, which has close correlation with different stages of PD and severities of bradykinesia. Several studies have researched on the posture stability of PD patients with instrumented balance analysis (*e.g.* force platform) or more advanced posture analysis with body sensors (Maetzler et al. (2012); Palmerini et al. (2011); Blaszczyk and Orawiec (2011)). In those works, the analysis of posture and stability needs subjects in quiet standing and to follow some sway protocols. Sway related parameters are measured by an inertial sensor attached to lower back. However, the posture of trunk can be considered from a different point of view other than the standing stability analysis. In the early stage of PD, the posture of bradykinesia patient appears very little differences from healthy control, but the trunk leans forward as the symptom progresses during standing and walking (Palmerini et al. (2011)). It proves that PD patients with higher severity are highly risky to fall (Blaszczyk and Orawiec (2011)). The trunk posture could help quantify bradykinesia and besides, the trunk leaning forward could happen to healthy control with humpback. Thus, trunk posture can be a predictable way for many situations, such as discriminate bradykinesia and detect falling.

None of existing approaches to bradykinesia quantification consider the concurrent motions of adjacent body segments, because they merely analyze single joint/segment by single inertial sensor. However, for human limb bradykinesia, a thorough quantification of all adjacent joints will be more efficient. In Chapter 2, a body motion tracking system is developed, which correlates multiple wireless IMUs mounted on the body segments to build a body model for motion tracking. This model-based technique allows IMUs to be arbitrarily placed on body segments and it is unnecessary to know their position in advance. Besides tracking single body segment and estimating its motor function, it also makes it feasible to analyze the relationship between any segments of the model. The model parameters such as joint positions in global frame and angle between body segments can be estimated easily. Therefore, a model-based approach for quantifying bradykinesia from lower extremity is introduced in this chapter.

PD patients with lower extremity bradykinesia suffer from impaired leg motor ability. The proposed model-based quantification approach is capable of estimating the rotation angle of hip and knee joints according to updated position and orientation of thigh and shank segments in the global frame. Since higher step frequency and shorter step length are the representative behavior for discriminating lower extremity bradykinesia from other PD symptoms, angle and frequency-spectrum based features are consequently chosen for quantification: average angle change rate, energy and entropy of both knee and hip joint angle. Selected features can best describe low extremity bradykinesia characters. Extracted features are correlated with UPDRS-III scores that rated by clinician and they are used for training classifier for future classification of new data. Model-based approach provides an effective and convenient quantification solution that overcomes the limitation of current subjective observations in labs. Moreover, the wireless capability of applied tracking system can upload monitored data to the database, which enables the remote diagnosis and clinician-patient interactions.

4.2 Human Lower Extremity Modeling and Joint Angle Estimation

4.2.1 Human Lower Extremity Modeling

For bradykinesia in PD, the impairment of motor function on lower extremities affects the daily living of patients more than upper extremities. Therefore, lower extremities are chosen for modeling and analysis. A human lower extremity (leg and foot) can be modeled as a kinematic chain comprises three segments (thigh, shank and foot) and three joints (hip, knee and ankle). It has five rotational Degrees of Freedom (DoFs), as are shown in Figure 4.1: hip has three (flexion-extension α_{18} , internal-external α_{19} and abduction-adduction α_{20}), knee has one (flexion-extension α_{21}) and ankle is considered as 1-DoF joint (flexion-extension α_{22}). In this chapter, patients' gait does

not covered in the research and ankle rotation is excluded. Correspondingly, two IMUs are mounted on the front thigh near knee and on the front lower shank near ankle, for hip and knee joint. According to our previous research, those positions are considered to have less effect from soft tissue artifact.

A global frame \mathbb{R} is defined and the rotations of hip coordinate Σ_{hip} are captured within \mathbb{R} . As the adjacent joint of hip, knee coordinate Σ_{knee} only considers its rotation corresponding to Σ_{hip} , so that rotations of knee joint are closely related to the hip joint's position and the inertial data from IMU of knee frame are closely correlated with hip mounted IMU's output. Ankle joint position is related to both knee joint position and the posture of shank rotating around knee joint. The absolute angles of hip and knee are estimated from the actual posture of connected body segments within \mathbb{R} . The absolute angle of hip is estimated by the spacial posture of lower trunk and thigh and the angle of knee is estimated by the spacial posture of thigh and shank. During walking, lower trunk is assumed to be vertical. IMUs are attached to body segments and, therefore, directly measure segment orientation generated by combined movements from all the prior joints.

Joint motions are captured by corresponding IMU and the joint quaternion \mathbf{q} computed inside the IMU is outputted for representing 3D rotations. Quaternion provides a convenient mathematical notation for representing orientations and rotations of objects in 3D. Quaternion-based rotation representation is adopted in view of its superiority, compared to Euler angles they are simpler to compose and avoid the problem of singularities (gimbal lock), and compared to rotation matrices they are more numerically stable and more efficient. Any rotation in three dimensions can be represented as a combination of an axis vector and an angle of rotation. Quaternion gives a simple way to encode this axis-angle representation in four numbers and apply the corresponding rotation to a position vector representing a point relative to the origin in \mathbb{R}^3 . It is a vector quantity of the form

$$\mathbf{q} = q_0 + q_1\mathbf{i} + q_2\mathbf{j} + q_3\mathbf{k} = (q_0, \vec{q}) \quad (4.1)$$

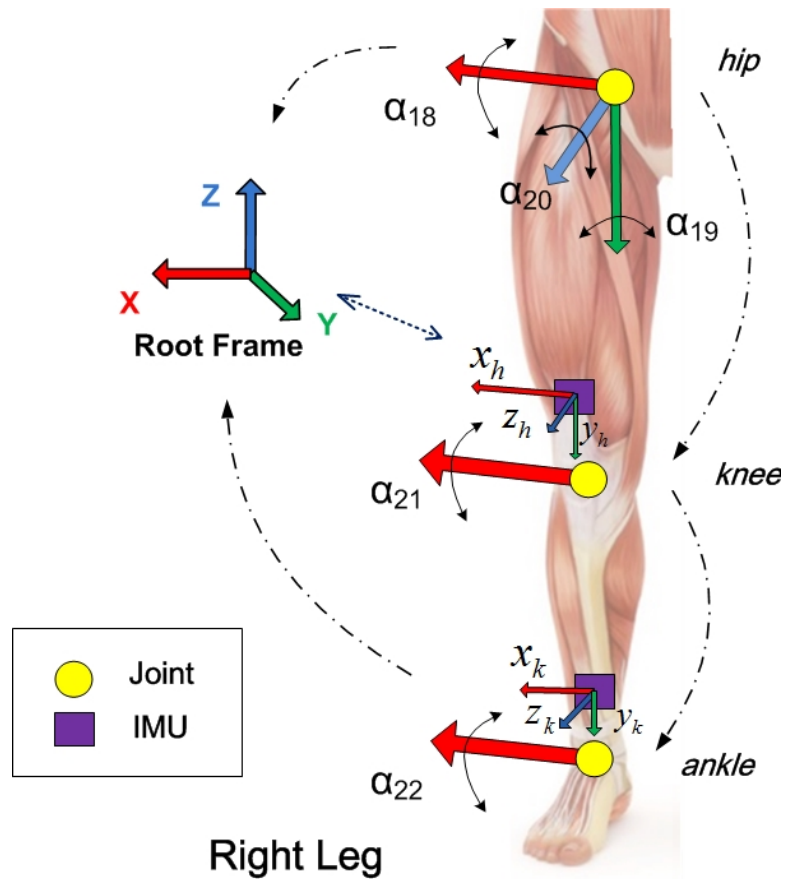


Figure 4.1: Kinematic modeling of a human lower extremity

where i, j and k are basis elements of a quaternion, q_0 is the scalar component of \mathbf{q} and $\vec{q} = (q_1, q_2, q_3)^T$ is the vector component. Given that $\omega = [\omega_1, \omega_2, \omega_3]^T$ represents the unit axis of rotation and $\theta \in \mathbb{R}$ represents the angle of rotation about ω , another form for quaternion is as $R\mathbf{q} = (\cos(\theta/2), \omega \sin(\theta/2))$. Thus, the corresponding rotation is extracted by setting

$$\theta = 2 \cos^{-1} q_0 \quad , \quad \omega = \begin{cases} \frac{\vec{q}}{\sin(\theta/2)} & \text{if } \theta \neq 0, \\ \mathbf{0} & \text{otherwise,} \end{cases} \quad (4.2)$$

The rotation angles of hip joint α_{18}, α_{19} and α_{20} and knee joint α_{21} are expressed by measured quaternion $H\hat{q}$ for hip frame and $K\hat{q}$ for knee frame. Two quaternions interpret the movements of two lower extremity joints. Applying quaternion achieves high computational efficiency, instead of traditionally applying the product of several rotational matrixes, such as from $R(\alpha_{18})$ to $R(\alpha_{21})$ for expressing rotations of lower extremity.

4.2.2 Angle Estimation of Leg Joints

By updating quaternions of each joint during the movements, their rotation angles around each axis can be decomposed from updated quaternions. However, mounting an IMU on human body acts more random than to follow any strict regulations and the orientation of mounted IMU could be in any direction. Thus, in order to reliably measure the rotations of joint, IMU orientation is calibrated, and the mapping relationship between IMU and joint coordinate is calculated for later transformation. A calibration procedure is designed in our previous research to estimate the IMU orientation, no matter how a subject mounts it to the body.

IMU shares the same coordinate with \mathbb{R} , which is an essential prerequisite. Before mounting IMUs on the body, a human initial posture is required for both mounting IMUs and coupling local joint frames to \mathbb{R} . When an IMU is mounted, its orientation with respect to (*w.r.t.*) \mathbb{R} is calculated from inertial output. Compared with

corresponding joint frame, a rotational transformation is generated and represented by ${}_X^Y q$, which denotes the quaternion representation of rotational relationship from X frame to Y frame. Thus, during tracking the leg motions, quaternion of each joint is updated by a product of corresponding IMU quaternion and their relationship quaternion.

Initially, IMUs are calibrated within \mathbb{R} . After being attached to the leg, their orientation measurements are rotated from initial orientation ${}_{\mathbb{R}} q_0$ to ${}_{IH} \hat{q}$ for the IMU corresponding to the hip and ${}_{IK} \hat{q}$ for the IMU corresponding to the knee. During this process, the subject is asked to stand still as pre-defined posture in order to mount the IMUs and calibration. The local coordinate of the hip and knee refer to \mathbb{R} are initially defined as ${}_{\mathbb{H}} q_{initial}$ and ${}_{\mathbb{K}} q_{initial}$ for the initial posture. The rotational relationship quaternion ${}_X^Y q$ between local joint coordinates and their corresponding IMU orientations are shown as

$$\begin{aligned} {}_{IH}^H q &= {}_{\mathbb{H}} q_{initial} \otimes {}_{IH} \hat{q}^* \\ {}_{IK}^K q &= {}_{\mathbb{K}} q_{initial} \otimes {}_{IK} \hat{q}^* \end{aligned} \quad (4.3)$$

where IH and IK denote the corresponding IMUs for hip joint and knee joint. The quaternion product \otimes is used to describe compounded orientations, which is based on the Hamilton rule Horn et al. (1988), and ${}_a^b q^* = {}_b^a q$ denotes the conjugate of a quaternion ${}_a^b q$. The relationship quaternion ${}_{IH}^H q$ and ${}_{IK}^K q$ will be used for updating real-time rotation measurements of thigh around hip ${}_{\mathbb{H}} \hat{q}$ and shank around knee ${}_{\mathbb{K}} \hat{q}$ joint:

$$\begin{aligned} {}_{\mathbb{H}} \hat{q} &= {}_{IH}^H q \otimes {}_{IH} \hat{q} \\ {}_{\mathbb{K}} \hat{q} &= {}_{IK}^K q \otimes {}_{IK} \hat{q} \end{aligned} \quad (4.4)$$

Lower extremity bradykinesia gradually impacts motor function of lower extremity. When the symptom gets worse, the patient is suffering highly bended joint

during walking and in difficulty to stand up caused by hip rotation. Based on this, two rotation angles are measured for feature extraction and quantification, which are hip flexion-extension and knee flexion-extension. In order to avoid the impact of rotation superposition on estimating Euler angles directly from quaternion, hip angle is calculated from intersection angle between lower trunk and thigh, knee angle is between thigh and shank. The estimation of joint position and segment posture are described below.

The assumed position of the hip (H) joint is ${}^R\hat{P}_H$ and the translational calculation from hip to knee (K) p_{HK} is achieved by combining ${}^R\hat{P}_H$ and initial spacial relationship of knee relative to hip ${}_0p_{HK}$ within Σ_{hip} :

$$p_{HK} = {}^R\hat{P}_H + {}_0p_{HK} \quad (4.5)$$

As the subject moves, the quaternion of hip-IMU (short for the IMU corresponding to hip) ${}^R_H\hat{q}$ is continuously updated. With hip measurements are calculated, the knee joint position can be updated by:

$$\begin{aligned} \theta_H, \omega_H &\leftarrow {}^R_H\hat{q} \\ \{\theta_H, \omega_H, p_{HK}\} &\xrightarrow{\text{exp map}} {}^R\hat{P}_K \end{aligned} \quad (4.6)$$

where ${}^R\hat{P}_K$ denotes updated knee position within \mathbb{R} .

For adjacent shank segment, the updated knee position is ${}^R\hat{P}_K$ and the translational calculation from knee to ankle (A) p_{KA} is achieved by:

$$p_{KA} = {}^R\hat{P}_E K + {}_0p_{KA} \quad (4.7)$$

Then, the position of ankle joint can be updated by:

$$\begin{aligned} \theta_K, \omega_K &\leftarrow {}_K\hat{q} \\ \{\theta_K, \omega_K, p_{KA}\} &\xrightarrow{\text{exp map}} {}^R\hat{P}_A \end{aligned} \quad (4.8)$$

The rotations of two joints of leg are represented by $\{\theta_H, \theta_K\}$ and their corresponding twists are $\{\hat{\xi}_H, \hat{\xi}_K\}$. The exponential map for twists of each joint is in the form of $e^{\theta\hat{\xi}}$ and the connection of joints is demonstrated by product of all joints' exponential maps:

$$\prod_{i=H}^K e^{\theta_i \hat{\xi}_i} = e^{\theta_H \hat{\xi}_H} \cdot e^{\theta_K \hat{\xi}_K} \quad (4.9)$$

and if we let $g_{knee,ankle}(0)$ represent the initial configuration of ankle *w.r.t.* knee joint, the final configuration of ankle *w.r.t.* hip $g_{hip,ankle}$, connected by rotation angles $\Theta = (\theta_H, \theta_K)$ is given by

$$\begin{aligned} g_{hip,ankle}(\Theta) &= \prod_{i=H}^K e^{\theta_i \hat{\xi}_i} \cdot g_{knee,ankle}(0) \\ &= \exp\left(\sum_{i=H}^K \theta_i \hat{\xi}_i\right) \cdot g_{knee,ankle}(0) \end{aligned} \quad (4.10)$$

The final configuration contains the position of the target joint. Thus, once the knee and ankle joint position are achieved, our interested hip flexion-extension and knee flexion-extension angles are easily estimated.

4.3 Model-based Bradykinesia Quantification

4.3.1 Bradykinesia Feature Selection

Model-based bradykinesia quantification approach is another practical application of developed human body motion tracking system. A trunk and lower extremity model is reconstructed from the exponential maps of connected body segments, as introduced in Section 4.2, whose twist movements are captured and measured by IMUs mounted on the segments. Developed motion tracking mechanism is advanced by its robustness to IMU placement, which means the reconstruction of human model can be achieved regardless of the placement and orientation of corresponding IMU (to the joint).

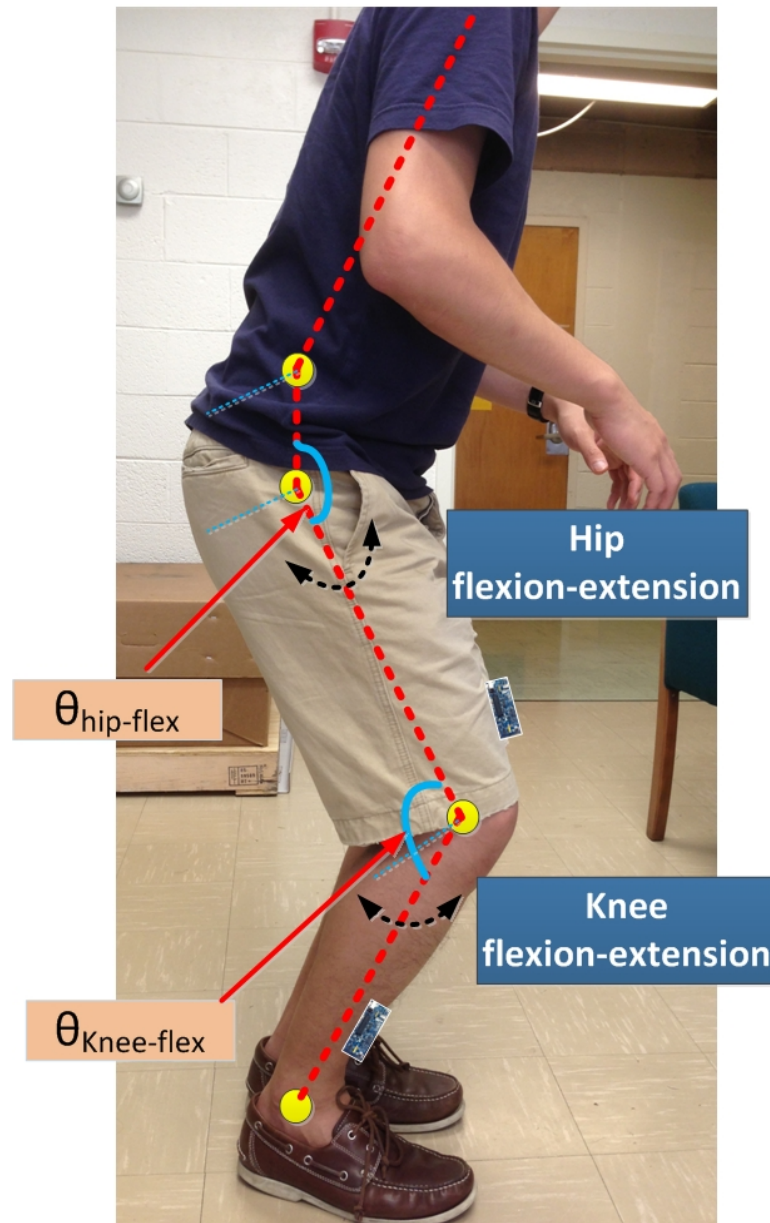


Figure 4.2: Two rotations of lower extremity used for extracting bradykinesia features

An IMU provides acceleration a , angular velocity ω and quaternion q of leg segments. The quaternion representation can properly represent the twist motion of each joint, therefore, the quaternion of hip joint ${}^H\hat{q}$ and knee joint ${}^K\hat{q}$ are employed and to estimate the position of knee and ankle joint. As are shown in Figure 4.2, hip flexion-extension $\theta_{hip-flex}$ and knee flexion-extension $\theta_{knee-flex}$ are the interested angles for monitoring and quantifying bradykinesia. The quaternion representation is capable of estimating the 3D rotations of corresponding joint, and if needed, each involved angles can be decomposed from quaternion to analyze separately. Aiming at those two concerned angles, features for quantification are mainly selected and extracted from angle related parameters.

Angle Related Features

Bradykinesia in PD is characterized by higher step frequency and shorter step length than healthy control, induced by impaired motor function of lower extremity. Refer to these characters, rotary angle of corresponding segments are calculated and directly segmented for feature extraction. The angle data is divided into a 3s duration window and 75% overlapping. Using moving window technique considers that a shorter window would bring heavy computation and a longer window, in the opposite, would reduce the resolution and accuracy of extraction.

Three angle related features are extracted from the angle data, as listed below. Among the features, 1 is angle-based feature; 2 and 3 are frequency-spectrum based features, which are extracted from the frequency-spectrum of the signal using the fast Fourier transform. In order to remove the effects from tremor and high frequency noise, the concentrated frequency for low extremity bradykinesia is 1-3Hz and for healthy control is 0.3-1Hz for normal walking.

1. Average angle change rate:

The average change rate of angle ($^{\circ}/s$) calculates the average changes of relative joint angle between two connected body segments in a certain time. It is defined

as

$$\bar{\theta} = \frac{\theta(i+1) - \theta(i)}{1/f} \quad (4.11)$$

where f is the frequency of the signal.

2. Angle change energy:

Bradykinesia behaves as higher frequency but lower amplitude than healthy control when leg segments rotating around joints, thus, the energy (unit: dB/s) is considered as a feature. From the frequency-spectrum of the signal, the energy is given as

$$E = \frac{1}{2} \sum f P(f) \quad (4.12)$$

where $P(f)$ is signal spectrum. It is expected to be lower for patients with bradykinesia than for healthy controls.

3. Spectrum entropy:

The high energy concentration in specific frequency also reflects the character of signal. Thus, the spectrum entropy H is calculated as follows:

$$H = - \sum_f p(f) \log p(f) \quad (4.13)$$

where $p(f) = \frac{P(f)}{\sum_f P(f)}$. The entropy measures the negative natural logarithm of the conditional probability that two sequences in a signal that are similar for m points are similar for $m+1$ points. For the pure sine wave, it closes to 0. Thus, it is expected to be lower and closer to 0 for healthy controls than patients with bradykinesia.

The severity of PD bradykinesia correlates with the amplitude and frequency of the joint rotation. The three features can commendably describe the character of bradykinesia for lower extremity, and the feature vector is defined as:

$$F = [\bar{\theta}, E, H] \quad (4.14)$$

Two angles, $\theta_{hip-flex}$ and $\theta_{knee-flex}$, which rotate about hip and knee joint are utilized. Corresponding $F_{hip-flex}$ and $F_{knee-flex}$ are calculated. Lower extremity angle are extracted three angle related features for each 3 seconds segment, and if monitored signal lasts for 20 seconds, then there are 23 segments and the total features are $2 \times 3 \times 23 = 138$. For PD patients, extracted features clearly describe the symptom compared with healthy control, and it guarantees the needs for classifying their bradykinesia symptom and keeping low computational complexity for quantification.

4.3.2 Bradykinesia Severity Classification

Classified features are correlated with the comprehensive score of UPDRS III for quantification. The feature vector which contains features of both healthy control and subjects with different severities are sent to HMM for training. Their corresponding UPDRS (as in Table 4.1) are sent to HMM as observation states. After training the HMM, dataset are randomly merged with leave-one-out mechanism to validate the performance of HMM classification. By going through all the dataset and leaving each subject outside the dataset once, total results are averaged.

Table 4.1: UPDRS of bradykinesia

0	None
1	Minimal slowness
2	Mild degree of slowness
3	Moderate slowness
4	Marked slowness

Many research in this field apply heuristic rules to classify bio-signal, such as decision tree and fuzzy logic, or apply statistical rules, such as discriminant analysis, k-NN and HMM. HMM is a statistical model that can better describe the characteristics of time dependent signal and can be well characterized as a parametric

random process. It preserves structural information of characteristic signal and no thresholds used by the heuristic rules are needed. The supervised studying mechanism enables HMM to learn new model and optimize current classification strategy based on its intrinsic probability-based discrimination. Therefore in our research where multiple features are requested for classification, HMM is chosen because of its adaptation.

A HMM is defined by a brief triplet $\lambda = (A, B, \pi)$, where A is the matrix of state-transition probabilities, B is observation probabilities and π is the vector of initial state probabilities. Classic Baum-Welch algorithm is adopted to estimate HMM parameter by maximizing the likelihood $P(O|\lambda)$ using an iterative procedure. Viterbi method is chosen to find the most likely state sequence in the model that produces the observations and optimize the model construction.

In order to train the HMM to make general use for different patients, a discrete HMM trained by multiple features is proposed as Figure 4.3 shows.

The state space consists of 5 patterns: 0-4, which represents the severity from scale 0 to scale 4. The state transitions are equiprobable and the classification result is mainly determined by the observation probability, which is obtained through calculating the probability of particular output sequence. In the training process, we only consider possible state transitions, such as the direct transitions between scale 0 (no visible tremor) and other scales (0-1, 0-2, 0-3, 0-4), the transitions between neighbor scales (0-1, 1-2, 2-3, 3-4). Even though in practice, the data extracted from a period of time mostly belong to one state, it is practical to take the transitions between different scales into consideration, since the purpose of developed system is for long term monitoring but short term in-lab observations.

The severity classification can be considered as a decoding procedure. Each moment a transition from scale 0 to other scale begins, it is noted as the start of the symptom; similarly, the end is defined as the moment that other scale returns to scale 0. Corresponding features from a subject's measurements are selected for the HMM and marked with the severity scale that estimated professionally by a clinician.

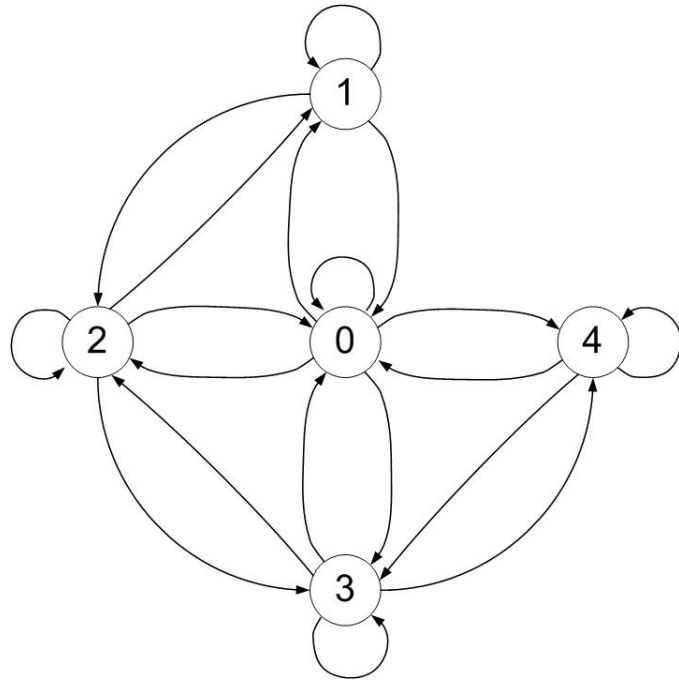


Figure 4.3: HMM for bradykinesia classification

After fulfilling the HMM training with dataset including various severity scales, a leave-one-out mechanism is applied to validate the classification and evaluate the availability of proposed model-based approach.

4.4 Experiments

In this section, the experimental procedure and results of proposed classification method are presented. The simulation of lower extremity bradykinesia is started by defining two different cases: none and moderate. Calculated angles of two joints (hip and knee) are extracted by applying aforementioned feature extraction methods.

Selected features are used for training HMM classifier, which is followed by leave-one-out validation to assess the model-based quantification.

4.4.1 Experimental Design

The task performed for quantification of bradykinesia is walking. Before the test, each subject is asked to get familiar with the task and his/her bradykinesia is evaluated once using UPDRS III. After mounting the IMUs on the body and calibration process, the subject is asked to stand and then walk four yards forward and stop. For each subject, the walking data from the test are used to train the HMM for walking with corresponding scale as the observation state. The subjects involved in the tests include healthy subjects and bradykinesia subjects. The purpose of the task is using model-based approach to discriminate PD patients with different severities of bradykinesia from healthy control and to quantify bradykinesia from lower extremity.

4.4.2 Signal Pre-processing

Our model-based approach can estimate the angle of lower extremity joints during walking. The frequency-spectrum signal for feature 2 and 3 is pre-processed by a bandpass filter to eliminate high frequency noise and the frequency of involuntary movement, such as tremor. The main frequency range for lower extremity bradykinesia had not been reached a consensus, since very little research in this field. Referred to the observation of patient's walking from videos who is suffering bradykinesia, the frequency is higher than healthy control ($0.3-1Hz$) and about in the range of $1-3Hz$, verified by simulated walking. A clear evaluation of bradykinesia could be achieved if tremor signal ($3-12Hz$) can be removed from the signal. Erroneously applying bandpass filter would remove valuable information, thus the chosen of filter range for lower extremity bradykinesia is $1-3Hz$. Once removed, the tremor would not impact on our quantification results.

4.4.3 Bradykinesia Simulation

Feature Extraction

The bradykinesia simulation tests the walking of healthy controls and moderate bradykinesia patients. Two healthy controls are asked to simulate the walking of a PD patient with moderate bradykinesia and also perform the walking of a healthy control with normal speed. Subjects are asked to stand first and walk four yards forward and stop. Each subject simulates bradykinesia walking twice and normal walking once. For each joint, 29 segments are captured from two subjects' simulation data, which contains 1358 samples. In these segments, 19 segments are from simulated bradykinesia and 10 segments are from normal walking. Since the angle data from both hip and knee joint are sampled at the same time, the total of 58 segments is processed. Figure 4.4 show a screenshot of the video taken during the test and concurrently reconstructed human motion by developed motion tracking system.

For each angle, three features are extracted: angle average change rate, energy and spectrum entropy. Figure 4.5 and Figure 4.6 show the segments of captured joint angle data and extracted features. On the bottom are corresponding severities for HMM training.

Bradykinesia Severity Classification

For bradykinesia severity classification, the leave-one-out cross-validation technique is employed to validate the HMM performance. The training process considers the transition among state 0 and 1. The validation is also applied to single feature training HMM, which only uses single feature to classify our data, so that to compare with training HMM using multiple features. The features we selected for extraction from angle data can clearly describe the characteristics of healthy control walking and bradykinesia walking, and discrepancies in angle-related features can be expected: the symptoms of lower extremity bradykinesia during walking is higher frequency, smaller joint angle and smaller step length, meanwhile, the features are based on

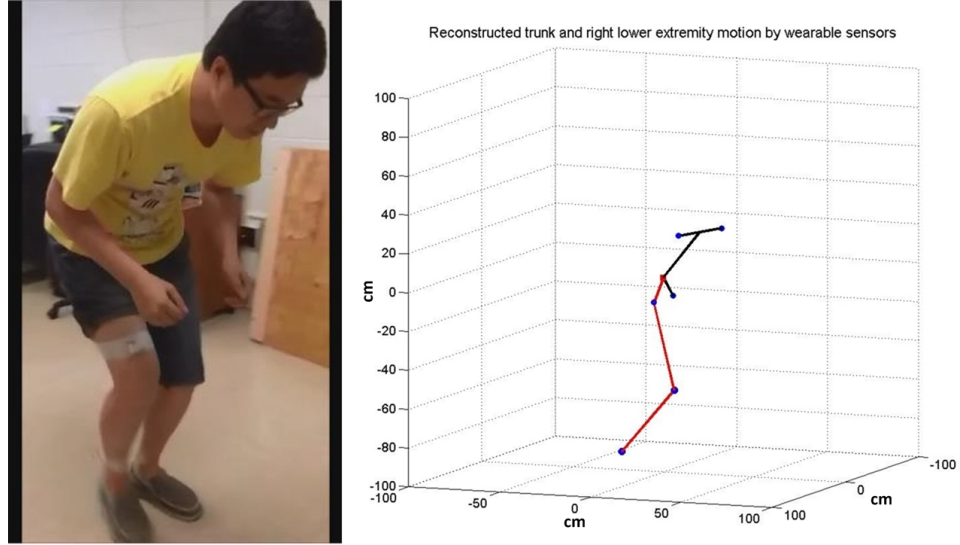


Figure 4.4: A screen shot of the video during the test and concurrently reconstructed body motions

frequency-spectrum and change rate of angle. The pertinent features guarantee the efficiency of classification and its high accuracy.

The performance of validation is defined as the average accuracy of matching the classification states with predefined states of segments. The results of the bradykinesia severity classification, by validating simulated data from both hip joint and knee joint, achieve 100% accuracy. Benefit from appropriate features, in our tests, the single feature trained HMM also achieves 100% accuracy for classification, as in Table 4.2 presents.

4.5 Discussion and Summary

In this chapter, a model-based quantification approach for classifying and assessing low extremity bradykinesia of PD patients is proposed. The model-based approach

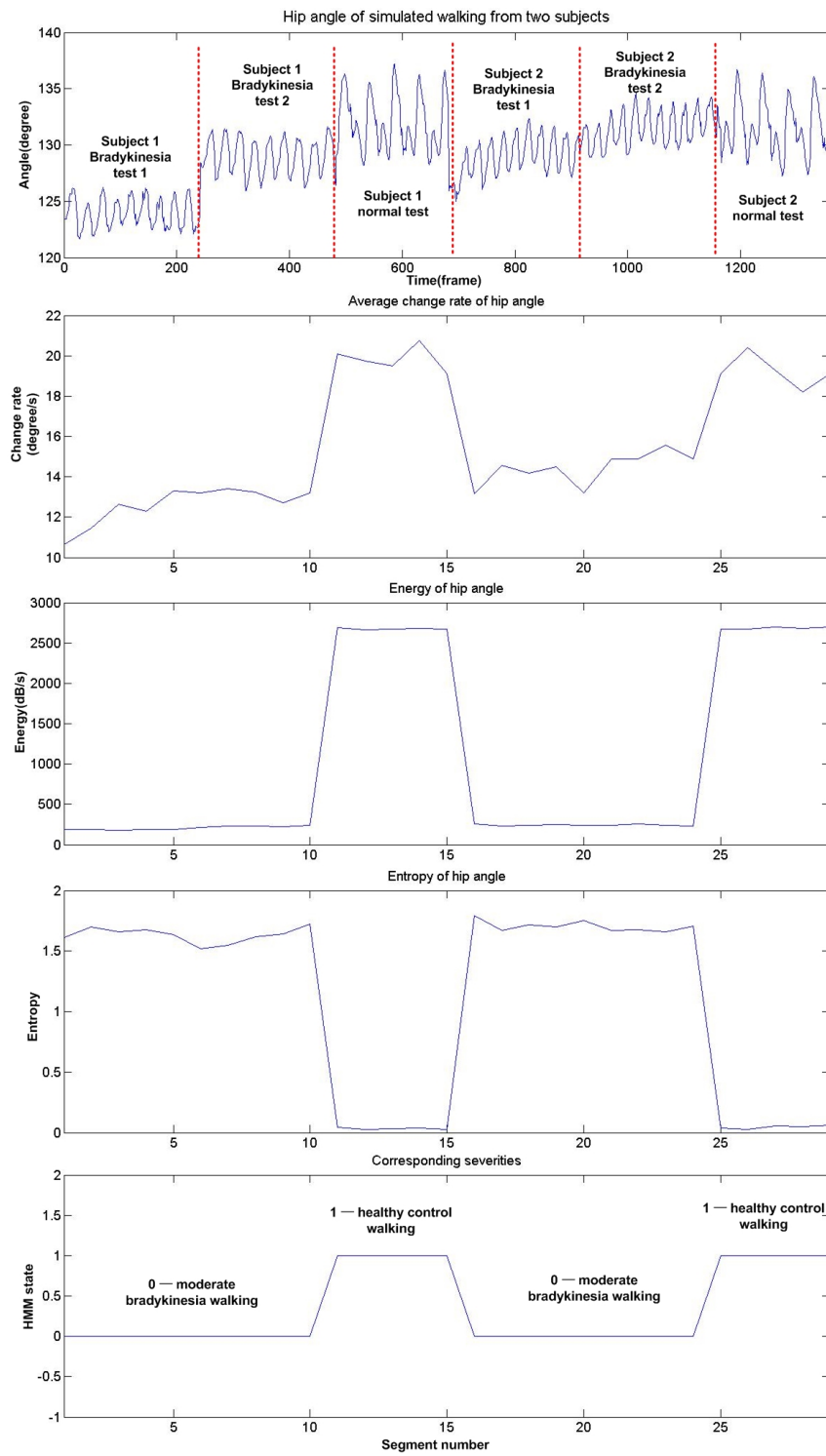


Figure 4.5: Segments of hip joint angle data, extracted three features and corresponding severities for HMM training.

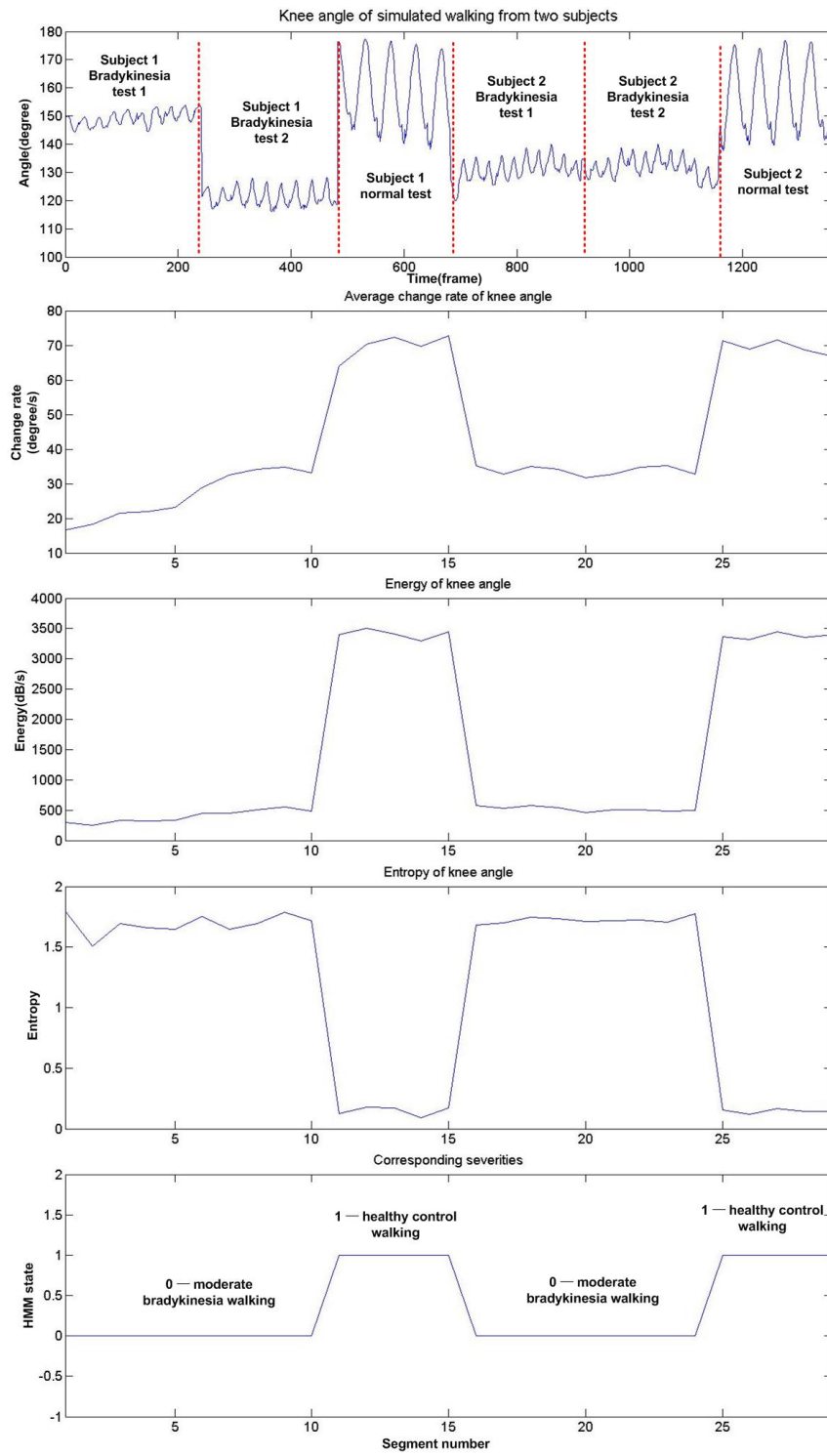


Figure 4.6: Segments of knee joint angle data, extracted three features and corresponding severities for HMM training.

Table 4.2: Classification results of three features HMM with leave-one-out technique for hip and knee joint angle

<i>Hip</i>		Classified as		Leave-one-out Validation Accuracy per Class
Class	0	1		
0	957	0		100%
1	0	401		100%
Overall Accuracy				100%

<i>Knee</i>		Classified as		Leave-one-out Validation Accuracy per Class
Class	0	1		
0	957	0		100%
1	0	401		100%
Overall Accuracy				100%

is advanced for its robustness to the arbitrary placement of IMUs, since a human model can be reconstructed and it does not limit the attachment of IMUs to certain positions. It simplifies the setup of the system without losing accuracy. Moreover, it provides clear information about joint motions and spatial correlation between body segments of a human model. Compared with current research which regularly uses acceleration and/or angular velocity as raw data, model-based approach estimates the joint angles based on updated neighbor joint position, which could neglect the impact from ambient noises, such as gravitational component and other intentional body movements. Estimated angles are analyzed by extracting three angle-related features which best describe the signal characteristics and sent to a discrete HMM for training and classification. HMM classification results correlate with clinical UPDRS to evaluate and quantify the severity of bradykinesia. In our simulated tests, appropriate features and HMM classifier conduce to high classification accuracy.

If the HMM is trained with a larger dataset, the new data can achieve more accurate classification. The HMM employed in proposed classifier is discrete, which means that continuous data are divided and sorted into different bins in HMM model.

The bin to bin transition probabilities are trained previously. If new input are sorted into the bin that does not have probability to other bins, the classification will have errors. That is why more training data can definitely increase the accuracy of HMM classification. Besides, it is apparent that choosing appropriate features can reduce the bin numbers when training the HMM classifier, thereby increasing the efficiency of classification.

Due to the matter of lacking real dataset, PD bradykinesia walking is simulated by healthy controls. In order to make sure the comparability with real bradykinesia walking, videos are used as references. Because of the apparent discrepancy between the bradykinesia walking and healthy walking, the accuracy of HMM classification is expected to be high. Even though different healthy subjects are requested to simulate the pathological walking, to simulate diverse severities without references is a tough problem. Besides, people have different gaits but more or less similar leg movements during walking. That is the reason why the two subjects in the normal walking tests have similar joint angles of lower extremity. If more angle data from different severities and subjects are collected, the practicability of the system will be more persuasive, nevertheless with more training data probability-based HMM classifier would still maintain high classification accuracy. Currently, very little research are focusing on the analysis of motor function of lower extremity and quantification of joint motions. Thus, there is no direct comparison with others, which also illustrates the novelty of proposed approach in the quantification of lower extremity bradykinesia.

Developing a reliable and convenient quantification approach for PD symptom is considerable important from the clinical point of view. It can be used for in-lab evaluation, off-line follow-up and remotely monitoring the progression of PD after therapy. The new approach may change the clinician's concentration from short term in-lab observation to long term assessment during daily life, since the fact that PD symptoms vary throughout the day. In addition, our system is small, low energy consumption and accessible for capturing daily motions, thus, it is potentially usable in home, outdoor and clinical environments to evaluate the progression of PD. The

proposed model-based quantification approach can make the diagnosis of bradykinesia more flexible. Especially for advanced stage patients who have difficulties in walking, the remotely diagnosis would be helpful for clinician to assess the evolutive disease and make decisions for the appropriate treatments. Proposed approach can be applied to the monitoring of body status of the elderly, such as discriminating fall from lay down, and it is capable of quantifying other symptoms of PD, such as the progression of trunk stability of body bradykinesia and deterioration of rigidity.

Chapter 5

Inertial-Based Pedestrian Positioning for Indoors

Abstract

This chapter presents a wearable IMU based pedestrian positioning system for indoors. A HMM is introduced to pre-process the sensor data and classify walking states. It also complements local minimum angular rate value for capturing the occurrence of each step. ZUPT algorithm is implemented to correct the walking velocity at step stance phase when errors existed. A novel acceleration-based approach combined with gyroscope data is implemented to achieve a better heading estimation. Proposed method is capable of reducing accumulated drift errors from gyroscopes and avoiding electromagnetic perturbation to magnetometers compared with conventional PDR system. Experimental results demonstrate the positioning system achieves approximately 99% accuracy.

5.1 Introduction

Outdoor navigation and tracking systems have been developed and widely used for decades. Some technologies, such as Global Positioning System (GPS) and cellular-based approaches, are able to provide accurate geographical and absolute position information. However, GPS is unreliable in dense “urban canyons” and not available inside the buildings due to the signal blockage. A few hybrid systems improve the performance. The integration of GPS and local beacon positioning systems achieve better results in calculating one’s position. This technique could also be extended to indoor environment, which is referred to as “network based positioning systems” ([Renaudin et al. \(2007\)](#)). They use pre-installed beacons as infrastructure to locate and track moving objectives, *i.e.* Bluetooth, Ultra Wide Band, WiFi and Radio-Frequency Identification (RFID) ([Renaudin et al. \(2007\)](#); [Gu et al. \(2009\)](#)).

Local beacon positioning systems provide absolute position information with high accuracy. However, their performance is still restricted by the basic elements of the techniques. They requires pre-installed infrastructure, which is time consuming and not practical in unknown environments. The communication between signal transmitters and receivers is easily interrupted by contextual noises. Furthermore, it is not economical to equip every point of the buildings with beacons. Consequently, beacon-free methodologies for indoor navigation are becoming popular in recent years.

As a beacon-free method, IMU provides a more promising and self-contained solution for position estimation. Sensor-based PDR system has been researched for computing the absolute position and orientation of a pedestrian. Conventional PDR system utilizes accelerometers to detect step occurrence and estimate stride length indirectly. Gyroscopes and compasses are used to measure the orientation changes. Due to the inaccuracy of vulnerable sensors, however, the accumulated errors would affect the estimation results. Thus, PDR system was developed by combining GPS for outdoors in the work of [Sun et al. \(2009\)](#); [Chen et al. \(2010\)](#); [Cho et al. \(2010\)](#) and RFID for indoors in the work of [Renaudin et al. \(2007\)](#) to

reduce drift errors. Compared with those approaches whose IMU was mounted on the upper body, i.e. Kourogi et al. (2010); Shin et al. (2010) attached sensors on the waist, many systems mounted IMU on pedestrian's shoe (Beauregard (2007); Jimenez et al. (2009)). Besides, ZUPT technique was applied to reduce the drift errors from gyroscopes and limit the overall inaccuracy (Ojeda and Borenstein (2007)).



Figure 5.1: A pedestrian positioning system design

This chapter presents a wearable IMU pedestrian positioning system for indoor environment (Figure 5.1). ZUPT algorithm is implemented to correct the walking velocity at step stance phase. Based on human physiologic characters, the foot mounted PDR system is more sensitive to the foot displacements and the data collected is more reliable for measuring the acceleration and orientation information. Three main elements are taken into account: step length estimation, step detection and heading determination.

Step length has a close relationship with the step frequency and walking velocity. Godha et al. (2006) adopted constant parameters as the step length, which is far from realistic for pedestrians with different walking patterns. Linear model for the relationship between step frequency and stride length was created in the work of Lee

and Mase (2001); Sun et al. (2009); Jimenez et al. (2009). However, the parameters should be uniquely adjusted for each individual but not for general use. Real-time measuring of step length performs more efficient. Ultrasonic sensors attached to one's shoes, measure the displacement of each step (Yeh et al. (2007)). It requires a line of sight between the shoes, which can work well in flat terrain but may not for rough terrain. ZUPT algorithm is considered to be more reliable and available for users with any walking patterns (Ojeda and Borenstein (2007); Beauregard (2007); Jimenez et al. (2009)). According to the idea that resetting the walking velocity to zero at step stance phase, ZUPT algorithm powerfully lowers the accumulated drift in step length estimation. So we executed our step length measurement based on ZUPT algorithm.

Many effective methods are developed for step detection, such as peak detection, zero-crossing and pitch signals analysis (Ojeda and Borenstein (2007); Sun et al. (2009); Chen et al. (2010, 2009); Jirawimut et al. (2003)). However, for irregular motions, peak misdetection will occur because some peak in acceleration during normal and irregular movement can be very similar. In order to improve the detection accuracy, some pre-processing are utilized to identify the valid acceleration readings from the whole walking movements, such as probabilistic neural network in the work of Sun et al. (2009). Ojeda and Borenstein (2007) found that during each step stance, angular velocity from pitch signal has a local minimum value which can be directly measured as the onset and end of each step. In the developed positioning system we implement this simple solution. In order to further reduce step misdetection, we introduce a HMM to capture the onset/end of each step. Furthermore, HMM works effectively as a classification mechanism during pre-processing.

Built-in Gyroscopes and Magnetic compass are able to determine a user's heading (Sun et al. (2009); Chen et al. (2009)). Gyroscope offers relatively accurate turn rate and magnetic compass provides absolute heading respect to the magnetic north when the environment has low magnetic distortion (Ojeda and Borenstein (2007)). Although either of these two sensors is eligible for measuring the turning, the sensor

drift of gyroscopes and unpredictable perturbation of magnetic field severely affect their accuracy in application. We novelly combined lateral acceleration and angular velocity from gyroscope for heading determination, which could avoid the perturbation to magnetometer from local disordered magnetic field.

In this chapter, a HMM is introduced for classifying the activities and rectifying the step misdetection when estimating positions. Local minimum value of angular velocity performs well for helping HMM detect steps. A novel combination of lateral acceleration and angular velocity are used for azimuth measurement and experimentally shown to achieve high accuracy for short-term and long-term indoor navigation.

5.2 System Overview

A wearable IMU pedestrian positioning system is developed and tested by a series of experiments. The architecture of the system is shown in Figure 5.2. IMU detects the movements and transmits the sensor data to positioning algorithm after signal pre-processing. Acceleration and angular rate data are integrated for step length calculation and orientation determination, which work as two inputs of position estimation. The magnetometer has good performance when used for outdoor orientation determination. Since we focus on the indoor application with random interference, the proposed system is mainly based on accelerometer and gyroscope information but leaves magnetometer for outdoor research.

The IMU pedestrian positioning system consists of two major parts: activity classification module and pedestrian dead reckoning module. The activity classification module pre-processes the sensor data and classifies different activities by HMM. During one's movement, different moving states exist in continuous sequence. Some of them could be very similar to each other, which is difficult to be distinguished apart only by sensor data. HMM is based on the relationship between current state's probability and last state's. Even if some unexpected incidents happen, such as hit

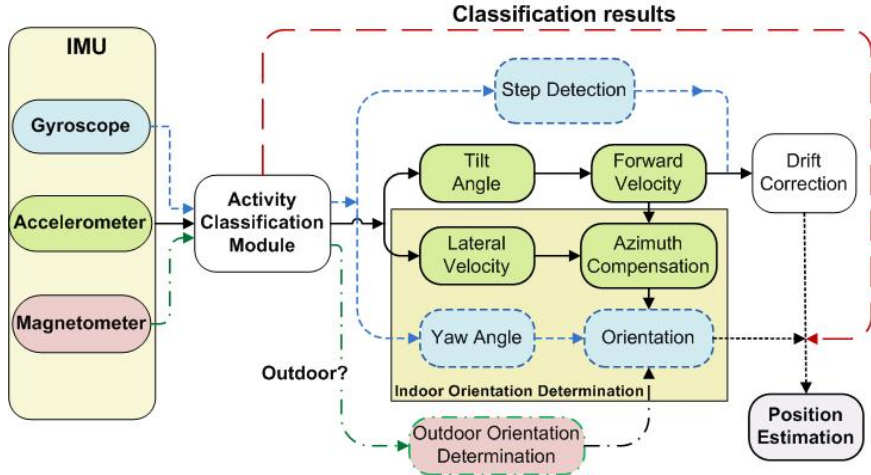


Figure 5.2: The architecture of position estimation system

something or fall, the probability-based method would not be affected easily. New data can be added to model without affecting learnt HMM and learn incrementally. Besides, HMM is easier to be analyzed and developed for implementations.

Many PDR systems utilize the combination of gyroscope and digital compass for the heading determination. However, this combination should work well in the environments without electromagnetic interference, or with very low interference. Because in our experimental environment, digital compass is vulnerable to surrounding interference, so we decided to use the accelerometer to substitute magnetometer. The novel integration of accelerometer and gyroscope is shown to be an accurate alternative for indoors, especially under interferential situations.

Lateral velocity is integrated from lateral acceleration, and combined with forward velocity through trigonometric operations, an azimuth θ_{acc} is calculated. Although the yaw angle mainly represents the heading orientation θ_{gyro} , its accuracy is not satisfactory due to the sensor errors. However, the calculated azimuth derived from

acceleration data can compensate the underestimation of gyro orientation very well, as follows: $\theta = W_1 \cdot \theta_{acc} + (1 - W_1) \cdot \theta_{gyro}$. The parameters W_1 is determined and preset by experiments. Finally, this high accuracy orientation information guarantees a decent position estimation result.

5.3 Activity Classification

As a stochastic machine, HMM is characterized by the triplet briefly $\lambda = (A, B, \pi)$, where A is the matrix of state-transition probabilities, B is the matrix of observation probabilities. π is the vector of initial state probabilities. The observation symbols can be continuous or discrete. In this chapter, a discrete HMM is employed to perform the real-time activity classification.

The parameter estimation plays an important role in the model construction, and is considered as an optimization problem. The classic Baum-Welch algorithm is adopted to solve this problem, which is obtained by maximizing the likelihood $P(O|\lambda)$ using an iterative procedure. On the other hand, Viterbi method is chosen to find the most likely state sequence in the model that produced the observations.

5.3.1 Model description

As is known, even two people are in the same walking or running pattern, the duration and frequency are discrepant more or less. If the traditional single-HMM model is used for different user, it has to be retrained to classify the activities, which would be time-consuming. Besides, traditional HMM model cannot be applied to complex activities for different people.

To address this problem, a novel activity model is proposed, which is shown in Figure 5.3. The topology of left one is ergodic (full-connected). The state space consists of 6 patterns: standing (S), walking (W), going upstairs (U)/downstairs (D), jogging (J) and running (R). The state transitions are equiprobable and the

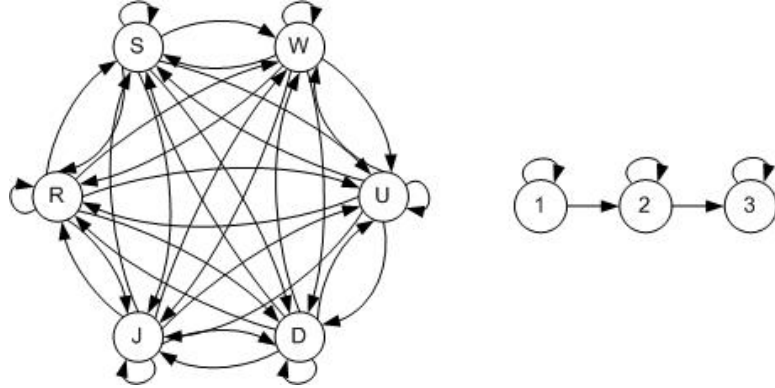


Figure 5.3: HMM for activity classification

state space is extensible depending on specific activity demands. The classification result is mainly determined by the observation probability, which is obtained through calculating the probability of particular output sequence. Each elementary HMM is considered as a left-right HMM, and associated to a state. As shown in the right of Figure 5.3 is the HMM of walking activity with three states. This level of HMM is built with different number of states according to the observation sequence. Other elementary models are similar. Consequently, a generic model is proposed by combining the elementary models.

5.3.2 HMM Training

In the training process, each elementary HMM is suitable for its respective patterns. The number of states for every model is specified empirically. Considering the complexity and performance, the parameters can be obtained through some experiments. In this work, there are 6 states for activity R and J model, 3 states for activity W model, 4 states for activity U and D model, and 2 states for activity model S. During

the training, optimal parameters are obtained by maximizing the local likelihood $P(O|\lambda)$ iteratively using the Baum-Welch algorithm.

5.3.3 Automatic Activity Classification

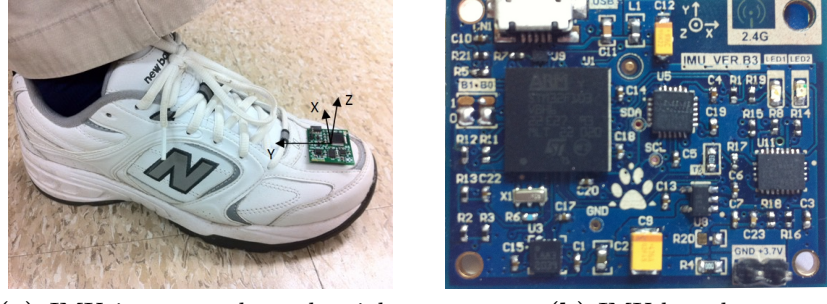
The activity classification can be considered as the decoding procedure. Viterbi algorithm is employed to find the most likely activity by given the observations using different elementary HMM. Figure 5.9a shows a series of activity classification results. The onsets and ends of all the activities are identified by the red line. The top letter indicates the activity state. Also for each activity, every step is captured accurately by HMM for further positioning. Figure 5.9b shows the zoom-in figure of the step intervals during walking.

5.4 Pedestrian Dead Reckoning

Pedestrians' walking is a cyclic pattern. Different placements of IMU mounted on the body reflect various results. In order to directly measure the foot behavior when one is walking, we mount our IMU on the upper surface of right foot (Figure 5.4a). Our PDR-based positioning algorithm includes four key elements: step detection, drift correction, heading determination and position estimation.

5.4.1 Step Detection

Ideally during normal walking, there exists a short portion of time Δt that lasts from the tiptoes touch the ground until they leave. Within Δt , the velocity of feet is zero relative to the ground. However due to some reasons, i.e. slipping ground, unsuitable shoe size and different walking patterns, ideal walking pattern is not practical. In order to properly calculate the step length of one's walking, it is necessary to identify this short portion of time. Encountering the above reasons, to find out the onset and



(a) IMU is mounted on the right foot

(b) IMU board

Figure 5.4: IMU board and its placement

end of Δt based on velocity is not achievable. So we find local minimum angular rate value of angular rate vector $\omega = (\omega_x, \omega_y, \omega_z)$ for our step detection.

The sampling frequency for utilized IMU is 50Hz, and for each time t_i , we sample the minimum absolute value as below:

$$\omega_i = \sqrt{\omega_{x,i}^2 + \omega_{y,i}^2 + \omega_{z,i}^2} \quad (5.1)$$

where ω_i is the minimum absolute value in time t_i . In order to determine the approximate onset and end of each step, a certain threshold K is chosen. If $\omega_i \leq K$, and it lasts at least for more than one sample, then we define this time i is the onset of the step. Next time when $\omega_i \geq K$, it represents the end of current step. As previously introduced, HMM also provides complementary detection results when pre-processes IMU data. In that case, the onset/end of steps could be correctly detected.

5.4.2 Drift Correction

When walking without any slip, the front sole holds still relative to the ground during Δt . So it is rational to extract the front sole as a point which has a zero velocity. Since Δt maintains for a period of time but not an instant, we consider that the acceleration of three axes would at least be zero at some time during this period. So step detection threshold K is employed for assuming where zero acceleration occurs. If at the end point of each step, the acceleration of three axes is not zero, then the bias is caused by drift. By resetting the acceleration to zero, the accelerometer drift can be effectively eliminated for each step. This is the main idea of ZUPT. Obviously, the drift occurs during the stride but not the stance phase. Each stride only lasts for a very short time and as the drift correction acts step by step, at least we could limit the accumulated error under a very small range.

$$\mathbf{v} = \int \dot{\mathbf{v}} dt = \int (\mathbf{a} - \mathbf{g}_l) dt \quad (5.2)$$

where $\mathbf{v} = (v_x, v_y, v_z)$ is the *velocity vector* of three components and $\mathbf{a} = (a_x, a_y, a_z)$ is the *acceleration vector* of three components. $\mathbf{g}_l = (g_x, g_y, g_z)$ represents the local gravity component in three axes.

We execute the above description to ground velocity. Equation (5.2) shows the computing of ground velocity by double-integrating the acceleration data and eliminating the local gravity components. As assumed, the front sole point should have both zero velocity and acceleration. If \mathbf{v} is not zero, we reset it to zero. Then the next step will have a zero starting, which means the drift errors generated by last step will not affect next one. Similarly, if the foot slips during one step, the errors will not be brought to next one.

5.4.3 Heading Determination

In this system, the IMU is placed on the upper surface of right foot. Due to the fact that people have diverse walking habit (toein, toeout) or different type of shoes (boots, sporting shoes), the initial orientation of IMU could be various, which will affect subsequent measurement of heading. Consequently, we initiate from computing of the tilt angle δ and deviation angle β .

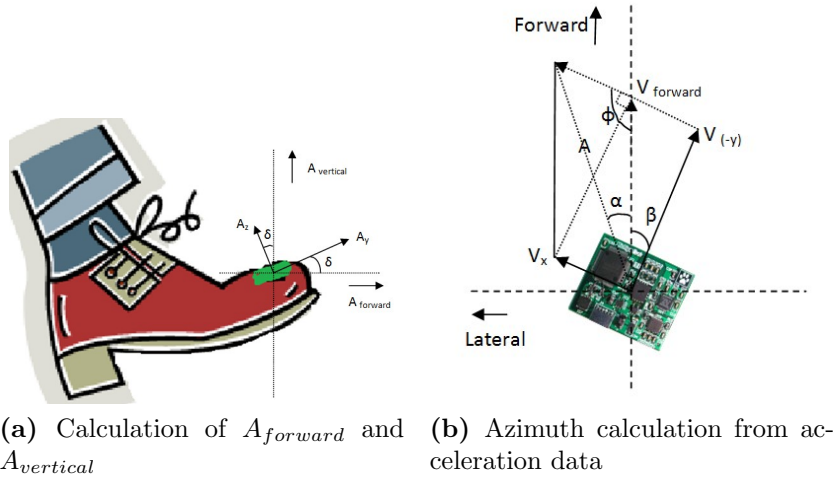


Figure 5.5: Some calculations for heading determination

The upper surface of a shoe may not be horizontal, and the initial state will be repeated every time the foot touches ground. This feature directly impacts the calculation of forward acceleration $A_{forward}$ and vertical acceleration $A_{vertical}$ (Figure 5.5a).

$$A_y = A_{yraw} - (-1) \sin \delta \quad A_z = A_{zraw} - (-1) \cos \delta \quad (5.3)$$

$$A_{forward} = A_y \cos \delta - A_z \sin \delta \quad (5.4)$$

$$A_{vertical} = A_y \sin \delta + A_z \cos \delta \quad (5.5)$$

where A_y and A_z are the acceleration data for Y -axis and Z -axis after removing the gravity components from raw acceleration data A_{yraw} and A_{zraw} in (5.3). Horizontal tilt angle δ is updated and utilized for $A_{forward}$ and $A_{vertical}$ by each sample. We also measure δ by *Quaternion* representation q_{se} , which is introduced in the work of [Hu et al. \(2010\)](#).

Many references determine their heading orientation based on gyroscope reading and magnetometer data. As we mentioned, however, the magnetic field is vulnerable to be interfered. The gyroscope was also tested for finding the orientation, but it turned out to be not accurate as we expected. Therefore we novelly fuse acceleration data and gyroscope data in order to achieve better results.

As Figure 5.5b shows, deviation angle β represents the angle between user's walking direction and IMU's heading direction. We develop an acceleration-based orientation estimation approach. When people is making a turn, the lateral velocity V_x and forward velocity $V_{forward}$ bring a trend, which towards a direction that is away from forward direction by angle α . Angle α is computed as:

$$\phi = \beta + \pi/2 \quad (5.6)$$

$$A^2 = V_x^2 + V_{forward}^2 - 2V_x \cdot V_{forward} \cos \phi \quad (5.7)$$

$$V_x^2 = A^2 + V_{forward}^2 - 2V_{forward} \cdot A \cos \alpha \quad (5.8)$$

Angle α represents the orientation θ_{acc} . From testing results, we find although θ_{acc} could describe the orientation better than θ_{gyro} measured by gyroscope, it does not accurately match the azimuth. Nevertheless, it works as an excellent complement to θ_{gyro} . We define a probabilistic relationship between θ_{acc} and θ_{gyro} , which is $\theta = W_1 \cdot \theta_{acc} + (1 - W_1) \cdot \theta_{gyro}$, where θ is the final azimuth and $W_1 \in [0.3 - 0.4]$ is the weight for θ_{acc} . The value of W_1 is from the Gaussian distribution of experimental measurements by testing the algorithm on each particular user. In our experiments, $W_1 = 0.33$ for indoor tests.

5.4.4 Position Estimation

Position estimation is a process of combining and coordinating the sensor data. After drift correction and heading determination, the position of pedestrian is estimated. Activity classification results are referred for the estimation. When successive sensor data generated from distinct moving patterns, some similar data would be mixed up and interfere the estimation results by false step. We classify some regular moving patterns and handle the sensor data in allusion to their character, so that to avoid step misdetection and reduce the along track error. Finally, the position can be estimated by coupling the distance with azimuth:

$$d = \int V_{forward} dt \quad h = \int V_{vertical} dt \quad (5.9)$$

$$(X_i, Y_i, Z_i) = (X_{i-1} + d \cos \theta, Y_{i-1} + d \sin \theta, Z_{i-1} + h) \quad (5.10)$$

where (X_i, Y_i, Z_i) are the estimated coordinate of sample i . θ is the angle changes from sample $i - 1$ to i in $X - Y$ plane.

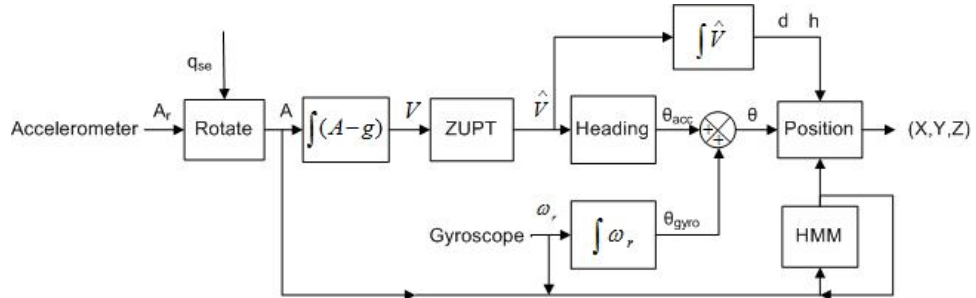


Figure 5.6: Position estimation with IMU

A block diagram for position estimation is shown in Figure 5.6. The position is determined by the horizontal and vertical displacement, with complementary azimuth

and classified state. The displacement is double integrated from accelerometer readings with heading estimation as an input. Gyroscope readings serve both the orientation compensation and classification model HMM. HMM which also includes the input from accelerometer and last classification state provides correct state for step detection.

5.5 Experiments

The hardware design of IMU is introduced in Section 1.5, as shown in Figure 5.4b. In this section, several experiments are developed to verify proposed system, including straight line walking, short term walking and long term walking.

5.5.1 Performance Evaluation

Some experiments are implemented in the $X - Y$ plane. The absolute error e_a for single experiment is depicted as:

$$e_a = \sqrt{x_e^2 + y_e^2} \quad (5.11)$$

where x_e and y_e are return position errors in X and Y directions, respectively. The absolute average error E_a and the relative average error E_r are defined to measure the system performance, which are shown as:

$$E_a = \frac{1}{n} \sum_{i=1}^n e_{a,i} \quad E_r = 100 \frac{E_a}{D} \quad (5.12)$$

where n is the number of our experiments. Similarly for 3D experiments, the absolute error and relative error in Z direction Z_a and Z_r are also computed.

5.5.2 Straight Line Walking

Before starting the experiment, a specific distance of $10m$ is measured and the starting and ending point are marked precisely. Figure 5.7 shows the reconstruction result of the straight line trajectory by using our algorithm. Two sets of experiments are implemented with normal walking speed and faster speed, about $2.6mph$ and $3.3mph$.

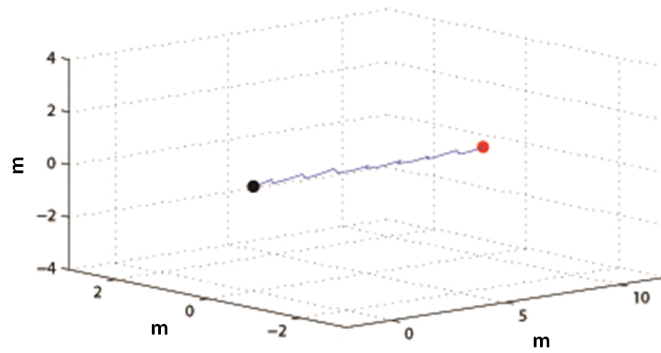


Figure 5.7: The reconstruction of straight line trajectory. Black point and red point represent the starting and ending point.

Each set of experiments are performed 5 times, and the absolute and relative average errors are calculated, while the y_e equals to 0. As shown in Table 5.1, the relative average errors are 0.55% and 0.31% respectively which are in high accuracy.

5.5.3 Short Term Walking

The proposed system also measures the instant position in real-time. The short term experiments include rectangle-shaped walking and U -shaped walking.

Table 5.1: Results of the straight line experiment

Index	$v = 2.6\text{mph}$			$v = 3.3\text{mph}$		
	$e_a(m)$	$E_a(m)$	$E_r(\%)$	$e_a(m)$	$E_a(m)$	$E_r(\%)$
1	0.063			0.024		
2	0.057			0.037		
3	0.060	0.055	0.55	0.021	0.031	0.31
4	0.034			0.032		
5	0.059			0.043		

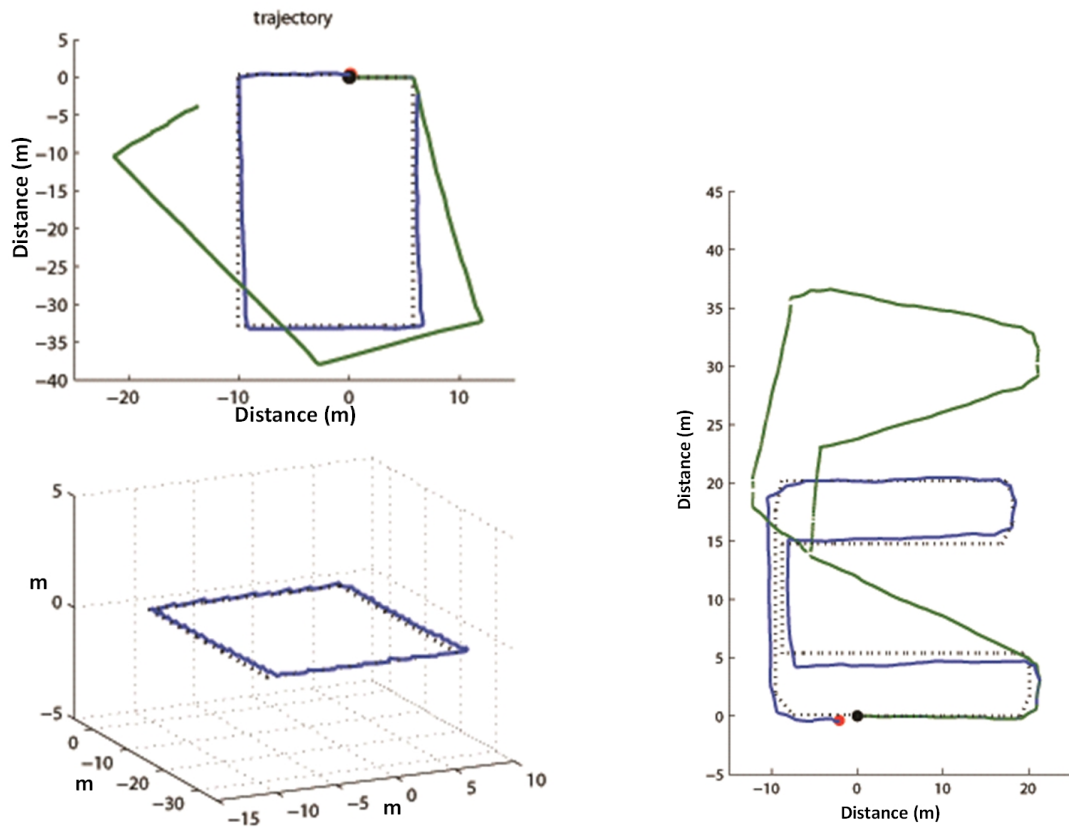
Rectangle-shaped Walking

One subject walks along a rectangle-shaped path, and goes back to the starting point finally. The length and width of the rectangle are $32.8m$ and $16m$ at the normal pace of 2.6mph . In Figure 5.8a (upper), the black dashed line represents designed trajectory. Compared with the result which only uses the gyroscope data (green line), the reconstruction result (blue line) based on our proposed system performs better. Figure 5.8a (lower) shows the 3D view of our reconstruction result, which follows the designed trajectory with high consistence. The difference between the starting and ending point is only $0.087m$, which is mainly caused by the heading error.

Similarly, this experiment is measured 5 times and calculates the absolute and relative average error. As shown in Table 5.2, both errors are smaller than 0.5, and can truly reach the actual requirement.

U-shaped Walking

U-shaped path is designed with the length is $226.5m$ in total. Actually it is similar with the rectangle walking. The reconstruction result is shown in Figure 5.8b. It is obvious that the reconstruction result using gyroscope is deviated from the designed



(a) The reconstruction of the rectangle trajectory

(b) The reconstruction of the U-shaped trajectory

Figure 5.8: Two short term walking experiments

trajectory further. Our system improves the performance greatly. The average errors are close to $1.20m$ and 0.52% . The detailed result is shown in Table 5.2.

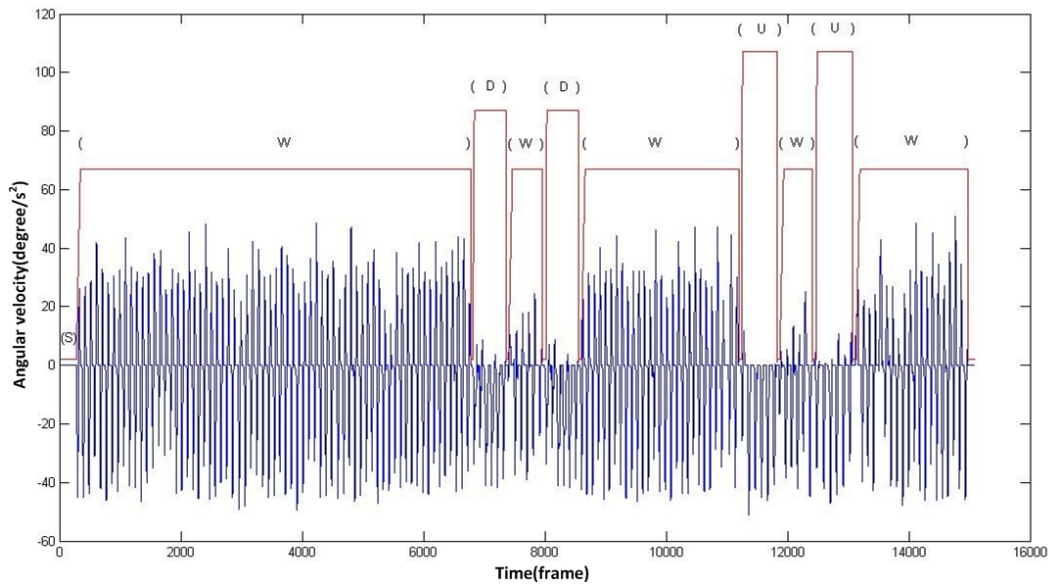
Table 5.2: Results of the rectangle-shaped and U-shaped experiment

Index	Rectangle-shaped			U-shaped		
	$e_a(m)$	$E_a(m)$	$E_r(\%)$	$e_a(m)$	$E_a(m)$	$E_r(\%)$
1	0.087			1.45		
2	0.079			1.11		
3	0.083	0.39	0.43	1.20	1.19	0.52
4	0.047			1.01		
5	0.081			1.15		

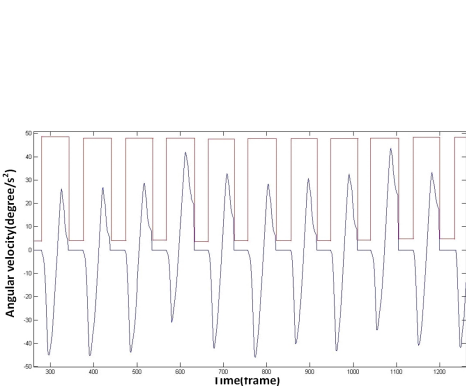
5.5.4 Long Term Walking

In proposed system, all three components of the velocity vector are applied. The Z -axis value is also calculated for vertical displacement. Figure 5.9c shows a complex 3D experiment with many activities, including walking (W), going downstairs (D) and upstairs (U) and standing (S). At first, the signal set is pre-processed using HMM to extract the onsets and ends of the activities (Figure 5.9a and 5.9b). Then the classification result is processed as the input of position estimation.

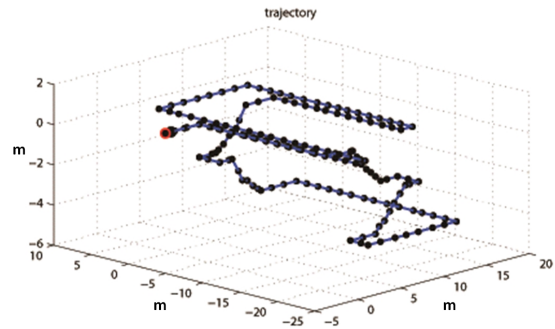
The approximated distance for the experiment is about $337m$ in total. It is repeated three times and their performance are evaluated by calculating the absolute and relative average error from $X - Y$ plane and Z direction. The position errors are summarized in Table 5.3. The error in $X - Y$ plane is 0.42% , while the vertical error is larger, averaging 1.52% .



(a) Activity classification using HMM



(b) zoom-in figure of walking part



(c) Walking trajectory reconstruction

Figure 5.9: Long term walking experiment

Table 5.3: Absolute and relative average error of the long term experiment

Index	Dist.(m)	Absolute(m)		Relative(%)	
		X-Y plane	Z axis	X-Y plane	Z axis
1	347				
2	330	1.42	0.05	0.42	1.52
3	335				

5.6 Summary

This chapter presents a wearable IMU pedestrian positioning system for indoors. HMM performs as activity classification to pre-process the sensor data, capture the steps and distinguish different moving patterns, such as walking, standing, jogging, running and going upstairs/downstairs, which are used for avoiding misdetection in position estimation. Local minimum absolute value of angular rate is utilized for detecting the onset/end of steps from gyro level. ZUPT algorithm corrects the sensor drift from acceleration data and resets the velocity to zero at each stance phase, which stops accumulating existing errors to next step. A novel acceleration-based approach for determining the heading orientation is developed, and combined with gyroscope data to achieve better azimuth estimation. Experiments are conducted to evaluate the accuracy of system. The overall errors are mostly under 1% except the vertical errors are around 2%.

Chapter 6

Conclusions and Future Work

In consideration of continuously tracking human motions, positioning human location and monitoring human health status in free-living environment, a human motion analysis system is developed to serve these purposes. It aims and achieves research goals as stated in Section 1.3: A human motion tracking system with wearable inertial sensors is developed for efficiently tracking free-living motions and reconstructing the human model; by applying the reconstructed model, a model-based approach is proposed for quantification of resting tremor and bradykinesia in PD, in order to validate the practical application of developed system; A pedestrian positioning system with wearable inertial sensors is developed for tracking position and recording itinerary for indoors.

6.1 Conclusions

A human motion tracking system with our developed wearable IMUs is developed. A well designed calibration procedure estimates the placement and orientation of attached IMUs, so that no specific measurement is needed for locating IMUs, which greatly reduces the complexity in configuring the system before use. The twists and exponential maps techniques, which are inspired from robotic manipulation and never used in human motion technique, are applied to describe body segment

movements, articulate segments by joints and reconstruct a body model accurately and conveniently. Compared with traditional high-order approach by multiplying rotational matrixes, low-order calculations from the twists and exponential maps techniques are more preferable in real-time tracking. The accuracy of developed system is assessed by comparisons with two commercialized motion capture systems. Accurately quantified analysis of joint angles based on built model provides the basis for applications which analyze human motor functions.

In order to prove the practicability of developed wearable motion tracking system in medical applications, resting tremor and bradykinesia in PD are quantified by model-based approaches. Wearable motion tracking system tracks a patient's body segment movements and these movements can be represented on the reconstructed human model. Based on the human model, rotational angles of involved upper extremity joints (elbow and wrist) and lower extremity joints (hip and knee) correlated with two symptoms (of resting tremor and bradykinesia) are estimated. Angle related features which can best describe symptom characteristics are extracted from estimated joint angles. Angle data with different severities rated by clinical UPDRS, plus corresponding rating, are used to train the discrete HMM classifier and trained HMM is capable of quantifying new angle data by determining the severity. Due to the lack of PD patients, simulated data with various severities captured from healthy subjects are employed to implement experiments. A leave-one-out validation technique validates the HMM performance. High accuracy (average over 99%) of proposed quantification approach preliminarily demonstrates its feasibility in improving present approaches in a more objective way.

Besides the tracking of human body motions, in order to complement the functions of human motion analysis system, a pedestrian positioning system based on wearable IMU is developed. A discrete HMM is introduced to detect step onset/end and classify the walking states. During each step, ZUPT technique is implemented to reset walking velocity drift at step stance phase, so that the drift generated when estimating step length and step height can be limited within a low level. In addition to estimating step

length and step occurrence, an accurate estimation of heading azimuth is essential. Since the conventional PDR system suffers gyro drift and magnetic field perturbation, a novel combination of lateral acceleration and angular velocity are used for the estimation, meanwhile replacing the vulnerable magnetometer. With the accurate heading, travelled itinerary of the subject in either 2D or 3D space can be tracked and monitored. Several tests include short term walking and long term walking with multiple walking states are conducted and the system performance is evaluated by calculating the absolute position errors between starting points and end points. The low overall error rate verifies the feasibility and usefulness of developed positioning system for indoor environment.

6.2 Future Work

This dissertation presents a promising human motion analysis tool that can potentially improve current medical approaches in continuous monitoring and tracking a subject's motions, health status and locomotion. This system has no limits to the implement environment and to the subjects. Both patients and elder person whose motor functions are needed to be concerned and investigated are available for wearing the system. The preliminary experimental results of each system verification and applications on PD quantification prove the practicability of proposed technique. Despite of those, more work is needed for further validating the performance of developed system. The future works are listed as follows:

1. Developed wearable body motion tracking system is advanced by its estimation of IMU placement. Although the IMU position where would be affected by less soft tissue artifact is suggested, the soft tissue artifact still exists. Therefore, one of the future works for this particular system is focusing on filtering approaches to further reduce the effects. Conducted experiments use steady and slow motions to simulate the motions of elder people. The other future work is

to exert rapid motions and more lifestyle movements to validate the stability of developed system and its potentiality for wider range of applicable people.

2. In order to validate the performance of wearable body motion tracking system in medical applications, a large number of dataset with various illness conditions is highly recommended. For the model-based quantification approach to symptoms in PD, limited simulations are employed, due to the lack of real data from PD patients. For probability based HMM classifier, more training data will definitely increase the accuracy of quantification. Therefore, one of future works of the applications will be collecting motion data from PD patients with different severities and further validating the quantification approach. Besides these two symptoms of PD, developed system will be investigated for quantifying other apparent symptoms of PD and illness, such as rigidity, body instability and fall. Besides, EMG of PD patient is going to be measured for the quantification of resting tremor to enhance potential PD diagnosis at early-stage and to discover the necessity of using both EMG and IMU in improving the PD quantification.
3. The pedestrian positioning system has been validated by indoor tests with short term and long term walking. More tests with longer distance and more complex walking states are suggested. Besides indoor use, developed positioning system can be combined with currently available positioning systems, such as GPS, cellular-based approach and local beacon technique, to calibrate our system when ambient calibration information can be received. So that the application of developed indoor positioning can be extended to more complicated unknown environment, meanwhile the system can self-calibrate to reduce the drift errors.

Bibliography

- Askari, S., Zhang, M., and Won, D. (2010). An emg-based system for continuous monitoring of clinical efficacy of parkinson's disease treatments. In *Annual International Conference of the IEEE Engineering in Medicine and Biology Society*, pages 98–101. [64](#), [66](#)
- Beauregard, S. (2007). Omnidirectional pedestrian navigation for first responders. In *4th Workshop on Positioning, Navigation and Communication*, pages 33–36. [121](#), [122](#)
- Blaszczyk, J. W. and Orawiec, R. (2011). Assessment of postural control in patients with parkinsons disease: Sway ratio analysis. *Journal of Human Movement Science*, 30(2):396–404. [96](#)
- Bregler, C. and Malik, J. (1998). Tracking people with twists and exponential maps. In *IEEE Computer Society Conference on Computer Vision and Pattern Recognition*, pages 8–15. [59](#)
- Chen, W., Chen, R., Chen, Y., Kuusniemi, H., and Wang, J. (2010). An effective pedestrian dead reckoning algorithm using a unified heading error model. In *IEEE/ION Position Location and Navigation Symposium*, pages 340–347. [120](#), [122](#)
- Chen, W., Fu, Z., Chen, R., Chen, Y., Andrei, O., Kroger, T., and Wang, J. (2009). An integrated GPS and multi-sensor pedestrian positioning system for 3D urban navigation. In *Joint Urban Remote Sensing Event*, pages 1–6. [122](#)
- Chen, X., Hu, S., Shao, Z., and Tan, J. (2011). Pedestrian positioning with physical activity classification for indoors. In *IEEE International Conference on Robotics and Automation*, pages 1311–1316. [45](#)
- Cho, D.-K., Mun, M., Lee, U., Kaiser, W., and Gerla, M. (2010). AutoGait: A mobile platform that accurately estimates the distance walked. In *IEEE International Conference on Pervasive Computing and Communication*, pages 116–124. [120](#)

- Cutti, A., Giovanardi, A., Rocchi, L., Davalli, A., and Sacchetti, R. (2008). Ambulatory measurement of shoulder and elbow kinematics through inertial and magnetic sensors. *Medical and Biological Engineering and Computing*, 46:169–178. [20](#), [21](#), [60](#)
- Dejnabadi, H., Jolles, B., Casanova, E., Fua, P., and Aminian, K. (2006). Estimation and visualization of sagittal kinematics of lower limbs orientation using body-fixed sensors. *IEEE Transactions on Biomedical Engineering*, 53(7):1385–1393. [60](#)
- Godha, S., Lachapelle, G., and Cannon, M. E. (2006). Integrated GPS/INS system for pedestrian navigation in a signal degraded environment. In *ION GNSS*, pages 26–29. [121](#)
- Grimaldi, G. and Manto, M. (2010). Neurological tremor: Sensors, signal processing and emerging applications. *Sensors*, 10(2):1399–1422. [64](#)
- Gu, Y., Lo, A., and Niemegeers, I. (2009). A survey of indoor positioning systems for wireless personal networks. *IEEE Communications Surveys & Tutorials*, 11(1):13–32. [120](#)
- Heldman, D., Filipkowski, D., Riley, D., Whitney, C., Walter, B., Gunzler, S., Giuffrida, J., and Mera, T. (2012). Automated motion sensor quantification of gait and lower extremity bradykinesia. In *Annual International Conference of the IEEE Engineering in Medicine and Biology Society*, pages 1956–1959. [94](#), [95](#)
- Heldman, D. A., Jankovic, J., Vaillancourt, D. E., Prodoehl, J., Elble, R. J., and Giuffrida, J. P. (2011). Essential tremor quantification during activities of daily living. *Parkinsonism and Related Disorders*, 17(7):537–542. [64](#), [65](#)
- Horn, B. K. P., Hilden, H., and Negahdaripour, S. (1988). Closed-form solution of absolute orientation using orthonormal matrices. *Journal of the Optical Society America*, 5(7):1127–1135. [32](#), [71](#), [101](#)

- Hu, S., Chen, X., and Tan, J. (2010). Pams: a wearable physical activity monitoring system for continuous motion capture in free-living environments. In *5th International Conference on Body Area Networks*, pages 233–239. [12](#), [131](#)
- Jankovic, J. (2008). Parkinsons disease: clinical features and diagnosis. *Journal of Neurology, Neurosurgery & Psychiatry*, 79(4):368–376. [64](#)
- Jimenez, A., Seco, F., Prieto, C., and Guevara, J. (2009). A comparison of pedestrian dead-reckoning algorithms using a low-cost mems imu. In *IEEE International Symposium on Intelligent Signal Processing*, pages 37–42. [121](#), [122](#)
- Jirawimut, R., Ptasiński, P., Garaj, V., Cecelja, F., and Balachandran, W. (2003). A method for dead reckoning parameter correction in pedestrian navigation system. *IEEE Transactions on Instrumentation and Measurement*, 52(1):209–215. [122](#)
- Jones, L. Y. (2009). *Great Expectations: America and the Baby Boom Generation*. Coward Mc Cann. [1](#)
- Jun, J.-H., Kim, J.-W., Kwon, Y., Eom, G.-M., Koh, S.-B., Lee, B., Kim, H.-S., Yi, J.-H., and Tack, G.-R. (2011). Quantification of limb bradykinesia in patients with parkinsons disease using a gyrosensor improvement and validation. *International Journal of Precision Engineering and Manufacturing*, 12(3):557–563. [94](#)
- Jung, Y., Kang, D., and Kim, J. (2010). Upper body motion tracking with inertial sensors. In *IEEE International Conference on Robotics and Biomimetics*, pages 1746–1751. [59](#)
- Kim, J.-W., Lee, J.-H., Kwon, Y., Kim, C.-S., Eom, G.-M., Koh, S.-B., Kwon, D.-Y., and Park, K.-W. (2011). Quantification of bradykinesia during clinical finger taps using a gyrosensor in patients with parkinsons disease. *Medical & Biological Engineering & Computing*, 49(3):365–371. [94](#), [95](#)

- Koop, M. M., Shrivitz, N., and Bront-Stewart, H. (2008). Quantitative measures of fine motor, limb, and postural bradykinesia in very early stage, untreated parkinson's disease. *Movement Disorders*, 23(9):1262–1268. [94](#), [95](#)
- Kurogi, M., Ishikawa, T., and Kurata, T. (2010). A method of pedestrian dead reckoning using action recognition. In *IEEE/ION Position Location and Navigation Symposium*, pages 85–89. [121](#)
- Kuipers, J. B. (2002). *Quaternions and Rotation Sequences: A Primer with Applications to Orbits, Aerospace and Virtual Reality*. Princeton University Press.
- Lee, J. K. and Park, E. (2009). A fast quaternion-based orientation optimizer via virtual rotation for human motion tracking. *IEEE Transactions on Biomedical Engineering*, 56(5):1574–1582. [60](#)
- Lee, S.-W. and Mase, K. (2001). Recognition of walking behaviors for pedestrian navigation. In *IEEE International Conference on Control Applications*, pages 1152–1155. [121](#)
- Lin, J. and Kulic, D. (2012). Human pose recovery using wireless inertial measurement units. *Physiol Meas*, 33(12):2099–2115. [5](#), [18](#), [60](#)
- Liu, H. and Chellappa, R. (2007). Markerless monocular tracking of articulated human motion. In *IEEE International Conference on Acoustics, Speech and Signal Processing*, volume 1, pages 693–696. [59](#)
- Louie, S., Koop, M. M., Frenklach, A., and Bronte-Stewart, H. (2009). Quantitative lateralized measures of bradykinesia at different stages of parkinson's disease: The role of the less affected side. *Movement Disorders*, 24(13):1991–1997. [94](#), [95](#)
- Luinge, H., Veltink, P., and Baten, C. (2007). Ambulatory measurement of arm orientation. *Journal of Biomechanics*, 40(1):78–85. [60](#)

Lundberg, A., Svensson, O., Nemeth, G., and Selvik, G. (1989). The axis of rotation of the ankle joint. *Journal of Bone & Joint Surgery, British Volume*, 71-B(1):94–99.

21

Maetzler, W., Mancini, M., Liepelt-Scarfone, I., Müller, K., Becker, C., van Lummel, R. C., Ainsworth, E., Hobert, M., Streffer, J., Berg, D., and Chiari, L. (2012). Impaired trunk stability in individuals at high risk for parkinson’s disease. *PLoS ONE*, 7:32240. 96

Mellone, S., Palmerini, L., Cappello, A., and Chiari, L. (2011). Hilbert-huang-based tremor removal to assess postural properties from accelerometers. *IEEE Transactions on Biomedical Engineering*, 58(6):1752–1761. 65

Ojeda, L. and Borenstein, J. (2007). Non-gps navigation with the personal dead-reckoning system. In *Unmanned Systems Technology IX*, volume 6561. SPIE. 121, 122

Palmerini, L., Rocchi, L., Mellone, S., Valzania, F., and Chiari, L. (2011). Feature selection for accelerometer-based posture analysis in parkinson’s disease. *IEEE Transactions on Information Technology in Biomedicine*, 15(3):481–490. 65, 96

Patel, S., Lorincz, K., Hughes, R., Huggins, N., Growdon, J., Standaert, D., Akay, M., Dy, J., Welsh, M., and Bonato, P. (2009). Monitoring motor fluctuations in patients with parkinson’s disease using wearable sensors. *IEEE Transactions on Information Technology in Biomedicine*, 13(6):864–873. 65, 90

Perez, R., Costa, U., Torrent, M., Solana, J., Opisso, E., Caceres, C., Tormos, J. M., Medina, J., and Gomez, E. J. (2010). Upper limb portable motion analysis system based on inertial technology for neurorehabilitation purposes. *Sensors*, 10(12):10733–10751. 21, 59

- Pons-Moll, G., Baak, A., Helten, T., Muller, M., Seidel, H.-P., and Rosenhahn, B. (2010). Multisensor-fusion for 3d full-body human motion capture. In *IEEE Conference on Computer Vision and Pattern Recognition*, pages 663–670. [59](#)
- Powell, H., Hanson, M., and Lach, J. (2009). On-body inertial sensing and signal processing for clinical assessment of tremor. *IEEE Transactions on Biomedical Circuits and Systems*, 3(2):108–116. [65](#)
- Renaudin, V., Yalak, O., Tom, P., and Merminod, B. (2007). Indoor navigation of emergency agents. *European Journal of Navigation*, 5(3):36–45. [120](#)
- Rigas, G., Tzallas, A., Tsipouras, M., Bougia, P., Tripoliti, E., Baga, D., Fotiadis, D., Tsouli, S., and Konitsiotis, S. (2012). Assessment of tremor activity in the parkinson’s disease using a set of wearable sensors. *IEEE Transactions on Information Technology in Biomedicine*, 16(3):478–487. [64](#), [65](#), [90](#)
- Rissanen, S., Kankaanpaa, M., Meigal, A., Tarvainen, M., Nuutinen, J., Tarkka, I., Airaksinen, O., and Karjalainen, P. (2008). Surface emg and acceleration signals in parkinsons disease: feature extraction and cluster analysis. *Medical and Biological Engineering and Computing*, 46:849–858. [64](#), [66](#), [82](#)
- Rissanen, S., Kankaanpaa, M., Tarvainen, M., Meigal, A., Nuutinen, J., Jakala and, P., Airaksinen, O., and Karjalainen, P. (2010). Discrimination of emg and acceleration measurements between patients with parkinson’s disease and healthy persons. In *Annual International Conference of the IEEE Engineering in Medicine and Biology Society*, pages 4878–4881. [64](#), [66](#)
- Rissanen, S., Kankaanpaa, M., Tarvainen, M., Novak, V., Novak, P., Hu, K., Manor, B., Airaksinen, O., and Karjalainen, P. (2011). Analysis of emg and acceleration signals for quantifying the effects of deep brain stimulation in parkinson’s disease. *IEEE Transactions on Biomedical Engineering*, 58(9):2545–2553. [64](#), [66](#)

- Rosenhahn, B. and Brox, T. (2007). Scaled motion dynamics for markerless motion capture. In *IEEE Conference on Computer Vision and Pattern Recognition*, pages 1–8. [59](#)
- Salarian, A., Russmann, H., Wider, C., Burkhard, P., Vingerhoets, F. J. G., and Aminian, K. (2007). Quantification of tremor and bradykinesia in parkinson’s disease using a novel ambulatory monitoring system. *IEEE Transactions on Biomedical Engineering*, 54(2):313–322. [64](#), [65](#), [90](#), [94](#), [95](#)
- Shin, S. H., Lee, M. S., Park, C. G., and Hong, H. S. (2010). Pedestrian dead reckoning system with phone location awareness algorithm. In *IEEE/ION Position Location and Navigation Symposium*, pages 97–101. [121](#)
- Sun, Z., Mao, X., Tian, W., and Zhang, X. (2009). Activity classification and dead reckoning for pedestrian navigation with wearable sensors. *Measurement Science and Technology*, 20(1). [120](#), [122](#)
- Tian, Y. and Tan, J. (2012). A fast adaptive-gain orientation filter of inertial/magnetic data for human motion tracking in free-living environments. In *Annual International Conference of the IEEE Engineering in Medicine and Biology Society*, pages 6760–6763. [12](#), [26](#)
- Tian, Y., Wei, H., and Tan, J. (2012). An adaptive-gain complementary filter for real-time human motion tracking with marg sensors in free-living environments. *IEEE Transactions on Neural Systems and Rehabilitation Engineering*, (99):1. [12](#), [26](#)
- Yeh, S.-Y., Chang, K.-H., Wu, C.-I., Chu, H.-H., and Hsu, J. Y.-J. (2007). GETA sandals: a footstep location tracking system. *Personal Ubiquitous Computing*, 11(6):451–463. [122](#)

Zhang, Z., Wu, Z., Chen, J., and Wu, J.-K. (2009). Ubiquitous human body motion capture using micro-sensors. In *IEEE International Conference on Pervasive Computing and Communications*, pages 1–5. [60](#)

Zhou, H., Hu, H., and Tao, Y. (2006). Inertial measurements of upper limb motion. *Medical and Biological Engineering and Computing*, 44:479–487. [59](#)

Zhu, R. and Zhou, Z. (2004). A real-time articulated human motion tracking using tri-axis inertial/magnetic sensors package. *IEEE Transactions on Neural Systems and Rehabilitation Engineering*, 12(2):295–302. [59](#), [60](#)

Vita

Xi Chen was born in Anshan, Liaoning, China in 1985. After graduation from North-eastern University in Shenyang, China with the Bachelor of Electrical Engineering degree, he headed for Michigan Technological University in Houghton, MI, USA in 2008 for further graduate study in the PhD program. He accepted a graduate research assistantship from the Department of Electrical and Computer Engineering from 2008 to 2012, and during those four years, he became a PhD candidate. He moved to Knoxville, TN in February 2012 and enrolled in the University of Tennessee at Knoxville in Fall semester of 2012. He graduated with a Doctor of Philosophy degree in Biomedical Engineering in August 2013.